UNCLASSIFIED

AD 432154

DEFENSE DOCUMENTATION CENTER

FOR

SCIENTIFIC AND TECHNICAL INFORMATION

CAMERON STATION, ALEXANDRIA, VIRGINIA

UNCLASSIFIED

NOTICE: When government or other drawings, specifications or other data are used for any purpose other than in connection with a definitely related government procurement operation, the U. S. Government thereby incurs no responsibility, nor any obligation whatsoever; and the fact that the Government may have formulated, furnished, or in any way supplied the said drawings, specifications, or other data is not to be regarded by implication or otherwise as in any manner licensing the holder or any other person or corporation, or conveying any rights or permission to manufacture, use or sell any patented invention that may in any way be related thereto.

64-10

432154

RTD TDR-63-3086

RTD
TDR
63-3086
DASA 1417

VULNERABILITY OF NUCLEAR WEAPON SYSTEMS TO FIRE - STUDIES OF BURNING EXPLOSIVES

Final Report

December 1963

CATALOGED BY DDC
AS AD No.

TECHNICAL DOCUMENTARY REPORT NO. RTD TDR-63-3086

Research and Technology Division
AIR FORCE WEAPONS LABORATORY
Air Force Systems Command
Kirtland Air Force Base
New Mexico

DDC
MAR 18 1964
TISIA B

Project 8809

This research has been funded by the
Defense Atomic Support Agency

(Prepared under Contract AF 29(601)-1959
by IIT Research Institute, Technology
Center, Chicago 16, Illinois)

432154

Research and Technology Division
Air Force Systems Command
AIR FORCE WEAPONS LABORATORY
Kirtland Air Force Base
New Mexico

When Government drawings, specifications, or other data are used for any purpose other than in connection with a definitely related Government procurement operation, the United States Government thereby incurs no responsibility nor any obligation whatsoever; and the fact that the Government may have formulated, furnished, or in any way supplied the said drawings, specifications, or other data, is not to be regarded by implication or otherwise as in any manner licensing the holder or any other person or corporation, or conveying any rights or permission to manufacture, use, or sell any patented invention that may in any way be related thereto.

This report is made available for study upon the understanding that the Government's proprietary interests in and relating thereto shall not be impaired. In case of apparent conflict between the Government's proprietary interests and those of others, notify the Staff Judge Advocate, Air Force Systems Command, Andrews AF Base, Washington 25, DC.

This report is published for the exchange and stimulation of ideas; it does not necessarily express the intent or policy of any higher headquarters.

Qualified requesters may obtain copies of this report from DDC. Orders will be expedited if placed through the librarian or other staff member designated to request and receive documents from DDC.

FOREWORD

This is the final report on Contract No. AF 29(601)-1959, IIT Research Institute Project A6000, performed during the period June 15, 1959 to November 30, 1962. The work was performed for the Air Force Special Weapons Center/Air Force Weapons Laboratory, Kirtland Air Force Base, New Mexico, under the guidance of Captain Lester McChristian, Air Force Project Engineer.

Personnel of IIT Research Institute who have contributed to this program are Joseph Cistano, Carl Foxx, William Hartmann, William Murphy, Richard Stauner and Arthur Takata. The author is indebted to Lt Colonel Gordon Jacks (formerly of FC/DASA) and Douglas Coder (Pantex) for their aid in the procurement of the high-explosive samples from the Pantex Division of Silas Mason, Mason and Hanger Company, Amarillo, Texas.

ABSTRACT

This report covers analytical and experimental studies of the behavior of burning Composition B and PBX 9404 under various degrees of confinement. These studies were undertaken to determine the properties of the gas, the conductive heat transfer to the explosive, the radiant heat transfer to the surfaces of the high-explosive and chamber, and the heat evolved by the burning of the explosive. The work resulted in a theory which describes the burning of the explosives under unconfined and confined conditions, and the ensuing pressure buildup during the period the explosive remains intact and the reaction is limited to its surface. The results are in good agreement with experimental measurements of pressure, gas temperature, chamber temperature, and heat flux to meters in the gas stream. Beyond a pressure of about 1000 psia, the samples of Composition B cracked causing an abrupt increase in the rate of pressure rise. The cause of these phenomena and the question of whether or not PBX 9404 cracks were not resolved. The results of this work may be used to predict the minimum order of explosion which may arise from a system that is exposed to heating.

PUBLICATION REVIEW

This report has been reviewed and is approved.

JOHN A. B. BOWER
Lt Colonel USAF
Chief, Synthesis Branch
Analysis Division

LOUIS W. PFLANZ, JR
Colonel USA
Director, Research Division
Field Command, DASA

JOHN D. COKE
Colonel USAF
Chief, Analysis Division
Air Force Weapons Laboratory

J. W. RAWLINGS
Colonel USAF
Deputy Chief of Staff
Research and Development
Field Command, DASA

CONTENTS

Page

1. INTRODUCTION 1

2. BASIC DATA AND FORMULAS PERTAINING TO THE BEHAVIOR OF BURNING COMPOSITION B AND PBX 9404. 3

a. Heat Released by Burning Composition B and PBX 9404 3

b. Enthalpy of Composition B and HMX 6

c. Conductive Heating of Burning Composition B 6

d. Total Equilibrium Enthalpy of Gas Released by Burning Composition B, RDX, and HMX 11

e. Specific Heat and Thermal Conductivity of Steel Chamber. 18

f. Radiation from Gas Evolved by Burning Explosives . . 18

(1) Derivation of Fundamental Radiation Equation . . 21

(2) Radiation Passing Through the Circumferential Boundary of a Cylindrical Volume of Gas 24

(3) Radiation Passing Through the Faces of a Cylindrical Gas Volume 28

3. BURNING OF COMPOSITION B AND PBX 9404 UNDER PRESSURES OF 1 TO 3 ATMOSPHERES 35

a. Experimental Studies of Burning Explosives Under Low Pressures 35

b. Confined and Unconfined Burning of Composition B . . 35

c. Unconfined Burning of PBX 9404 50

d. Theoretical Analysis of the Effects of Burning High-Explosives Under Low Pressure 55

(1) Analysis of the Effects of Burning Composition B Under Low Pressures 58

(2) Preliminary Analysis of the Effects of Burning PBX 9404 Under Low Pressures. 73

CONTENTS (Continued)

Page

4. BURNING OF COMPOSITION B AND PBX 9404 UNDER HIGH PRESSURES 75

a. Experimental Results from High Pressure Burning of Composition B 75

b. Experimental Results from High Pressure Burning of PBX 9404. 89

c. Theoretical Analysis of the Effects of Transient Burning of High-Explosives (High Pressure) 94

5. SUMMARY AND CONCLUSIONS. 103

REFERENCES 105

APPENDIX 107

DISTRIBUTION. 111

LIST OF ILLUSTRATIONS

Figure		Page
1	"Open" Chamber for Heat and Temperature Measurements	4
2	Heat Released by Burning Composition B	7
3	Enthalpy of Composition B and HMX	8
4	Conductive Heating of Composition B	12
5	Total Enthalpy of Composition B Gas	16
6	Total Enthalpy of HMX or RDX Gas	17
7	Schematic of a Gas and a Surface Element	22
8	$F(\beta'_g P_g R)$ versus $\beta'_g P_g R$	25
9	Radiation Received by Circumferential Boundary of Gas Volume	26
10	$P_1(z, a = \frac{1}{6} ft, \beta'_g P_g)$	29
11	Radiation Received by End Face of Gas Volume	30
12	$S_1(z, a = \frac{1}{6} ft, \beta'_g P_g)$	33
13	Cross Section of "Vented" Test Chamber	36
14	Electric Heater and Heat Flow Meter	39
15	Gas Temperature (Burning Rate Composition B, 2.5 ft/hr)	40
16	Gas Temperature (Burning Rate Composition B, 3.5 ft/hr)	41
17	Gas Temperatures (Burning Rate Composition B, 5 ft/hr	42
18	Gas Temperatures (Burning Rate Composition B, 7.5 ft/hr)	43
19	Gas Temperatures (Burning Rate Composition B, 10 ft/hr)	44
20	Meter Temperatures (Burning Rate Composition B, 3.5 ft/hr)	45

LIST OF ILLUSTRATIONS (Continued)

Figure		Page
21	Meter Temperatures (Burning Rate Composition B, 5 ft/hr)	46
22	Meter Temperatures (Burning Rate Composition B, 7.5 ft/hr)	47
23	Meter Temperature (Burning Rate Composition B, 10 ft/hr)	48
24	Effect of Vent Hole on Burning of Composition B	49
25	Chamber Temperatures (Burning Rate of Composition B, 2.5 ft/hr	51
26	Gas Temperatures (Burnring Rate PBX 9404 5.0 ft/hr.	52
27	Chamber Temperatures (Burning Rate PBX 9404 5.0 ft/hr	53
28	Chamber Temperatures (Burning Rate PBX 9404 5.0 ft/hr	54
29	Gas Temperature (Composition B)	61
30	Inlet and Exit Mass Flow to Chamber (Distance-Composition B and Vent - 2 ft)	70
31	Inlet and Exit Mass Flow to Chamber (Distance-Composition B and Vent - 0.5 ft)	71
32	Inlet and Exit Mass Flow to Chamber (Distance-Composition B and Vent - 0.1 ft)	72
33	Cross Section of "Closed" Test Chamber	76
34	Side View of "Closed" Chamber for High-Pressure Burning	77
35	Bottom View of "Closed" Chamber for High-Pressure Burning	78
36	Type-A Ion Probe and Associated Circuit	80
37	Type-B Ion Probe and Associated Circuit	81
38	Method of Inserting Thermocouples and Pressure Probe Through Chamber Wall	82

LIST OF ILLUSTRATIONS (Continued)

Figure		Page
39	Pressure Time History (Composition B, ℓ = 1.75 inches)	89
40	Pressure Time History (Composition B, ℓ = 8 inches)	84
41	Pressure Time History (Composition B, ℓ = 17.75 inches)	85
42	Composition B Pieces Found in Chamber Following Ejection of Top Cover Plate	86
43	Plastic Failure of Chamber (Composition B)	90
44	Brittle Fracture of Chamber (Composition B)	91
45	Effect of Explosion on Inner Surfaces of Chamber (Composition B)	92
46	Remains of Chamber from Detonation of PBX 9404	93

LIST OF TABLES

Table		Page
I	Strand Burning Rate of Composition B	10
II	Constituents of Gas from Burning Composition B (P_g = 1 Atmos.)	14
III	Constituents of Gas from Burning RDX and HMX (P_g = 1 Atmos.)	15
IV	Properties of Gas Evolved by Burning Composition B	19
V	Properties of Gas Evolved by Burning RDX or HMX .	19
VI	Specific Heat and Thermal Conductivity of Plain Carbon Steel	20
VII	Summary of Analytical Results	60
VIII	Gas Temperatures (Composition B)	62
IX	Meter Temperatures (Composition B)	64
X	Temperature Rises of Chamber at 10 Minutes After Start of Burning Composition B	67
XI	Temperature Rises of Chamber at 20 Minutes After Start of Burning Composition B	68
XII	Temperatures and Pressures from Burning Composition B in Chamber with ℓ = 1.75 inches	98
XIII	Temperatures and Pressures from Burning Composition B in Chamber with ℓ = 8.0 inches	99
XIV	Temperatures and Pressures from Burning Composition B in Chamber with ℓ = 17.5 inches	100

1. INTRODUCTION

Numerous accidents have occurred in which nuclear weapon systems have become involved in fire. From 1956 to 1963 a number of weapon systems have been purposely exposed to fire to ascertain the behavior of the high explosive and the electronic circuits. The results of these tests are presented in the DASA Reports 1060, 1066, 1234, and 1276 (see Bibliography). For purposes of safety, information is generally required pertaining to the minimum ignition time of the high explosives, the likelihood of a high-explosive detonation, and the likelihood of a nuclear detonation.

The ignition times of nuclear weapon systems have been predicted to within 20 percent. This was accomplished by building models of critical regions of the weapon system and exposing the models to the desired rate of heating. A detailed discussion of modeling techniques is presented in the DASA Report 1130.

The likelihood of a nuclear detonation from heating of the high-explosive is dependent on the behavior of the various electronic circuits and on the condition of the HE system at the time of delivery of any critical electrical signal. DASA Report 1276 describes the behavior of a number of electronic circuits within actual weapon systems that were exposed to fire. Detailed laboratory studies of the behavior of the various electronic components in high temperature environments have been conducted by organizations such as Sandia Corp., Albuquerque, New Mexico. From such work, it is possible to conservatively estimate the probability of a nuclear detonation of a given weapon system in a fire environment.

Work has also been conducted to develop means of predicting whether a given weapon system would or would not explode in a given fire environment. This work was initiated by a feasibility study in 1956 by I I T Research Institute to explore the possibility of developing means of predicting HE explosions and means of preventing such explosions. This study indicated that such an endeavor appeared promising and led to the studies covered in this report.

The results of the initial study are presented in the DASA Report 1234. In this study, cylinders of Composition B were burned at the bottom of tubular chambers. Vents were provided at the top of the chamber to vary the rate of pressure build-up. This work revealed that the behavior of burning explosives under pressures of 1 to 2 atmospheres is reasonably reproducible and therefore amenable to prediction. Measurements of thermal irradiation at various locations within the gas stream indicated that thermal radiation is the principal source of heat flow to the thin layer, i.e., approximately 0.05 inches, of explosive undergoing reaction. Thermal radiation is of less significance at higher pressures of the order

of tens of atmospheres due to the rapid increase in the heat conduction from the hot gas with pressure. It was found that vent holes having a cross-sectional area of about 1 percent or more of the area of the burning explosive were sufficient to maintain near-atmospheric pressures in the chamber.

This report covers the experimental and theoretical studies of the behavior of burning Composition B and PBX 9404 under pressures as high as several hundred atmospheres. Section 2 presents the significant properties of the explosive and test chamber required for the theoretical studies and develops a theory describing the flow of thermal radiation from the hot gas stream. Section 3 discusses the experimental burning of the high explosives under pressures of 1 to 3 atmospheres. In addition, several analyses were conducted to predict the burning velocity, the gas temperatures, the thermal irradiation from the gas stream, the temperatures of the test chamber and the gas flow through the vent holes. A comparison of the results of the experimental and analytical studies ranges from good to excellent.

Section 4 discusses the burning of Composition B and PBX 9404 under pressures as high as several hundred atmospheres. This was achieved by burning the explosive material in closed chambers which were held together by rods of varying strength. The void volume within the chamber was varied to explore its effect on the pressure history of the gas. The results of the analytical studies covered in Section 3 were used to predict the pressure history of the gas evolved by burning Composition B and was found to be in good agreement with the experimental data for pressures as high as about 1000 psia. At pressures in excess of this level, the rate of pressure rise increases very abruptly. The cause of this abrupt pressure rise is attributed to the increase of burning area caused by cracking of the Composition B. Insufficient data were found to conduct a similar analysis of the burning of PBX 9404.

2. BASIC DATA AND FORMULAS PERTAINING TO THE BEHAVIOR OF BURNING COMPOSITION B AND PBX 9404

This section covers the basic data and formulas required for subsequent theoretical studies which describe the behavior and effects of the burning explosives under various environments. The theoretical studies will be presented later in the report.

a. Heat Released by Burning Composition B and PBX 9404

The heat released by the burning of a given mass of explosive plays a sensitive role in affecting the heating and rate of burning of high-explosive materials. A preliminary study of the heat released by burning Composition B under pressures of 1 to 2 atmospheres is presented in the DASA Report 1234. Additional data were acquired under the present program from a literature study and by experimentation. In these experiments, a given mass of Composition B or PBX 9404 was burned to completion in the tubular chamber shown in Figure 1. The chamber was insulated with a light-weight insulation (rockwool), to deter the escape of heat from the chamber. The top of the chamber was partially closed by a disk that was formed from high-temperature insulating brick to minimize radiant heat loss. A large hole was provided through the center of the disk to allow the gases to escape at a sufficiently fast rate so that a near-atmospheric pressure was maintained within the chamber. The explosives were ignited by preheating the exposed surface with a 122-watt electrical heater for 15 minutes and passing a current of 10 amperes through a 0.56 ohm wire embedded across the face of the explosive. The burning velocities of the Composition B and the PBX 9404 were 2.5 and 5.0 ft/hr respectively, and were found to be consistent and uniform throughout the tests. Most of the heat released by the burning was either absorbed by the steel chamber or escaped with the gas. Small corrections in the data were made for the heat absorbed by the insulating materials, for the heat generated by the electric heater and igniter, and for the energy associated with the velocity of the escaping gas.

The heat absorbed by the chamber from the burning of each pound of high-explosive was determined by measuring the temperatures and specific heat of the chamber and substituting these data into the following formula:

$$Q(\text{chamber}) = \frac{1}{M} \int_{0}^{v} C_{stl} \, (T - T_o) \rho_{stl} \, dv \qquad (1)$$

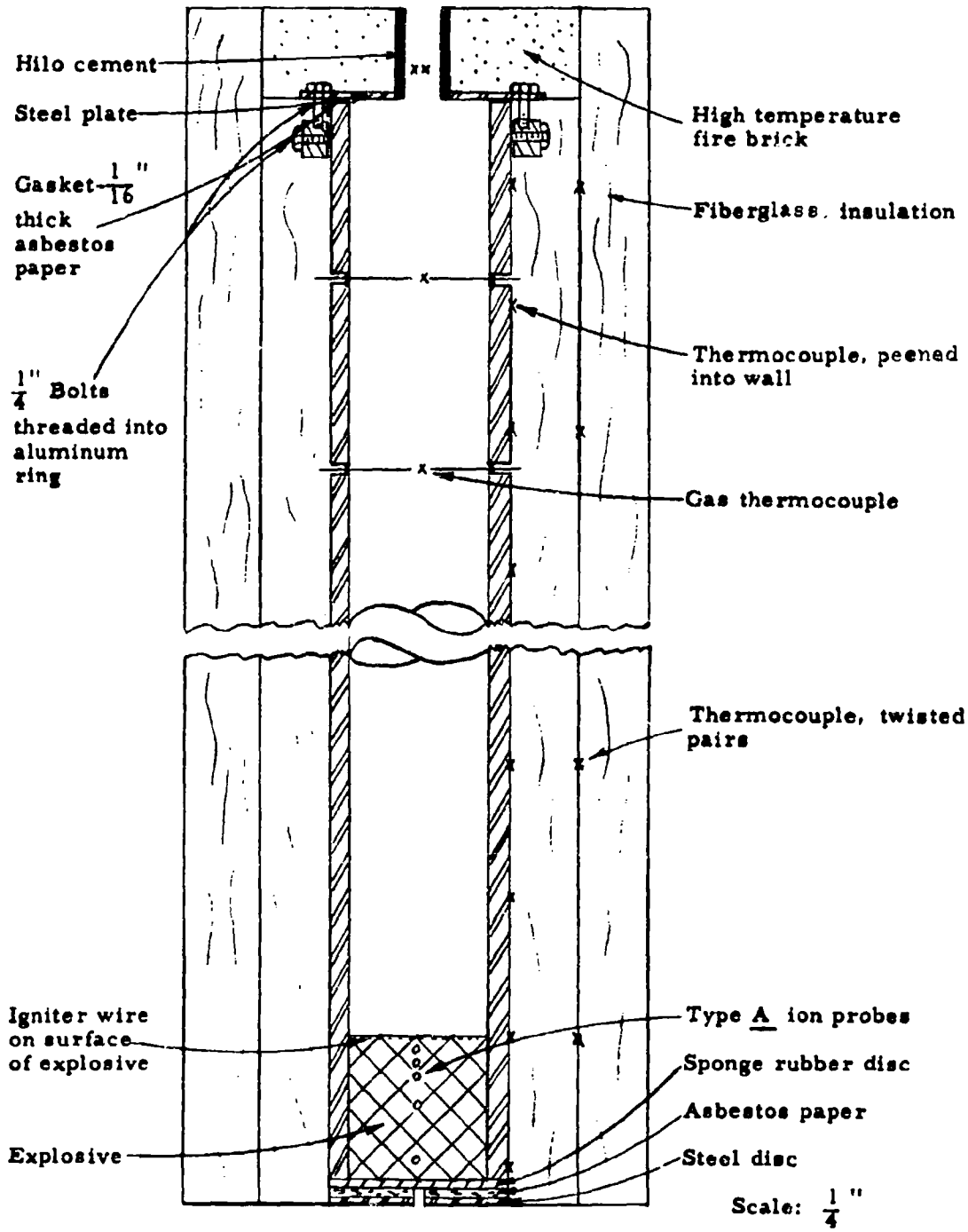

Fig. 1 "OPEN" CHAMBER FOR HEAT AND TEMPERATURE MEASUREMENTS

where

Q (chamber)	=	heat absorbed by steel chamber from the burning of a pound of explosive, B/lb.
M	=	total mass of explosive, lb
C_{stl}	=	specific heat of steel = 0.12 B/lb °R
T	=	temperature of an increment of the chamber, °R
T_o	=	initial temperature of the chamber, °R
ρ_{stl}	=	density of steel = 491 lb/ft^3
dv	=	volume of an increment of the chamber, ft^3
v	=	total volume of chamber, ft^3

A similar calculation was made to determine the heat absorbed by the insulating materials Q (insulation) using their temperature rises, specific heat, densities, and volumes. The heat which escaped with each pound of gas was evaluated by determining the total equilibrium enthalpy of the escaping gas (see Section 2d) above the enthalpy of the unheated explosive. This quantity of heat was determined by substituting the enthalpy into the following equation:

$$Q\ (\text{gas}) = \frac{1}{M} \int_0^M H(T)dM \qquad (2)$$

where

Q(gas)	=	heat per pound of escaping gas, B/lb
H(T)	=	enthalpy of gas above its value at ambient temperature, B/lb
dM	=	increment of gas mass, lb

The quantity of heat released by the burning of 1 pound of the high-explosive, Q_E is expressible as

$$Q_E = Q(\text{chamber}) + Q(\text{gas}) + Q(\text{insulation}) + Q(\text{misc}) \qquad (3)$$

Where Q(misc) refers to the small quantities of heat associated with the heater, ignitor, and kinetic energy of the escaping gas.

In addition, a literature study was conducted which revealed that the quantities of heat released by the slow decomposition of TNT, Cyclotol, 75/25 and RDX were 900, 675, and 900 B/lb, respectively[1], while the quantities of heat released by the explosion of TNT, Cyclotol, 75/25, Composition B, RDX and HMX were 1944, 2205, 2232, 2304, and 2441 B/lb, respectively (see Table A 1). The quantities of heat released by the explosions are considerably higher than those from the slow decomposition. Since the velocities of these two types of reactions bracket the burning velocities from the ARF experiments, it may be expected that the values of the heat released by burning a pound of a given explosive would lie between the values associated with the two reactions. To determine whether or not this is true, the heat released by a pound of Composition B was determined as a

function of the velocity of burning. The results are shown in Figure 2. The rate of heat release from Composition B at "zero burning velocity" was considered equal to that from Cyclotol 75/25 during slow decomposition. It may be noted that the values are reasonably consistent and that the heat released by the burning Composition B reaches a maximum at the relatively low velocity of about 40 ft/hr.

The heat released by burning PBX 9404 under atmospheric pressure was also measured and resulted in the following measurements: 2223, 2261, 2453, 2492 and 2736 B/lb. The average of these values is 2433 B/lb. Unfortunately no values could be found in the literature for the heat of explosion of PBX 9404. Since the major constituent of PBX 9404 is HMX, it appears reasonable that the heat of explosion of PBX 9404 would be close to that of HMX, i.e., 2441 B/lb. It may be observed that the difference between this value and the average value for slow burning is small and is much less than the experimental variations. From this it appears that the heat released by burning PBX 9404 is essentially independent of burning velocity.

b. Enthalpy of Composition B and HMX

The enthalpy of a high-explosive plays a very significant role in affecting its rate of burning. This is due to the fact that the virgin material must first be heated to temperatures of about 500 to 600°F before the material will react with any significant vigor. Unfortunately, no enthalpy data could be found above about 300°F. Values of the enthalpy of Composition B and HMX may be obtained from the specific heat values given in Table A-1. Curves of enthalpy versus temperature constructed from the data from Composition B and HMX are shown in Figure 3. These curves were extrapolated to the higher temperatures by assuming that the heats of fusion of HMX and RDX are equivalent to that of TNT. Due to the uncertainties of this extrapolation, the extrapolated portions of the curves are shown as dashes. No account was taken for possible vaporization of the high-explosive material. The curve for Composition B was taken from the DASA Report 1234.

c. Conductive Heating of Burning Composition B

During burning, an explosive is heated by radiation (to be discussed later) and by conduction from the hot gases. At pressures in excess of a few hundred atmospheres, conduction is the dominant source of heat flow to the reacting explosive. A literature search was conducted to find any data which either would indicate the conductive heat flux or could be used to determine the flux. Fortunately, a substantial amount of strand burn data was found in a Picatinny Arsenal report for Composition B.[3] These data indicate the burning velocity as a function of pressure and were obtained by burning a long thin rod of the explosive in an environment which was maintained

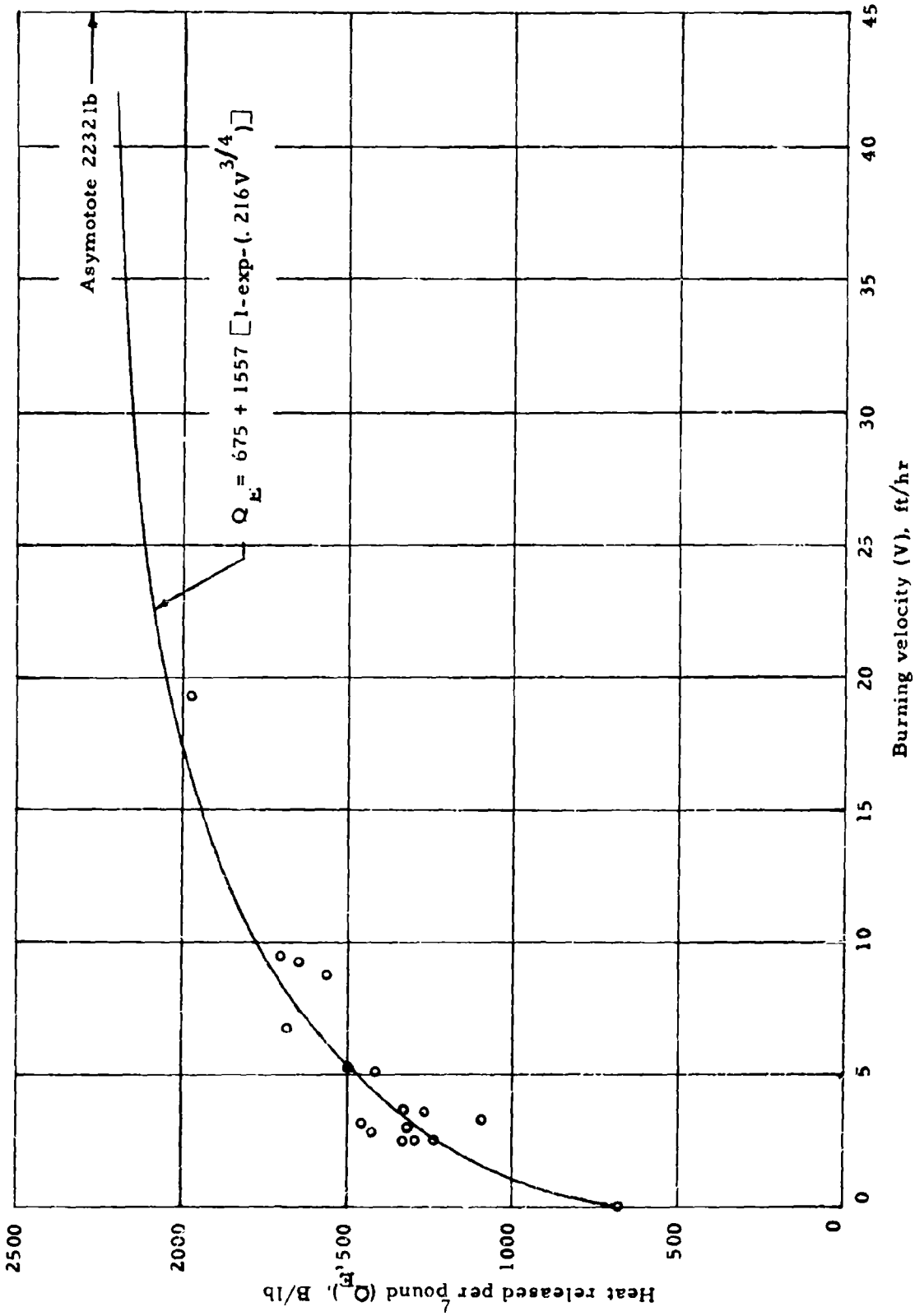

Fig. 2 HEAT RELEASED BY BURNING COMPOSITION B

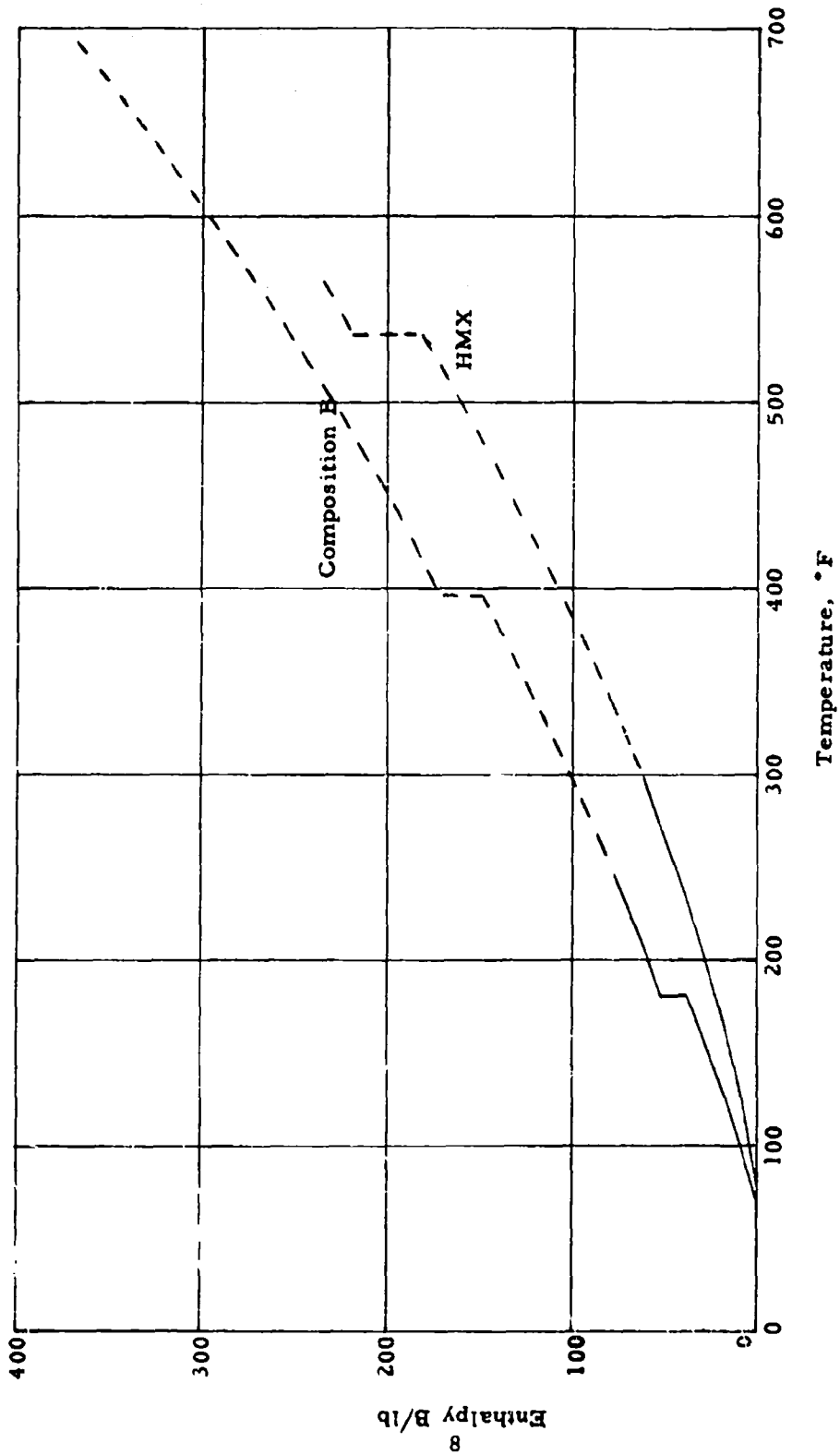

Fig. 3 ENTHALPY OF COMPOSITION B AND HMX

at constant pressure. This was accomplished by use of a chamber whose volume is large compared to that of the gas evolved by explosion. The velocities of burning of Composition B are presented in Table I for pressures ranging from 136 to 2041 atmospheres. Since thermal radiation is not a significant source of heat flux at these pressures, it is possible to utilize the Arrenhius relationship and the data generated in the DASA Report 1234 to determine the conductive heat flux to the reacting explosive at the several pressures. In IITRI's previous study, it was found that the thickness of the layer of Composition B undergoing reaction was about 0.05 inch or 0.0042 foot. This layer consisted of foam whose density was found to range between 1/3 to 1/6 of that of the solid explosive. This was determined by slowly heating a bath of liquid Composition B until it burst into flame. In the present study the density of the foam layer will be considered as 1/6 of that of the virgin Composition B. This yields a foam density of 105/6 or 17.5 lb/ft^3. The Arrenhius relationship, which was discussed in the DASA Report 1234, is as follows

$$W = \rho_f x_f Z \exp. -(E/R_{go} T_f) \tag{4}$$

where

W	=	rate of mass flow per unit area, lb/ft^2 hr
ρ_f	=	density of foam = 17.5 lb/ft^3
x_f	=	thickness of foam = 0.0042 ft
Z	=	frequency factor = 1.14×10^{22}/hr
E	=	activation energy = 47,500 Cal/mole
R_{go}	=	univeral gas constant = 1.104 Cal/mole °R
T_f	=	temperature of foam, °R

The values of Z and E are assumed to be independent of temperature and equal to those of Cyclotol 75/25 shown in Table A 1. While the values undoubtedly vary with temperature, the inconsistencies of the values in the literature tend to overshadow this dependence.

Substituting the appropriate quantities into Eq. 4 yields

$$\begin{aligned} W &= (17.5)(0.0042)(1.14 \times 10^{22}) \exp. -(47,500/1.104T_f) \quad (5) \\ &= 8.38 \times 10^{20} \exp. -(43,025/T_f) \end{aligned}$$

The rate of mass flow may also be determined from the rate of burning v by

$$W = \rho_E V \tag{6}$$

where

ρ_E	=	density of virgin Composition B = 105 lb/ft^3
V	=	velocity of burning, ft/hr

Eliminating W from Eq. 5 and 6 solving for T_f yields

$$T_f = 43,025/\ln(7.981 \times 10^{18}/V) \tag{7}$$

Table I

STRAND BURNING RATE OF COMPOSITION B

Pressure, Atmospheres	Burning Rate, ft/hr
136	153
204	246
340	480
680	1071
1361	2001
2041	3126

This indicates the temperature of the foam as a function of the velocity of burning. The enthalpy, H, of the foam for each of the several velocities may be found from the data shown in Figure 3. Following this the rate of conductive heating, q_c, required to maintain each of the several velocities of burning may be expressed by (H = enthalpy above that at 70°F)

$$q_c = \rho_E H(T_f)V \tag{8}$$

This represents the rate of conductive heating as a function of the velocity. The relationship between the conductive heating and pressure may be obtained by the velocity-pressure data shown in Table I. A plot of the ratio of the conductive heating and the pressure is shown in Figure 4 as a function of pressure. A ratio was used to maintain a reasonable scale which allows a better appreciation of the effects of pressure. It may be noted that the conductive heating increases at a greater than linear rate with pressure at least up to 2000 atmospheres of pressure. It may also be observed that at near-atmospheric pressure the value of the conductive heating is about 25,000 B/ft^2 hr. This value may be compared with the value of 41,000 B/ft^2 hr which was determined in the previous study (see DASA Report 1234) by the subtraction of the substantial radiant flux (experimental) from the total heat flux (theoretical). Based on the accuracies of the techniques used, the agreement between the two values is gratifyingly good.

d. Total Equilibrium Enthalpy of Gas Released by Burning Composition B, RDX and HMX

The temperatures of the gas from burning explosives are sufficient to cause appreciable dissociation and ionization. As a result of this the specific heat increases significantly with temperature and is not accurately treated as a constant value over the temperatures of concern. The total enthalpy of the gas evolved during the burning of Composition B, RDX and HMX was computed as a function of temperature from 900°R to 6300°R assuming equilibrium conditions. This was accomplished by determining the composition of the gas and summing the heats of formations and enthalpies of the various species at each of several temperatures. The composition of the gas was determined using the techniques illustrated by Huff[4] and Eberhardt.[5] The chemical formulas of the high-explosives are as follows:

COMPOSITION B	.605	moles	$C_3H_6N_6O_6$ (RDX)
	.395	moles	$C_7H_5N_3O_6$ (TNT)
HMX	1	mole	$C_4H_8N_8O_8$
RDX	1	mole	$C_3H_6N_6O_6$

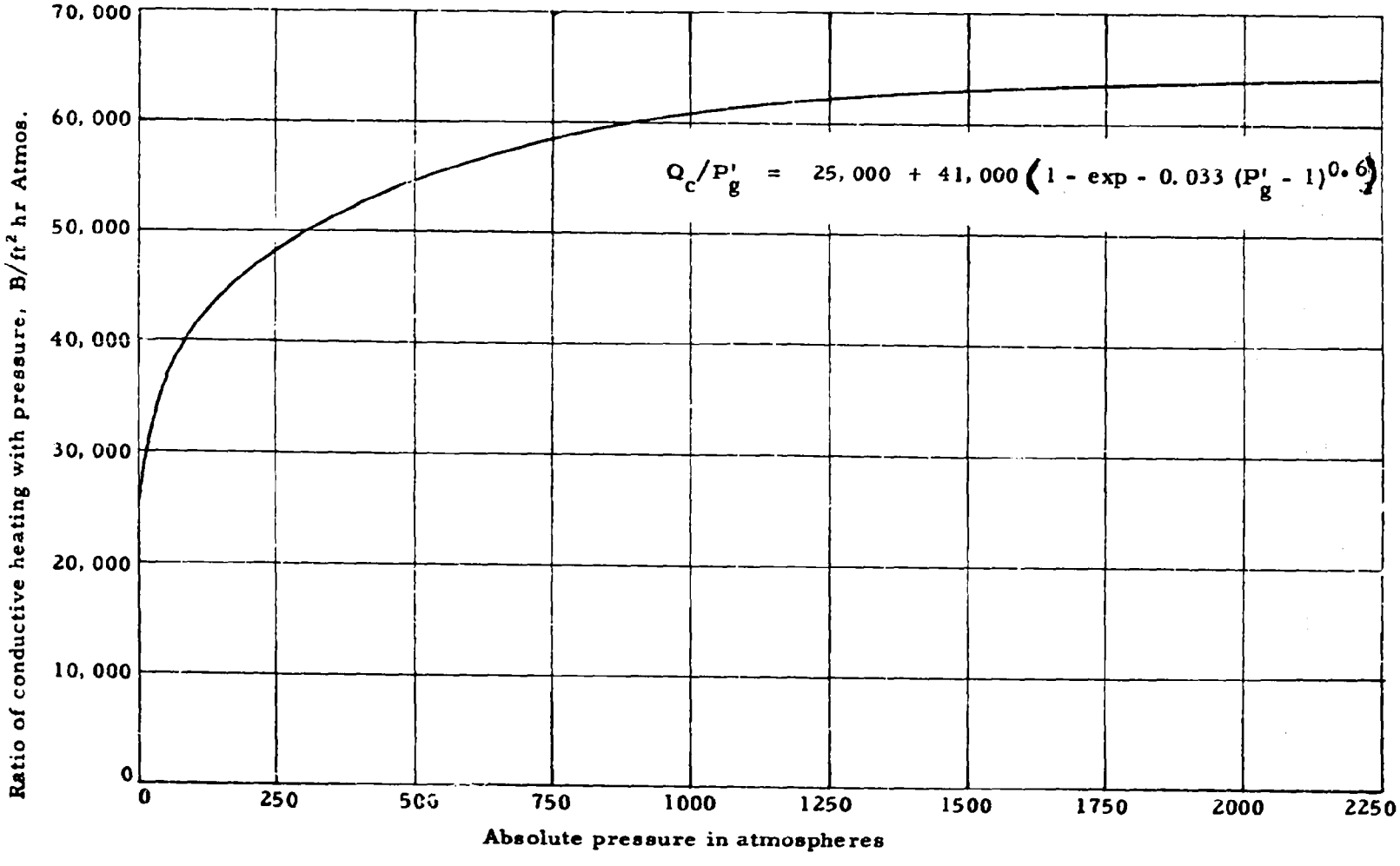

Fig. 4 CONDUCTIVE HEATING OF COMPOSITION B

It may be observed that the number of atoms in the HMX and RDX molecules differs only by a factor. As a result the composition and enthalpies of the gases associated with HMX and RDX will be identical under conditions of equilibrium and for equal temperatures and equal pressures. The percentages of the gas constituents associated with Composition B and HMX or RDX are summarized in Table II and Table III for a pressure of 1 atmosphere. The sums shown at the bottom of each column are not all 100 percent due to errors in rounding off the numbers. Calculations were also performed at 10 and 100 atmospheres. These calculations predicted small shifts in the composition of the gas. However, the effect of these shifts on the total enthalpy is quite small and will be neglected in the present study.

The total equilibrium enthalpy, H(T), was computed using the equation

$$H(T) = \frac{1.8}{M} \sum S_i \left[H_i + (\Delta H_f)_i \right] \tag{9}$$

where the factor of 1.8 is introduced to give values of H(T) in B/lb rather than Cal/gm and where

M	=	effective molecular weight of gas
S_i	=	moles of the ith constituent per mole of gas
H_i	=	enthalpy (sensible heat) per mole of the ith constituent
$(\Delta H_f)_i$	=	heat of formation of the ith constituent

The resulting values of the total equilibrium enthalpies of the Composition B and HMX and RDX gas were referenced to a temperature of 530°R (70°F) and are shown in Figures 5 and 6 respectively. In both cases it may be observed that the total enthalpy is definitely not linear with temperature. Therefore the specific heat, which is equal to the slope of the curve, changes vary appreciably with temperature. This is particularly true at the high temperatures. (The specific heats used here refer to the slopes of the total equilibrium enthalpy curves rather than the normal enthalpy curves in which the gas constituents remain invariant.)

From the data in Tables II and III, it is a simple exercise to determine the gas constant and the ratio of the "specific heat" as constant pressure to the "specific heat" at constant volume for each of the specified temperatures. To accomplish this, the apparent molecular weight of the gas was found by taking a weighted average of the molecular weights of the several constituents. The individual gas constants may be evaluated by dividing the universal gas constant, $1544 \frac{\text{ft-lb}}{\text{lb mole °R}}$, by the apparent molecular weights. The ratios of the "specific heats," k, may be found from the following well known equation

$$k = JC_p/(JC_p - R_g) \tag{10}$$

Table II

CONTITUENTS OF GAS FROM BURNING COMPOSITION B (P_g = 1 ATMOS.)

Gas Constituent	Mole Per Cent of Gas Constituents at Specified Temperatures						
	500°K (900°R)	1000°K (1800°R)	1500°K (2700°R)	2000°K (3600°R)	2500°K (4500°R)	3000°K (5400°R)	3500°K (6300°R)
CO	41.7	42.1	42.7	43.5	43.4	42.1	39.0
N_2	28.9	28.9	28.9	28.9	28.7	27.8	25.4
H_2	27.0	26.1	25.5	25.2	24.4	20.8	12.6
H_2O	0	0.9	1.4	1.7	1.8	1.5	0.7
CO_2	2.4	2.1	1.5	0.6	0.5	0.4	0.2
OH	0	0	0	0	0	0.2	0.5
H	0	0	0	0.1	1.2	7.2	21.0
NO	0	0	0	0	0	0	0.1
N	0	0	0	0	0	0.1	0.6
O_2	0	0	0	0	0	0	0
O	0	0	0	0	0	0	0.5
TOTAL	100.0	100.1	100.0	100.0	100.0	100.1	100.6

Table III

CONSTITUENTS OF GAS FROM BURNING RDX AND HMX (P_g = 1 ATMOS.)

Gas Constituent	Mole Per Cent of Gas Constituents at Specified Temperatures						
	500°K (900°R)	1000°K (1800°R)	1500°K (2700°R)	2000°K (3600°R)	2500°K (4500°R)	3000°K (5400°R)	3500°K (6300°R)
CO	2.8	15.0	20.3	22.8	24.0	24.8	24.2
N_2	33.3	33.3	33.3	33.3	33.2	31.1	25.3
H_2	30.8	17.9	12.5	10.4	9.3	9.1	8.6
H_2O	2.5	15.4	20.8	22.8	23.3	18.3	6.2
CO_2	30.5	18.6	13.0	10.5	9.3	6.6	2.1
OH	0	0	0	0	0.4	3.2	5.8
H	0	0	0	0.1	0.8	4.8	17.3
NO	0	0	0	0	0.1	0.6	1.4
N	0	0	0	0	0	0.1	0.6
O_2	0	0	0	0	0	0.8	1.9
O	0	0	0	0	0	1.1	7.0
TOTAL	99.9	100.2	99.9	99.9	100.4	100.5	100.4

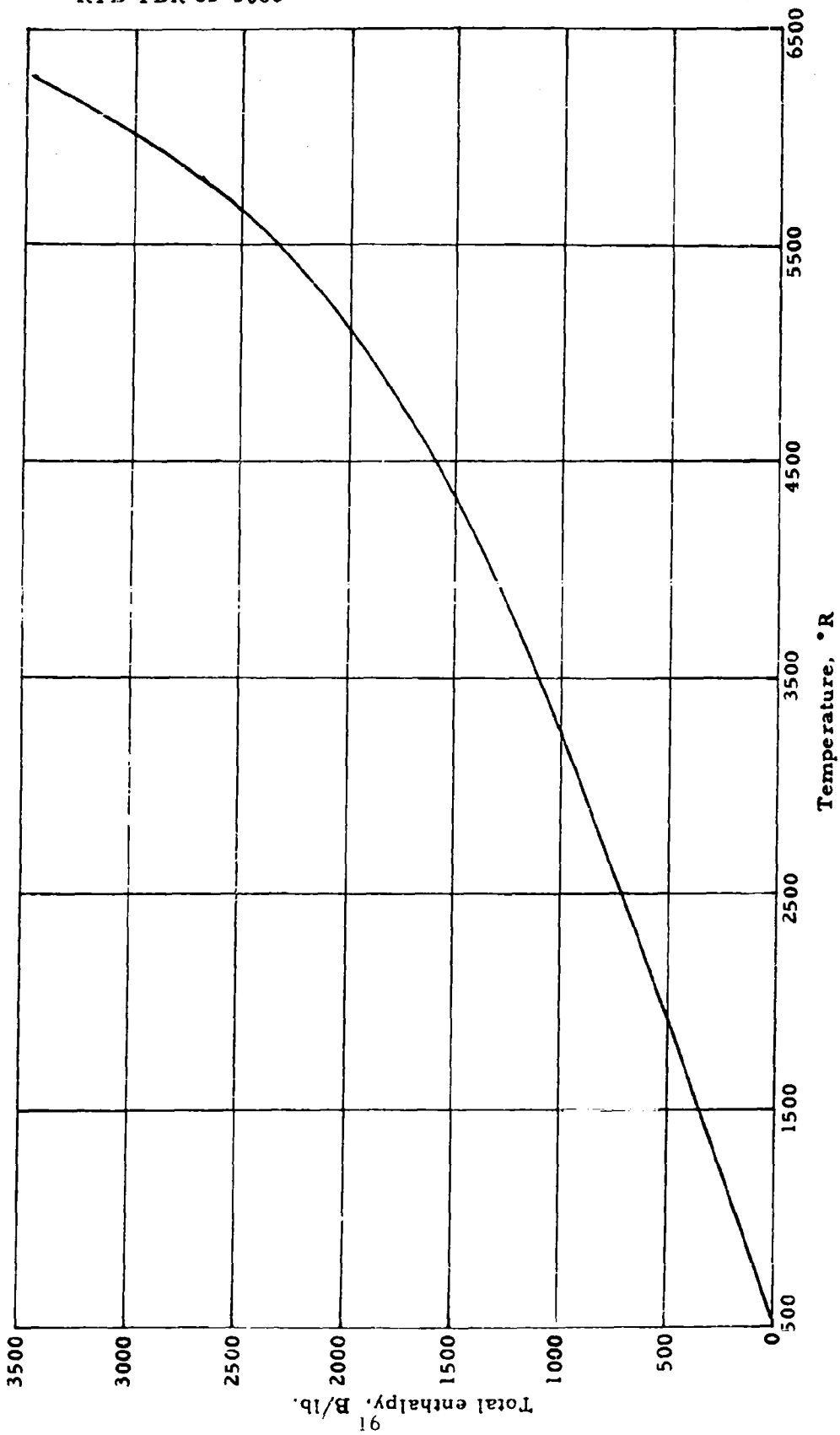

Fig. 5 TOTAL ENTHALPY OF COMPOSITION B GAS

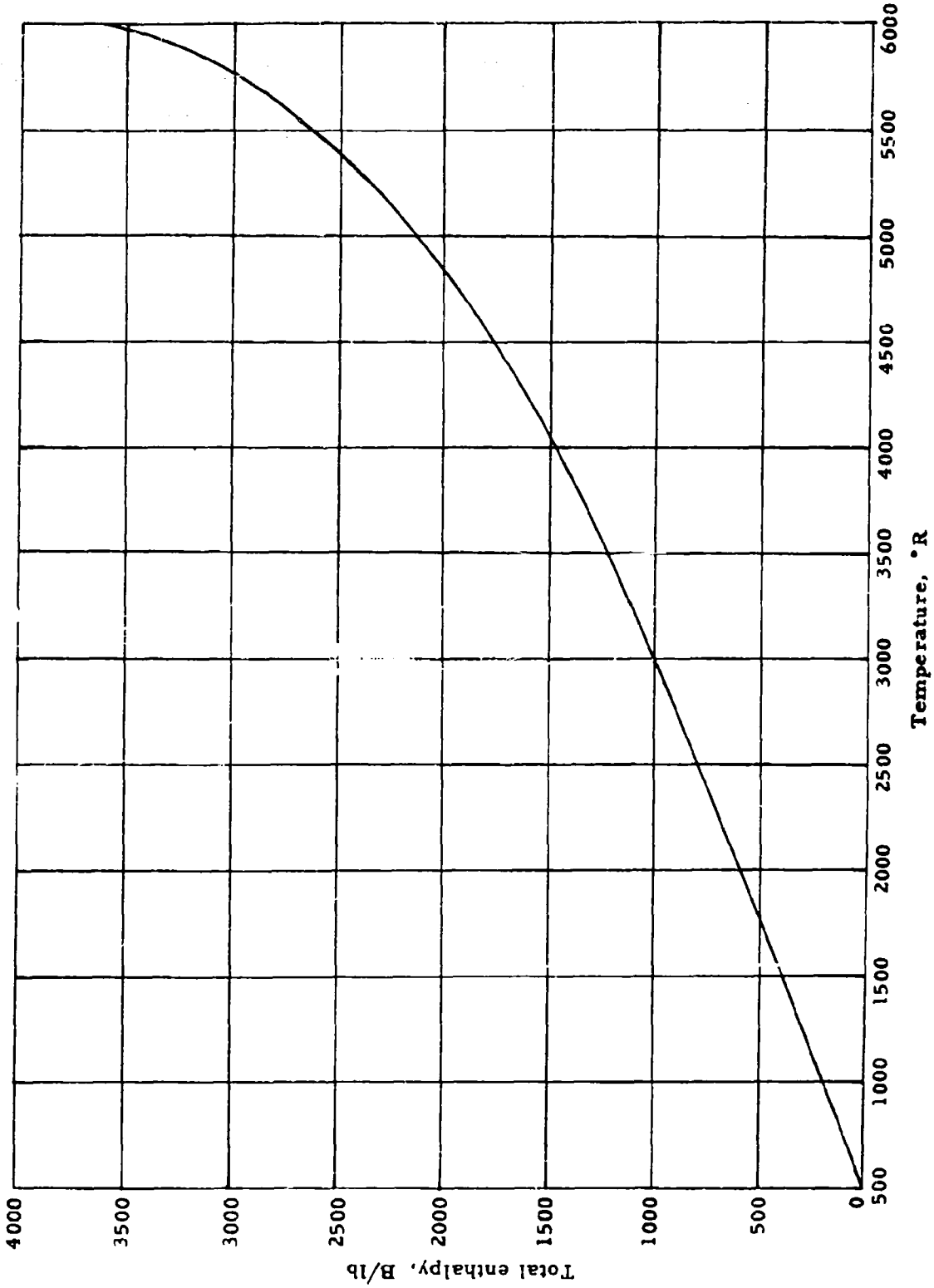

Fig. 6 TOTAL ENTHALPY OF HMX OR RDX GAS

The results are summarized in Tables IV and V, where

J = mechanical equivalent of heat = 778 ft-lb/B
R_g = gas constant, ft-lb/lb °R

e. Specific Heat and Thermal Conductivity of Steel Chamber

As described in Section 2 a, the steel chamber was used as a calorimeter to measure the heat evolved by burning explosive. Later in the report the temperature distribution along the length of the chamber will be computed and compared to the experimental temperatures. This will serve as one of several checks on the radiation theory presented in a subsequent section. Accurate values of the specific heat of the steel as a function of temperature are required in both cases. In addition a knowledge of the thermal conductivity is necessary for the computation of the temperature distribution along the length of the chamber. Values of the specific heat and thermal conductivity of ordinary carbon steel found in the literature[6] are listed in Table VI. Due to the importance of the specific heat for the calorimetric measurements, three enthalpy measurements of the steel were made between 72° and 212°F and also between 72° and 500°F. These measurements were made by dropping a heated sample of the steel into a water bath contained in a Dewar calorimeter. The temperature of the water bath was measured by a Beckman thermometer. These enthalpy measurements resulted in the following average-values of specific heat, C_{stl}

C_{stl} = .111 B/lb°F, 72 to 212°F
C_{stl} = .116 B/lb°F, 72 to 500°F

It may be observed that these average values compare quite favorably with the values shown in Table VI.

f. Thermal Radiation From Gas Evolved by Burning Explosives

A significant portion of the heat flux to a burning explosive at low pressures (of the order of tens of atmospheres) is generally due to thermal radiation.

Thermal radiation is emitted by the individual molecules and by the particles within the gas stream. The gases evolved by TNT-based explosives such as Cyclotols and Composition B contain appreciable quantities of such particles. The emission of radiation from the gas molecules evolved by the burning of such explosives is negligibly small compared to that from the cloud of particles. This will become more evident later in the report.

The first part of this section will be devoted to a derivation of the basic equation that prescribes the radiant emission from the particles contained in a gas at constant temperature and pressure. Following this, the equation will be used to determine the equations

Table IV

PROPERTIES OF GAS EVOLVED BY BURNING COMPOSITION B

Temperature °R	Molecular Weight	Gas Constant ft-lb/lb°R	Ratio of "Specific Heats"
900	21.4	72.1	1.37
1800	21.5	71.8	1.34
2700	21.5	71.8	1.29
3600	21.3	72.5	1.28
4500	21.2	72.8	1.20
5400	20.6	75.0	1.11
6300	19.0	81.3	1.06

Table V

PROPERTIES OF GAS EVOLVED BY BURNING RDX OR HMX

Temperature °R	Molecular Weight	Gas Constant ft-lb/lb°R	Ratio of "Specific Heats"
900	24.6	62.7	1.24
1800	24.8	62.3	1.24
2700	24.7	62.5	1.23
3600	24.6	62.8	1.19
4500	24.6	62.8	1.16
5400	22.6	68.3	1.08
6300	19.6	78.8	1.03

Table VI

SPECIFIC HEAT AND THERMAL CONDUCTIVITY
OF PLAIN CARBON STEEL
(DENSITY = 491 LB/FT^3)

Temperature °F	Specific Heat B/lb°F	Thermal Conductivity B/ft^2 hr°F
70	.100	37.2
100	.104	36.7
200	.110	35.1
300	.116	33.5
400	.120	32.0
500	.124	30.3
600	.134	29.0
700	.140	27.3
800	.159	26.0
900	.164	24.4
1000	.179	23.1
1100	----	21.8
1200	----	20.5
1300	----	19.0

describing the radiation emitted by a cylindrical volume of the gas. Thermal radiation will be divided into two parts... that arriving at the circumferential surface enclosing the cylindrical volume of gas and that arriving at the two faces at either end of the gas volume.

(1) Derivation of Fundamental Radiation Equation

There are four principal parts to the radiation equation. These are:

(a) The emission of radiation from a gas element.
(b) The divergence of the radiation in passing from an element to the target area.
(c) The attenuation of the radiation in passing from an element to the target area.
(d) The orientation of the gas element and target area with respect to each other.

Figure 7 represents a gas element and an increment of surface being irradiated. The radiation emitted by the particles in a gas element must be proportional to the size and density of the particles. If equal masses of the gas contain the same number and sizes of particles, the emitted radiation will be proportional to the gas density ρ_g. In addition the emission of radiation is inversely proportional to the wave length λ raised to a power close to 1.[7] For purposes of simplifying the expressions, the exponent will be taken as 1. Based on these arguments, the emission of heat radiation is approximately equal to the factor $\beta_g \rho_g dR/\lambda$, where β_g is a constant of proportionality and dR is the thickness of the gas element in the direction prescribed by the line between the element and the surface being irradiated. The amount of radiation emitted within a given increment of wave length is proportional to the product of monochromatic areal radiant intensity, $N_{B\lambda}^{g}$ and the increment of wavelength, $d\lambda$. As a result of geometrical considerations, only a fraction of the emitted thermal radiation is incident on the surface being radiated. This fraction is proportional to the product of the component of the vector representing the area of the gas element in view of the irradiated surface, $dA_g \cos\theta$, and the solid angle subtended by the surface being irradiated, $dA \cos\phi/R^2$. A portion of this radiation is intercepted by the cloud of the intervening particles. To determine the amount that is intercepted, consider a collimated beam of intensity I and of wave length λ passing through an element having a thickness of dR. The intensity of this beam will decrease in the following fashion

$$dI = -I\beta_g \rho_g dR/\lambda \tag{11}$$

Since the pressure and temperature of the gas are considered uniform ρ_g as well as β_g and λ are constants. Integration of this expression with $I = I'$ at $R = 0$ gives

$$I/I' = \exp. -(\beta_g \rho_g R/\lambda) \tag{12}$$

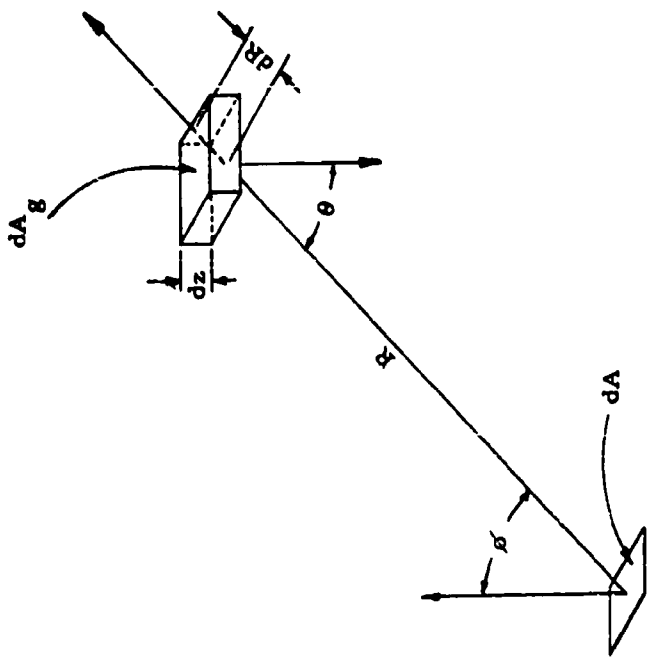

Fig. 7 SCHEMATIC OF A GAS AND A SURFACE ELEMENT

This indicates that the fraction of the radiation which passes through a gas element of thickness R is exp. $-(\beta_g \rho_g R/\lambda)$. As a result the radiation which is emitted from a gas element with wave lengths between λ and $\lambda + d\lambda$ and is incident on the surface may be described as follows

$$dq_r = \beta_g \frac{\rho_g dR}{\lambda} N_{B\lambda}(T_g) d\lambda dA_g \cos\theta \frac{dA \cos\phi}{R^2} \exp -(\beta_g \rho_g R/\lambda) \tag{13}$$

If dV_g represents the volume of the gas element, then $dV_g = dA_g dz$, and since $dz = dR \cos\theta$,

$$dA_g = dV_g / dR \cos\theta \tag{14}$$

Substitution of this into Eq. 13 yields

$$dq_r = \frac{\beta_g \rho_g N_{B\lambda}(T_g)}{\lambda} \frac{\cos\phi}{R^2} \exp -(\beta_g \rho_g R/\lambda) d\lambda dV_g dA \tag{15}$$

where

q_r = radiation incident on target area, B/ft^2 hr
β_g = constant of proportionality
ρ_g = density of gas, lb/ft^3
λ = wave length, cm

$$N_{B\lambda} = \frac{2C_1}{\lambda^5 \left[\exp (C_2/\lambda T_g) - 1\right]}, \quad B/ft^2 \text{ hr cm}^4 \tag{16}$$

T_g = absolute temperature of gas or particles, °R
C_1 = first radiation coefficient = $1.867 \times 10^{-9} \frac{B \text{ cm}^4}{ft^2 \text{ hr}}$
C_2 = second radiation coefficient = 2.58 cm °R
R = slant distance between gas element and target surface, ft
dV_g = volume gas element, ft^3
dA = incremental area of target surface, ft^2

It may be noted that the temperature of the gas and particles are used interchangeably. This is a result of an analysis of the heat transfer to the particles by Schack[7] which indicates that the temperatures of the gas and particles are essentially equal, due to the small dimensions of the particles.

To simplify the expression for dq_r, λT_g will be replaced by λ_o. Also the ideal gas law will be considered valid, i.e.,

$$\rho_g = \frac{P_g}{R_g T_g} \tag{17}$$

P_g = gas pressure, lb/ft^2
R_g = gas constant, ft-lb/lb °R

Integrating the part of Eq. 15 containing λ and substituting the relationships of Eqs. 16 and 17 gives

$$\beta_g \rho_g R \int_0^\infty \frac{N_B \lambda}{\lambda} \exp -(\beta_g \rho_g R/\lambda)\, d\lambda =$$

$$T^4_g \int_0^\infty \frac{2C_1 \exp -(\beta_g P_g R/R_g \lambda_o)}{\lambda_o^6 \left[\exp (C_2/\lambda_o) - 1 \right]} \cdot \frac{\beta_g P_g R d\lambda_o}{R_g} \tag{18}$$

$$= T^4_g F \left(\frac{\beta_g P_g R}{R_g} \right)$$

The function F is presented in Figure 8 with β_g/R_g represented by β'_g. Substitution of the above relationships into Eq. 15 yields

$$dq_r = T^4_g \frac{\cos \phi}{R^3} F(\beta'_g P_g R)\, dV_g dA \tag{19}$$

This is the basic equation describing the radiant flux that is emitted by an element of gas at uniform temperature and pressure and is incident on an area dA. The next section will apply this equation to the specific problems of computing the radiant fluxes from a cylindrical volume of gas.

(2) Radiation Passing Through the Circumferential Boundary of a Cylindrical Volume of Gas

The thermal radiation passing through the boundary at the sides of a cylindrical volume of gas generally represents a significant heat loss from the gas. A knowledge of this loss is of key importance in the analysis of the behavior of burning explosives, which will be covered in a later section. This section will be devoted to a derivation of an equation, that will be used later in the report, to determine the effects of this heat loss.

A diagram of a volume and surface element of a cylindrical volume of gas is shown in Figure 9. In the derivation, the temperature and pressure of the gas will be considered as constant throughout its volume.

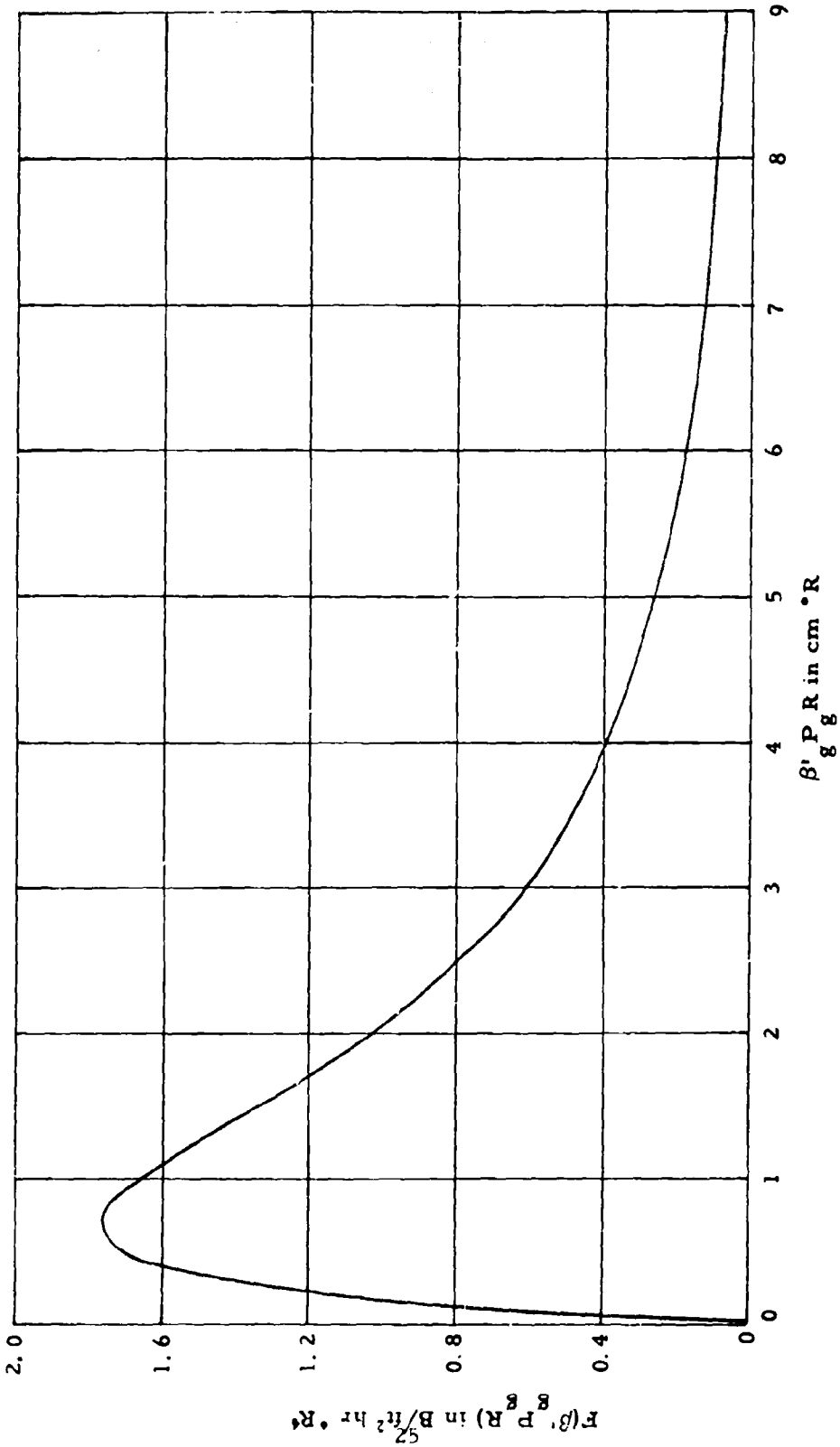

Fig. 8 $F(\beta'_g P_g R)$ versus $\beta'_g P_g R$

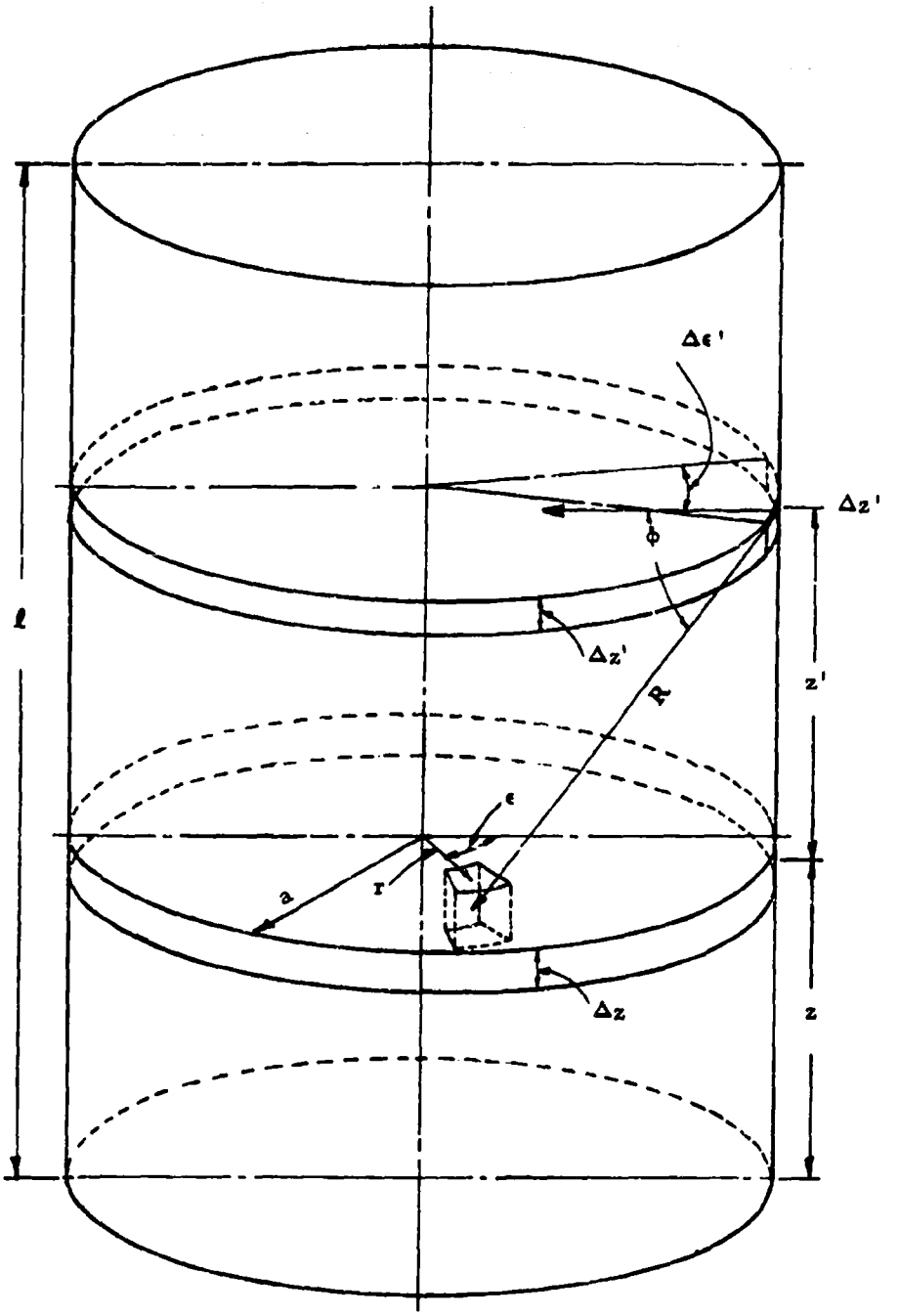

Fig. 9 RADIATION RECEIVED BY CIRCUMFERENTIAL BOUNDARY OF GAS VOLUME

From trigonometric relationships

$$R = (a^2 - 2ar\cos\epsilon + r^2 + z'^2)^{1/2} \tag{20}$$

$$\cos\phi = (a - r\cos\epsilon)/R \tag{21}$$

$$\Delta V_g = r\Delta\epsilon\Delta r\Delta z \tag{22}$$

$$\Delta A = a\Delta\epsilon'\Delta z' \tag{23}$$

Substitution of these relationships into Eq. 19 yields

$$\Delta q'_r = T^4_g \frac{(a - r\cos\epsilon)}{R^4} F(\beta'_g P_g R)\, r\Delta\epsilon\Delta r\Delta z a\Delta\epsilon'\Delta z' \tag{24}$$

The radiation which is emitted by a disc-shaped element of the gas and which passes through the circumferential boundary of the gas volume may be determined by integrating Eq. 24 as follows

$$\Delta q'_r = 4\pi T^4_g \left\{ \int_0^z \int_0^a \int_0^\pi \frac{(a - r\cos\epsilon)}{R^4} F(\beta'_g P_g R)\, ar\, d\epsilon\, dr\, dz' + \int_0^{\ell - z} \int_0^a \int_0^\pi \frac{(a - r\cos\epsilon)}{R^4} F(\beta'_g P_g R)\, ard\epsilon\, dr\, dz' \right\} \Delta z \tag{25}$$

In order to simplify this expression, let the function P_1 represent the following

$$P_1(z, a, \beta'_g P_g) = 4\pi a \int_0^z \int_0^a \int_0^\pi \frac{(a - r\cos\epsilon)}{R^4} F(\beta'_g P_g R)\, rd\epsilon\, dr\, dz' \tag{26}$$

Then Eq. 25 becomes

$$\Delta q_r' = T_g^4 \left\{ P(z, a, \beta_g' P_g) + P(\ell - z, a, \beta_g' P_g) \right\} \Delta z \qquad (27)$$

This represents the rate of heat loss from a gas disc which passes through the circumferential boundary of the gas volume (see Figure 9). Several plots of $P_1(z, a = 1/6 ft, \beta_g' P_g)$ are shown as functions of z in Figure 10 for several values of $\beta_g' P_g$. It may be observed that as $\beta_g' P_g$ increases, P_1 approaches its maximum value at decreasing values of z. In the limit, where the gas becomes completely opaque, the rate of heat loss would tend to approach the radiation emitted from the edge of the gas disc. The area of this edge is $2\pi a \Delta z$. From the Stefan-Boltzmann Equation

$$\lim \Delta q_r' \longrightarrow 2\pi a \Delta z \sigma T_g^4 \quad \text{as} \quad \beta_g' P_g \longrightarrow \infty \qquad (28)$$

where σ = Stefan-Boltzmann Constant = $.173 \times 10^{-8}$ B ft^2 hr°R^4.

Comparison of this expression with the right side of Eq. 27 shows that P_1 approaches $\pi a \sigma$ or (3.1416) (0.1667) (0.173×10^{-8}) = 0.906 $\times 10^{-9}$. It may be observed that this value is approached quite closely for $\beta_g' P_g$ = 30. This completes the derivation of the equation prescribing the radiant heat loss from a disc shaped element of gas through the circumferential boundary enclosing a gas volume of uniform temperature.

(3) Radiation Passing Through the Faces of a Cylindrical Gas Volume

The thermal radiation passing through the boundaries at either end of a gas volume represents an important source of heat loss by the gas. It also represents a significant source of heating of the reacting explosive since the explosive was situated at one end of the gas volume in experiments to be discussed later in this report. This section will be devoted to a derivation of an equation that will prescribe this radiant flow for various gas pressures and temperatures.

A diagram of a volume element and a surface element of a cylindrical volume of gas is shown in Figure 11. It should be observed that each gas element is encompassed by circles drawn from a point lying directly above the surface element. As was true on the previous analysis, the pressure and temperature will be considered as constant throughout the gas. From trigonometric relationships

$$\cos\phi = z/R \qquad (29)$$

$$R = (r^2 + z^2)^{1/2} \qquad (30)$$

$$\Delta V_g = \xi (r', r)\, r \Delta r \Delta z \qquad (31)$$

$$\Delta A = r' \Delta\epsilon' \Delta r' \qquad (32)$$

$$\xi = 2 \arccos (r^2 + r^2 - a^2)/2rr' \qquad (33)$$

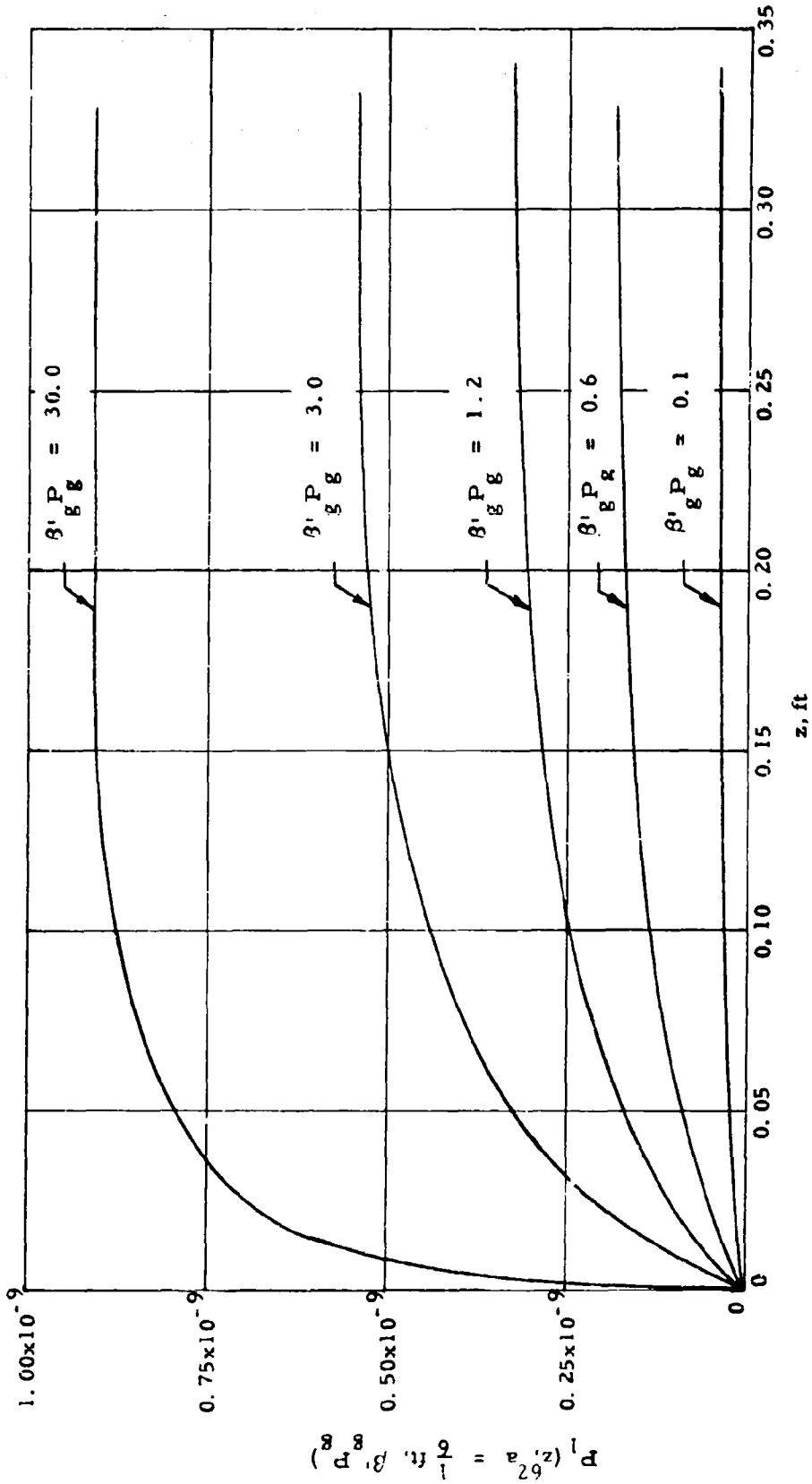

Fig. 10 $P_1(z, a = \frac{1}{6}$ ft, $\beta' P_g g)$

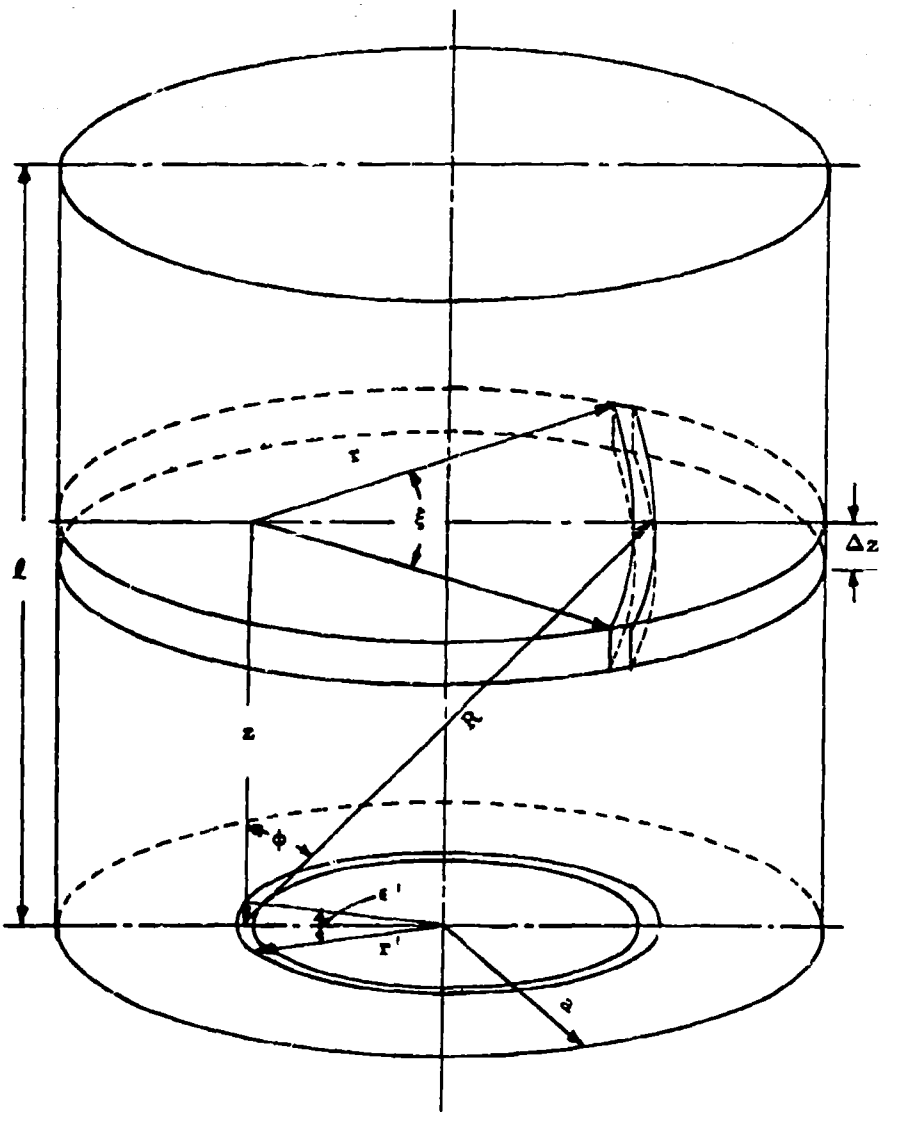

Fig. 11 RADIATION RECEIVED BY END FACE OF GAS VOLUME

Substitution of these relationships into Eq. 19 gives

$$\Delta q''_r = T^4_g \frac{z}{R^4} F(\beta'_g P_g R)\, \xi\,(r', r) r \Delta r \Delta z\, r' \Delta \epsilon' \Delta r' \tag{34}$$

From Figure 11, it may be noted that

$\xi = 2\pi$ for $r \leq a - r'$

$o < \xi < 2\pi$ for $a - r' < r < a + r'$

$\xi = o$ for $r \geq a + r'$

$$\Delta q''_r = T^4_g \int_o^a \left\{ \int_o^{a-r'} \frac{z}{R^4} F(\beta'_g P_g R)\; 2\pi\, r\, dr \right. \tag{35}$$

$$\left. + \int_{a-r'}^{a+r'} \frac{z}{R^4} F(\beta'_g P_g R)\, \xi\,(r', r)\, r\, dr \right\} 2\pi r' dr' \Delta z$$

This equation will be simplified by defining a function S_1 as

$$S_1(z, a, \beta'_g P_g) = \int_o^a \left\{ \int_o^{a-r'} \frac{z}{R^4} F(\beta'_g P_g R)\; 2\pi\, r\, dr \right. \tag{36}$$

$$\left. + \int_{a-r'}^{a+r'} \frac{z}{R^4} F(\beta'_g P_g R) \xi\,(r', r)\, r dr \right\} \cdot 2\pi\, r' dr'$$

Then Eq. 35 becomes

$$\Delta q''_r = T^4_g\, S_1(z, a, \beta'_g P_g) \Delta z \tag{37}$$

This represents the rate of heat loss from the element of gas to the end surface of the gas volume which is at a distance z. The loss to the other end of the gas volume is

$$\Delta q''_r = T_g^4 S_1 (\ell - z, a, \beta'_g P_g) \Delta z \tag{38}$$

The total radiant flux to the end surfaces may be found by integrating Eq. 37 and 38 with respect to z. Several plots of S_1 as functions of z are shown in Figure 12 for several values of $\beta'_g P_g$. It may be noted that S_1 increases with $\beta'_g P_g$. This should happen since the gas becomes increasingly opaque with larger values of $\beta'_g P_g$. In addition it may be expected from the Stefan-Boltzmann equation that

$$\lim q''_r = \lim T_g^4 \int_0^\infty S_1 \, dz = \pi a^2 \sigma T_g^4 \quad \text{as } \beta'_g P_g \rightarrow \infty \tag{39}$$

This relationship was found to be valid by integration of the S_1 function over sufficiently large values of z and $\beta'_g P_g$. This completes the presentation of the basic data and formulas. The subsequent sections will be devoted to a discussion of experimental studies of burning high-explosive and an application of these data and formula to explore the effects and behavior of burning explosives.

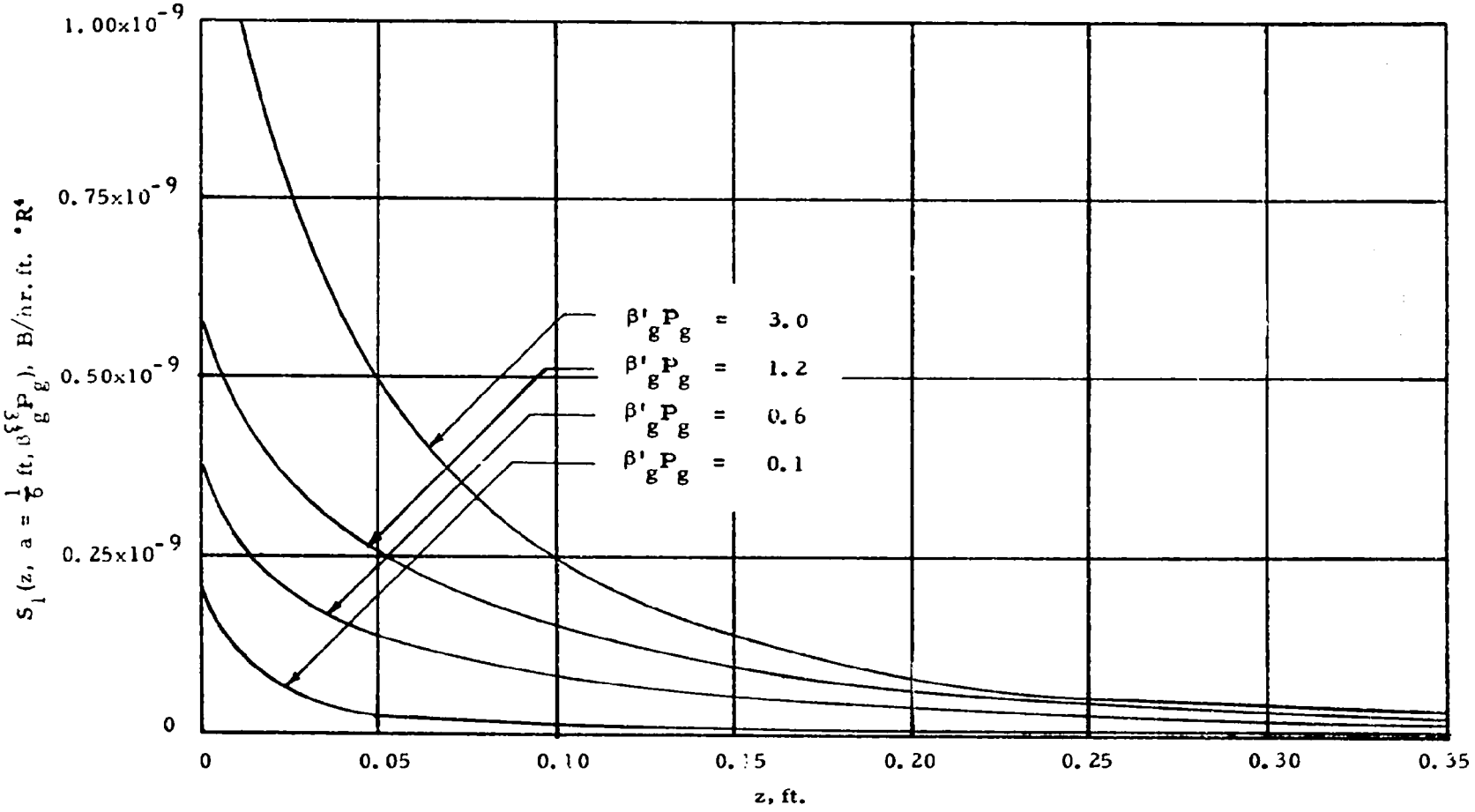

Fig. 12 $S_1(z,\ a = \frac{1}{6}FT, \beta'_g P_g)$

3. BURNING OF COMPOSITION B AND PBX 9404 UNDER PRESSURES OF 1 TO 3 ATMOSPHERES

Composition B and PBX 9404 burn at speeds between about 2 and 20 ft/hr under pressures from 1 to 3 atmospheres. Due to these low rates of burning, it is possible to make a number of reliable measurements that are not possible at the higher burning rates. Furthermore, a knowledge of the behavior of burning explosives under low pressures is necessary to predict their behavior after being ignited in environments of near-atmospheric pressures. A number of tests were conducted in this program to determine the behavior of burning explosives under small, slowly-increasing pressures. In these experiments, the temperature and irradiation were measured in the gas stream. Additional experiments were conducted to determine the heat released by the burning (see Section 2a). The first part of this section will describe the experiments and summarize the resulting data. The second part of this section will develop an analytical description of the burning and its effects, and will compare predictions with experimental data.

a. Experimental Studies of Burning Explosives Under Low Pressure

PBX 9404 burns approximately twice as fast as Composition B and results in considerably higher flame temperatures. The high temperatures of the gas stream are generally beyond the temperature range of ordinary thermocouples except at distances in excess of 2 feet from the PBX 9404 and under conditions of slow burning, i.e., pressures of about 1 atmosphere. As a result of the high temperatures, the experimental studies of PBX 9404 were limited to the unconfined burning in the "open" chamber indicated in Figure 1.

The experimental studies of the burning of Composition B were conducted under conditions in which the evolved gas was "confined" as well as "unconfined". The confinement was adjusted to vary the rate of increase of the gas pressure and of the burning velocity. The first part of this section will discuss the experimental studies of the "confined" and "unconfined" burning of Composition B. This will be followed by a discussion of the experimental studies of the "unconfined" burning of PBX 9404.

b. Confined and Unconfined Burning of Composition B

These studies are a continuation of those presented in the DASA Report 1234. Except for minor differences, the tubular chamber in which most of the high explosive was burned (see Figure 13), was essentially the same as that used previously (see DASA Report 1234). A ceramic liner was used to protect the thermocouple lead wires, to provide a means of mounting an electric heater and heat meters, and to deter the conduction of heat to the sides of the cylinder of explosive. To prevent the escape of gas, an aluminum gasket was used between

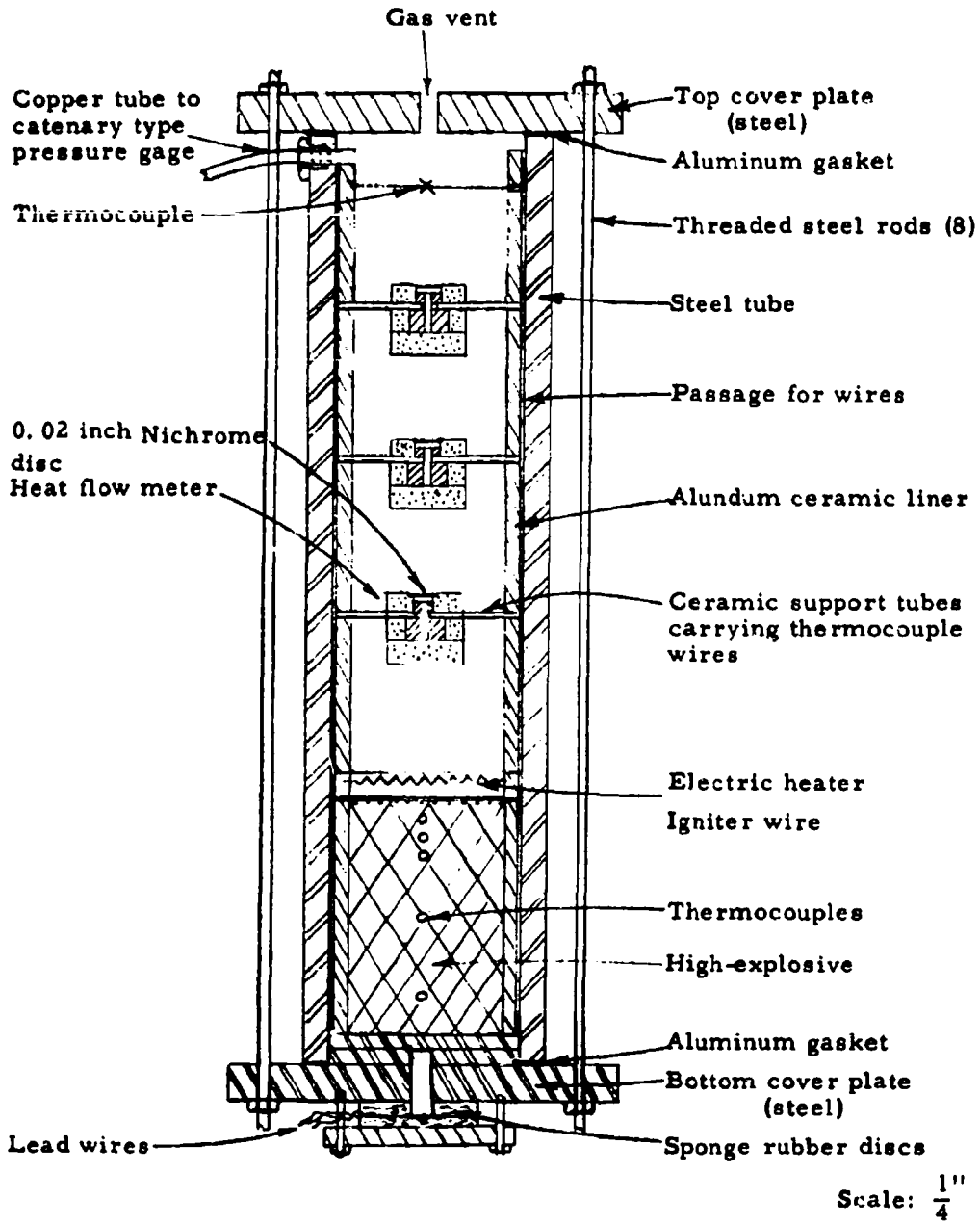

Fig. 13 CROSS SECTION OF "VENTED" TEST CHAMBER

the face at each end of the steel tube and the cover plate. Two rubber gaskets were used to seal the hole through the bottom cover plate. This hole was provided for the several thermocouple and electric wires. A small hole was drilled through the top cover plate to vent the gas and to allow a slow increase in the pressure and burning rate. The Composition B was heated with a 122 watt heater (see Figure 14) for 15 minutes prior to ignition. Ignition was accomplished by passing 10 amperes through a 0.56 ohm resistance wire embedded across the face of the cylinder of Composition B

The thermal irradiation at various locations in the gas stream was measured by the heat meter shown in Figure 14. The sensing element consisted of a 0.02-inch thick disk of Nichrome. The disk was kept as thin as possible to ensure a more rapid response time. Both surfaces of the disk and the upper face of the aluminum cylinder were blackened with stoveblack so that their values of emissivity and absorptivity approached 1 and were nearly equal. Under this condition, it is possible to determine the radiation incident on the upper face of the disk from the following relationship (see previous DASA Reports)

$$q''_r = 2\sigma T^4_m \tag{40}$$

where

q''_r = irradiation in B/hr ft^2

σ = Stefan-Boltzman Constant = 0.173×10^{-8} B/hr ft^2 °R^4

T_m = absolute temperature of disk in °R

Gas temperatures were measured both by bare and shielded 28-gage Chromel-Alumel thermocouple wires. No apparent differences could be detected between the data collected with the two types of thermocouples. However, it is not unlikely that the measured temperatures are slightly low since shielding is only partially satisfactory under transient conditions. Also, the gas flow was not sufficient to produce high convective heat transfer to the junction relation to the radiant losses from the thermocouples to the relatively cool walls of the assembly. An analysis indicated that the readings could be low as much as 200°F.

Gas pressures were measured by a catenary type pressure gage over the range 1 to 27 atmospheres. Due to the excessive heat, the gage was mounted in a 15-cubic-inch pressure vessel which was connected to the chamber by means of a 6-inch length of 1/4-inch copper tube. The rate at which the explosive burned was determined by locating thermocouples along the axis of the cylinder of explosive. A rapid increase in the temperature of each thermocouple indicated the passage of the burning front.

Preliminary heating of the surface of the Composition B was required to produce a reasonably vigorous burning corresponding to velocities of 2.5 ft/hr or higher. Very sluggish burning occurred in tests in which there was insufficient heating of the surface of the Composition B prior to ignition. The reason for this will become apparent during the discussion of the theoretical analysis of the factors affecting the burning. In each test, the Composition B commenced to burn with a velocity of about 2.5 ft/hr. The velocity remained at about this level provided there was sufficient venting of the gas, that is, when the ratio of the cross-sectional area of the vent hole to that of the surface of the burning explosive was in excess of about 0.006. With an area ratio between 0.003 and 0.006, the velocity increased slowly for a period up to 6 minutes. The temperature and the pressure of the gas rose gradually during this period. When a pressure of about 2 to 3 atmospheres was reached, the rate of burning and pressure increased very rapidly and either lifted or ejected the top cover plate. Curves of typical temperatures and pressures of the gas are shown in the DASA Report 1234.

A summary of the temperatures of the gas at various distances from the surface of the burning Composition B is shown in Figures 15 to 19 for several rates of burning. It may be observed that the temperature decreases quite rapidly with distance from the burning surface of the explosive. In addition it should be observed that the temperatures are greater with the higher rates of burning.

The temperatures of the heat meters are shown in Figures 20 to 23 as functions of distance from the burning surface for several rates of burning. It may be noted that the meter temperature increases according to the proximity of the meter to the explosive and also with the rate of burning. This, of course, is what one would expect and is consistent with the temperature distributions of the gas.

As was mentioned earlier, the size of the vent hole was varied to determine its effect on the pressure buildup within the chamber, and to acquire data at higher burning rates. With sufficiently large vents, the Composition B burned to completion with only a small buildup of pressure, i.e., less than 1 atmosphere. On the other hand, excessively small vents resulted in very appreciable pressure buildups which often broke or permanently lengthened the rods holding the cover plates, and thereby caused ejection of the top cover plate. The remainder of the chamber always remained intact. The effect of the size of vent may be measured according to whether it was or was not sufficient to prevent such a pressure buildup. A summary of the diameters of the vent hole which did and which did not cause an appreciable pressure buildup (i.e., of about 1 atmosphere) are shown in Figure 24. It may be noted that there is no sharp demarcation between the diameters of the vent hole for the two conditions. Thus while diameters as small as 0.222 inches resulted in uneventful burning, holes as large as 0.304 inches resulted in a noticeable increase of pressure and

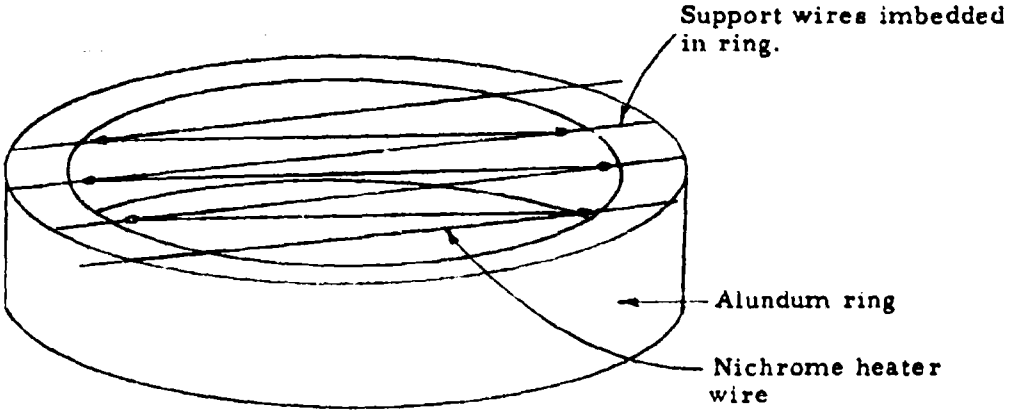

ELECTRIC HEATER Full Scale

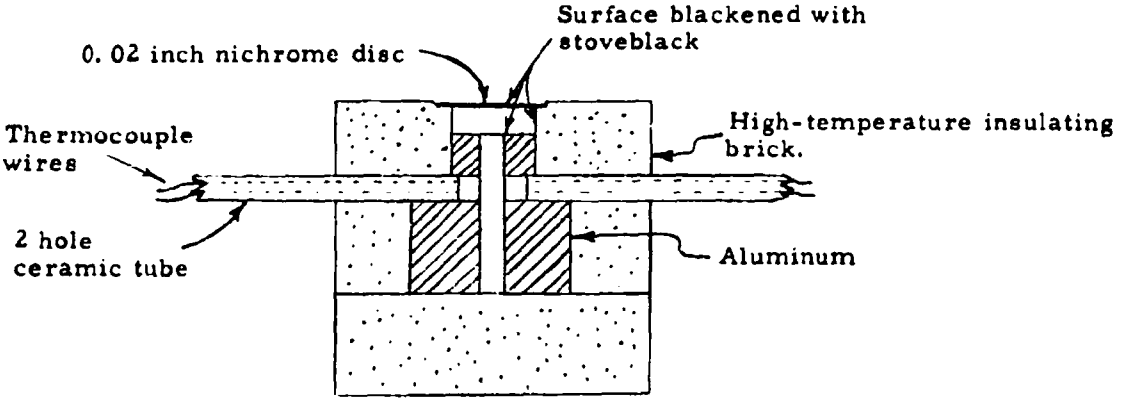

HEAT FLOW METER Full Scale

Fig. 14 ELECTRIC HEATER AND HEAT FLOW METER

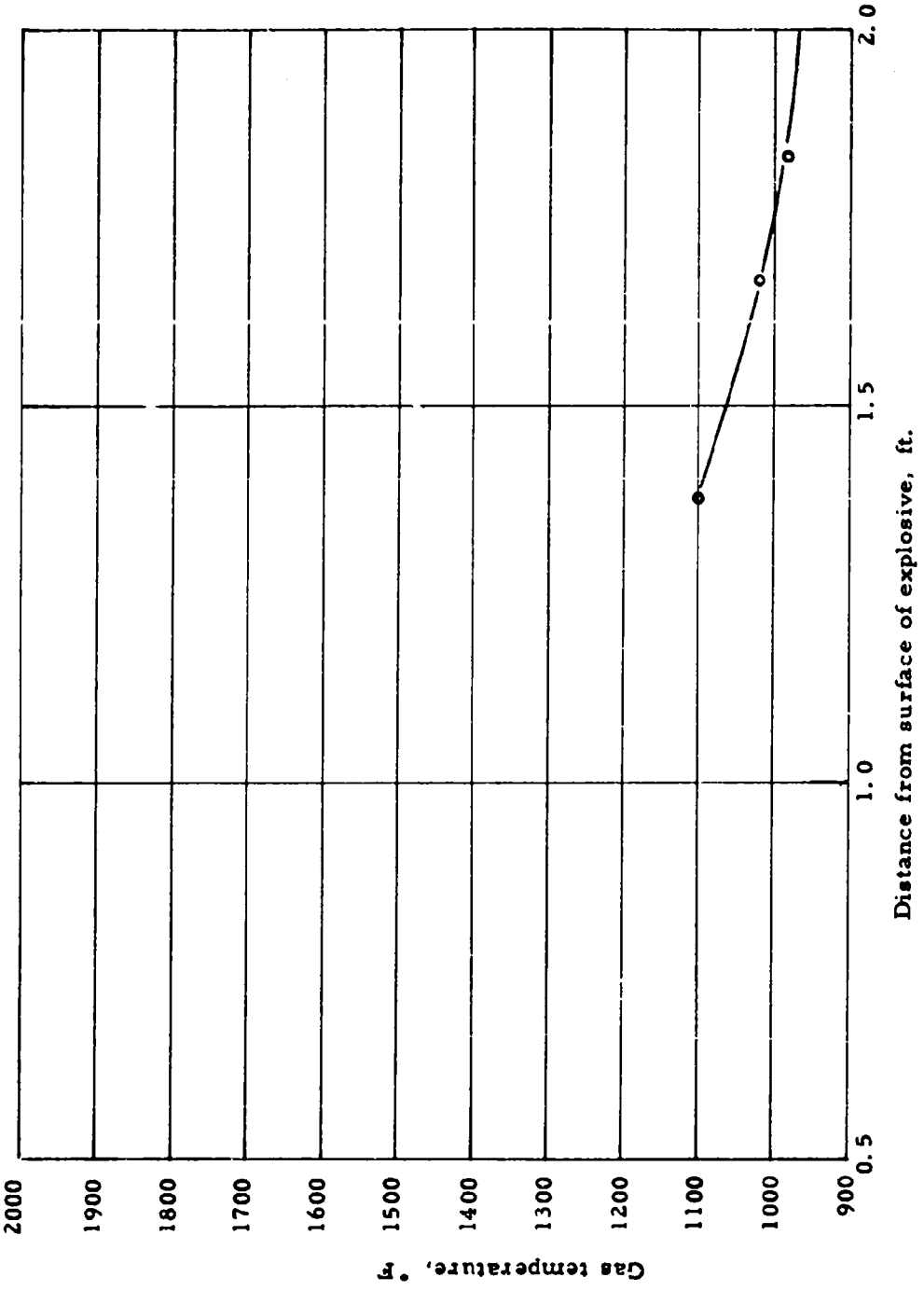

Fig. 15 GAS TEMPERATURE (BURNING RATE COMPOSITION B, 2.5 FT/HR)

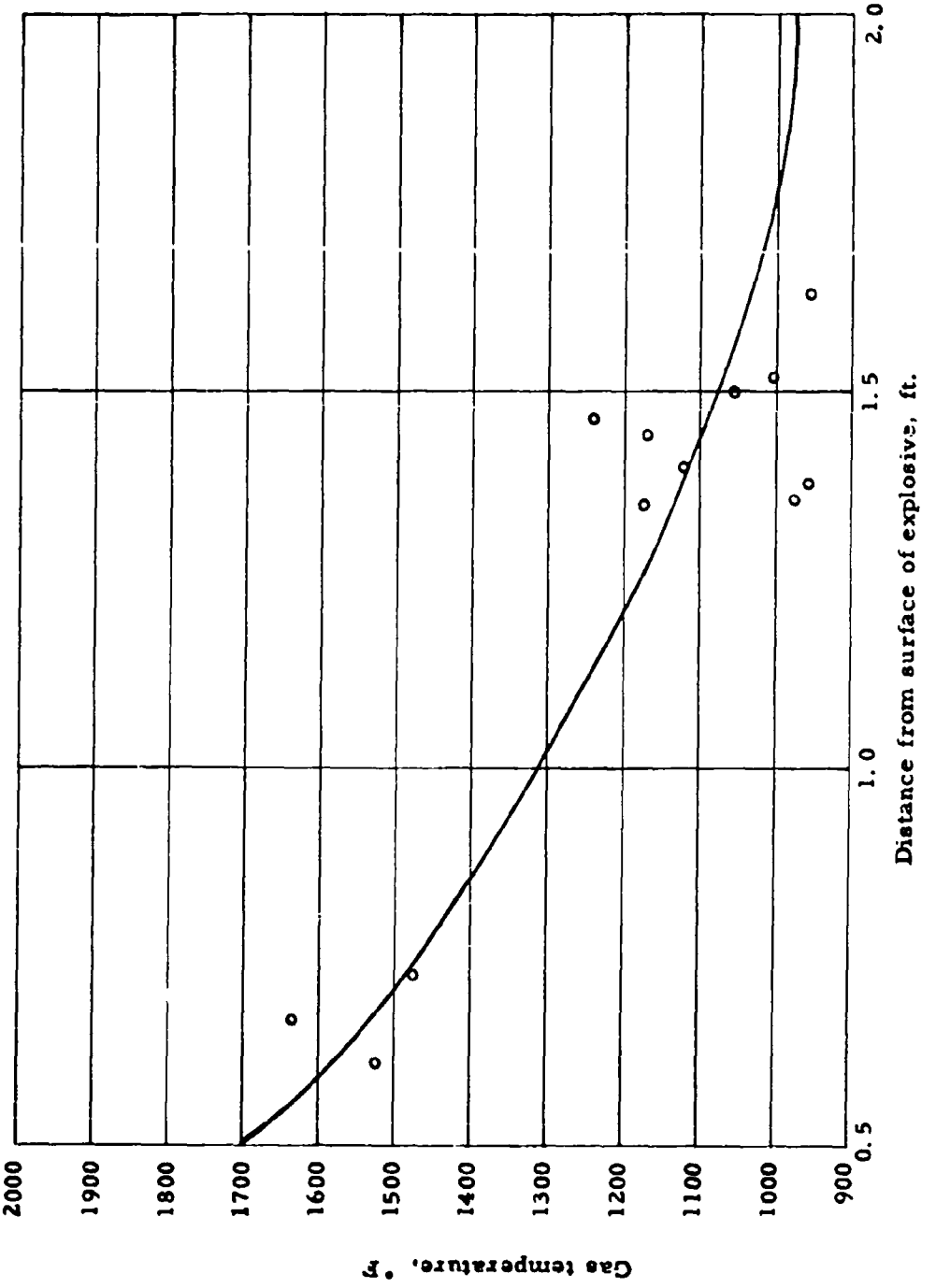

Fig. 16 GAS TEMPERATURE (BURNING RATE COMPOSITION B, 3.5 FT/HR)

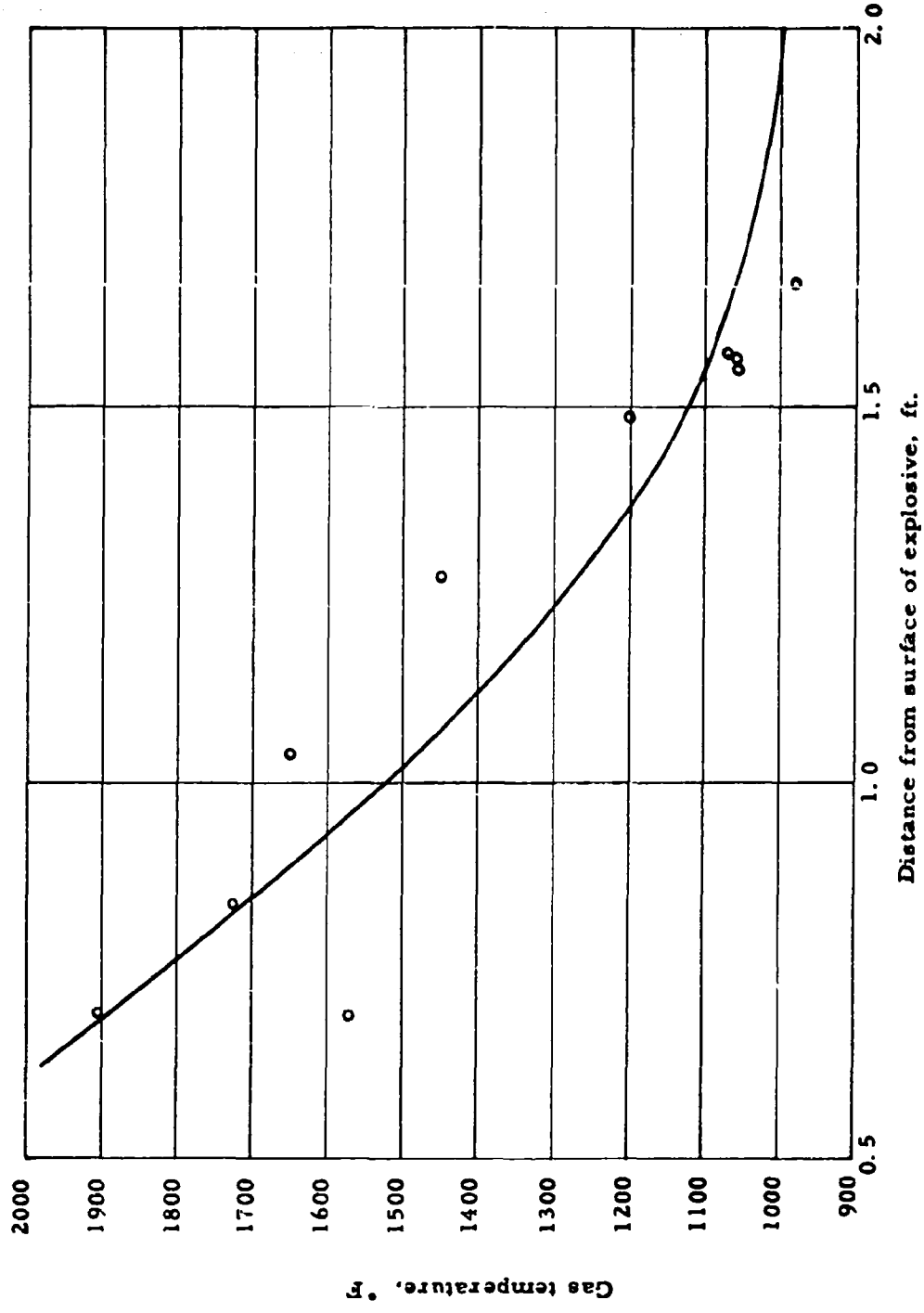

Fig. 17 GAS TEMPERATURES (BURNING RATE COMPOSITION B, 5 FT/HR)

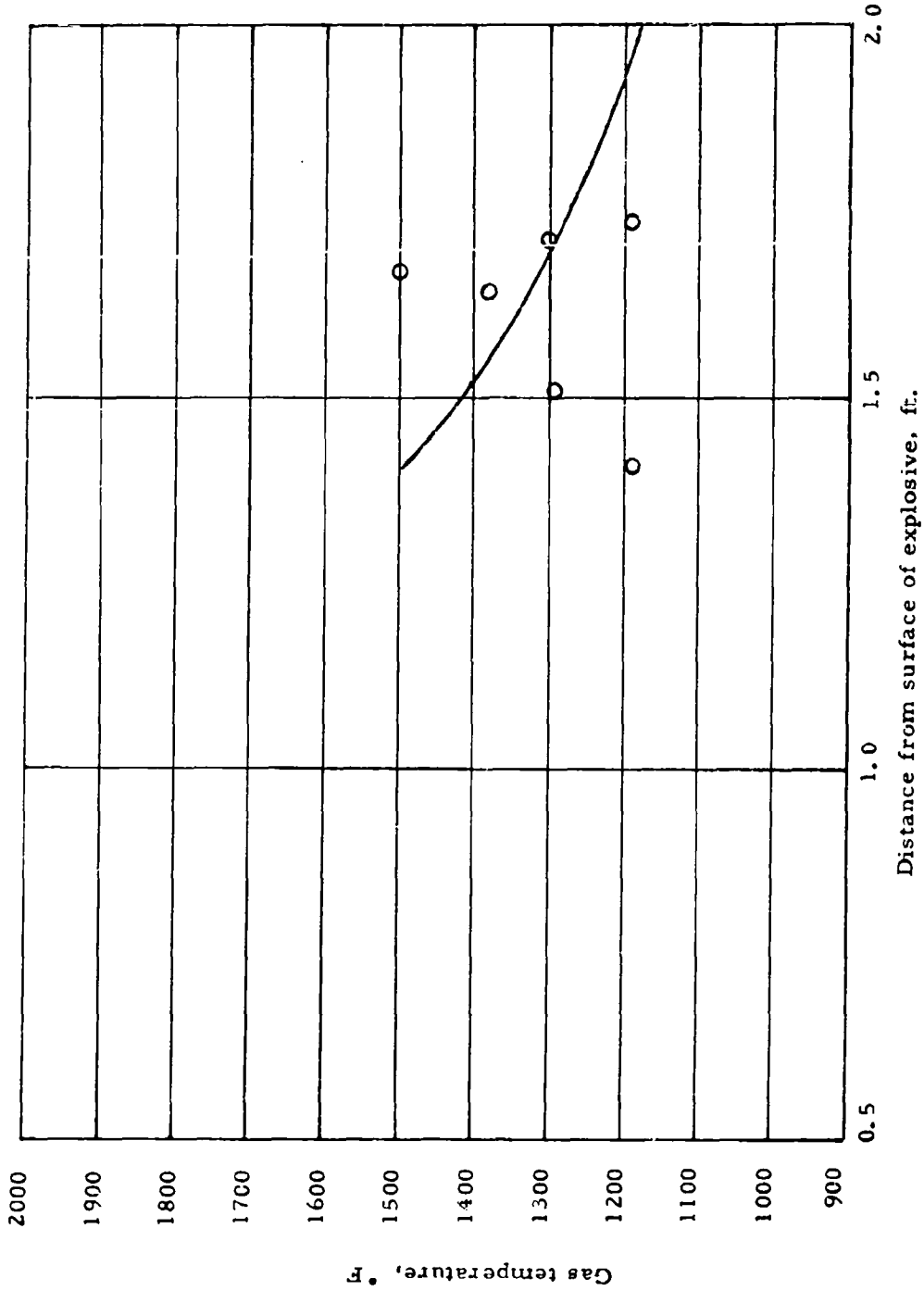

Fig. 18 GAS TEMPERATURES (BURNING RATE COMPOSITION B, 7.5 FT/HR)

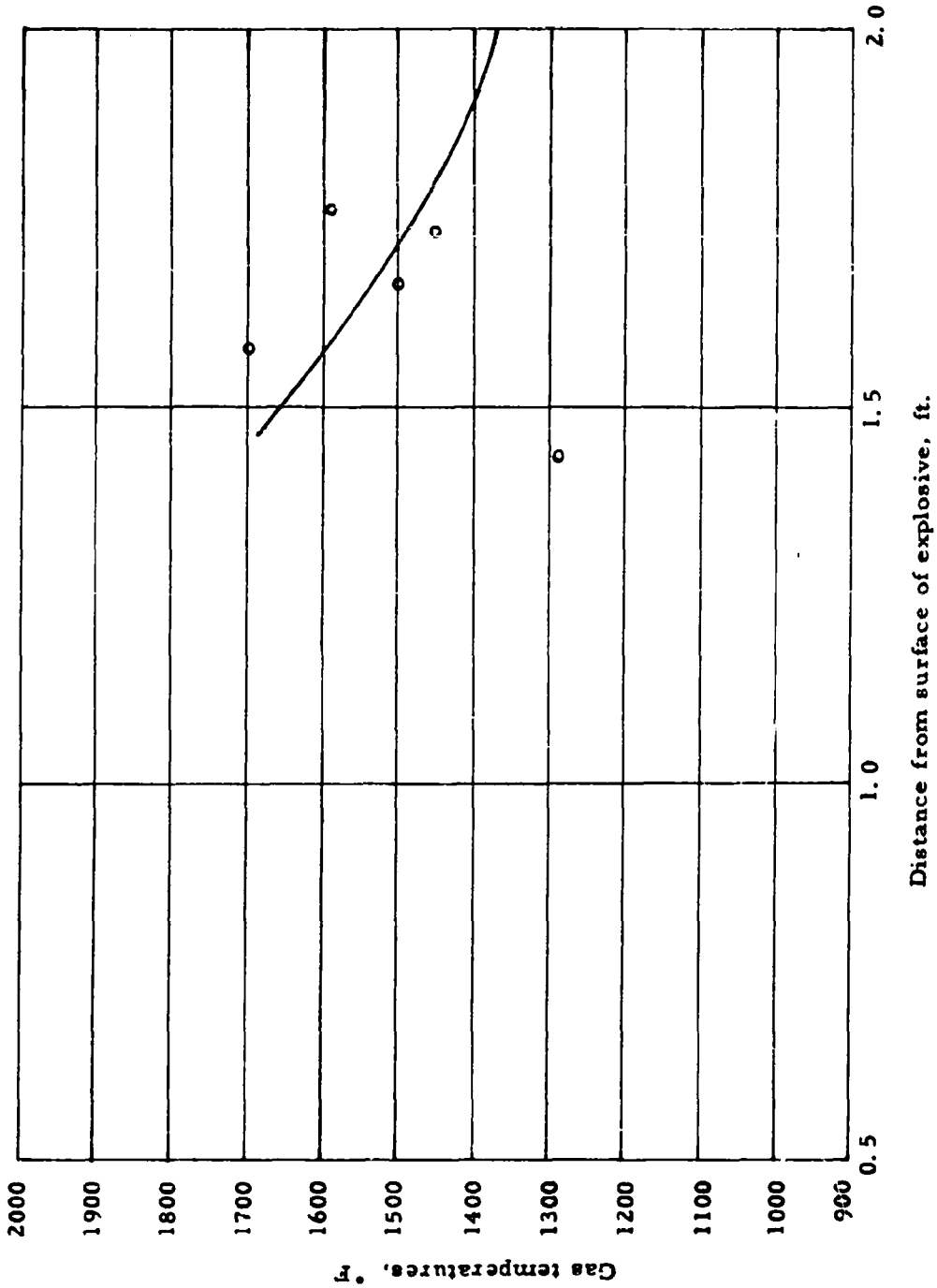

Fig. 19 GAS TEMPERATURES (BURNING RATE COMPOSITION B, 10 FT/HR)

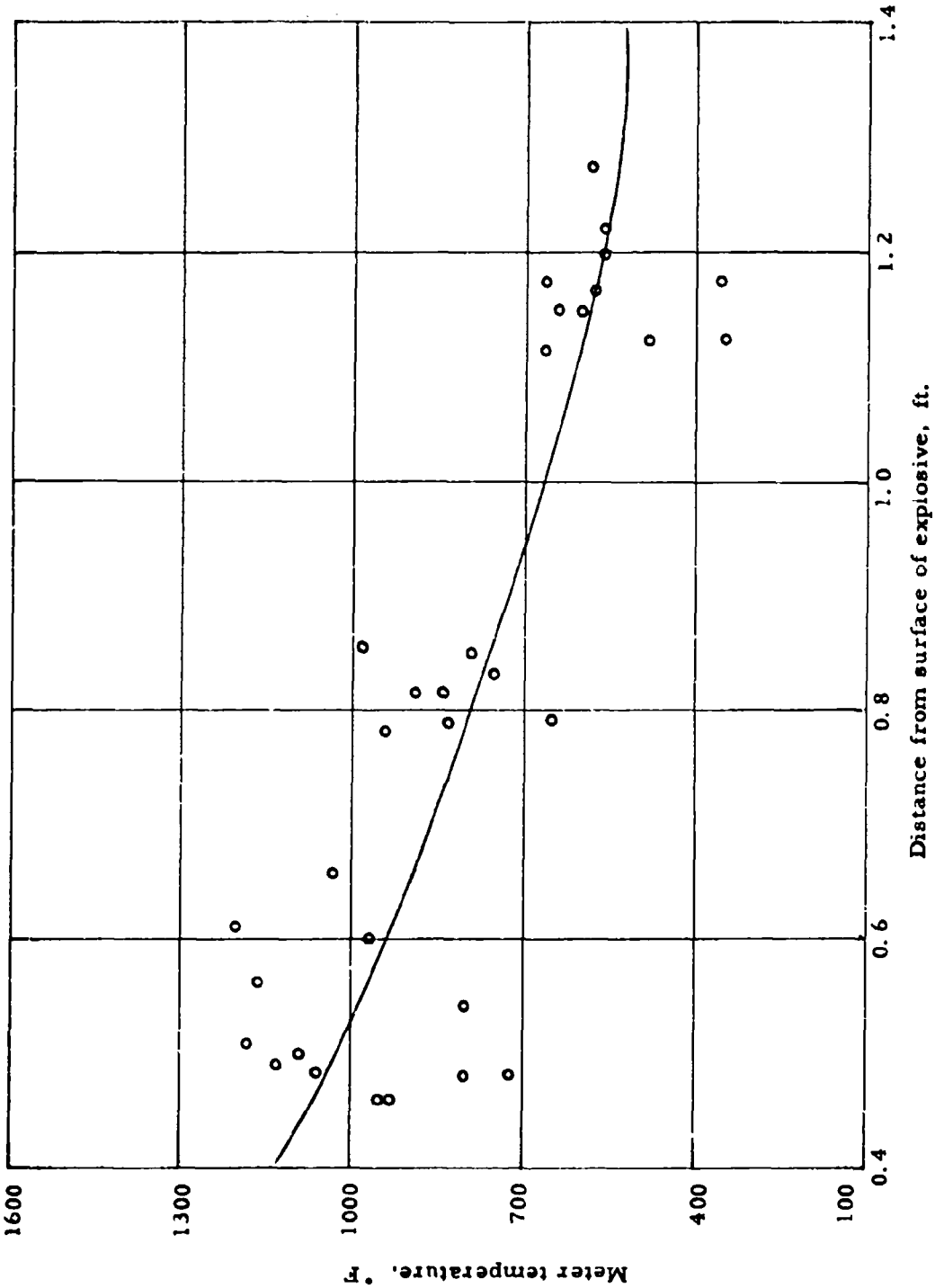

Fig. 20 METER TEMPERATURES (BURNING RATE COMPOSITION B, 3.5FT/HR)

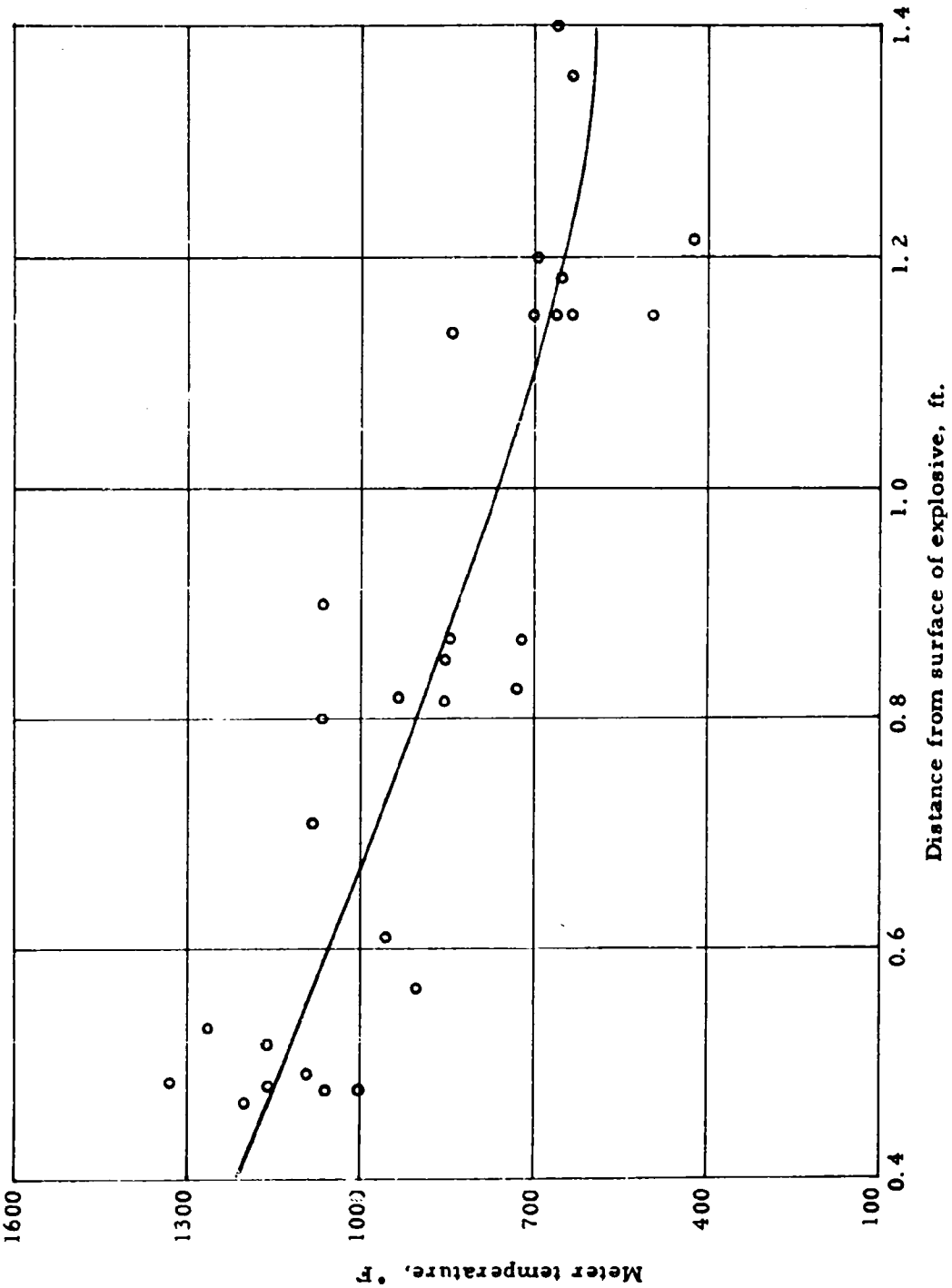

Fig. 21 METER TEMPERATURES (BURNING RATE COMPOSITION B, 5FT/HR)

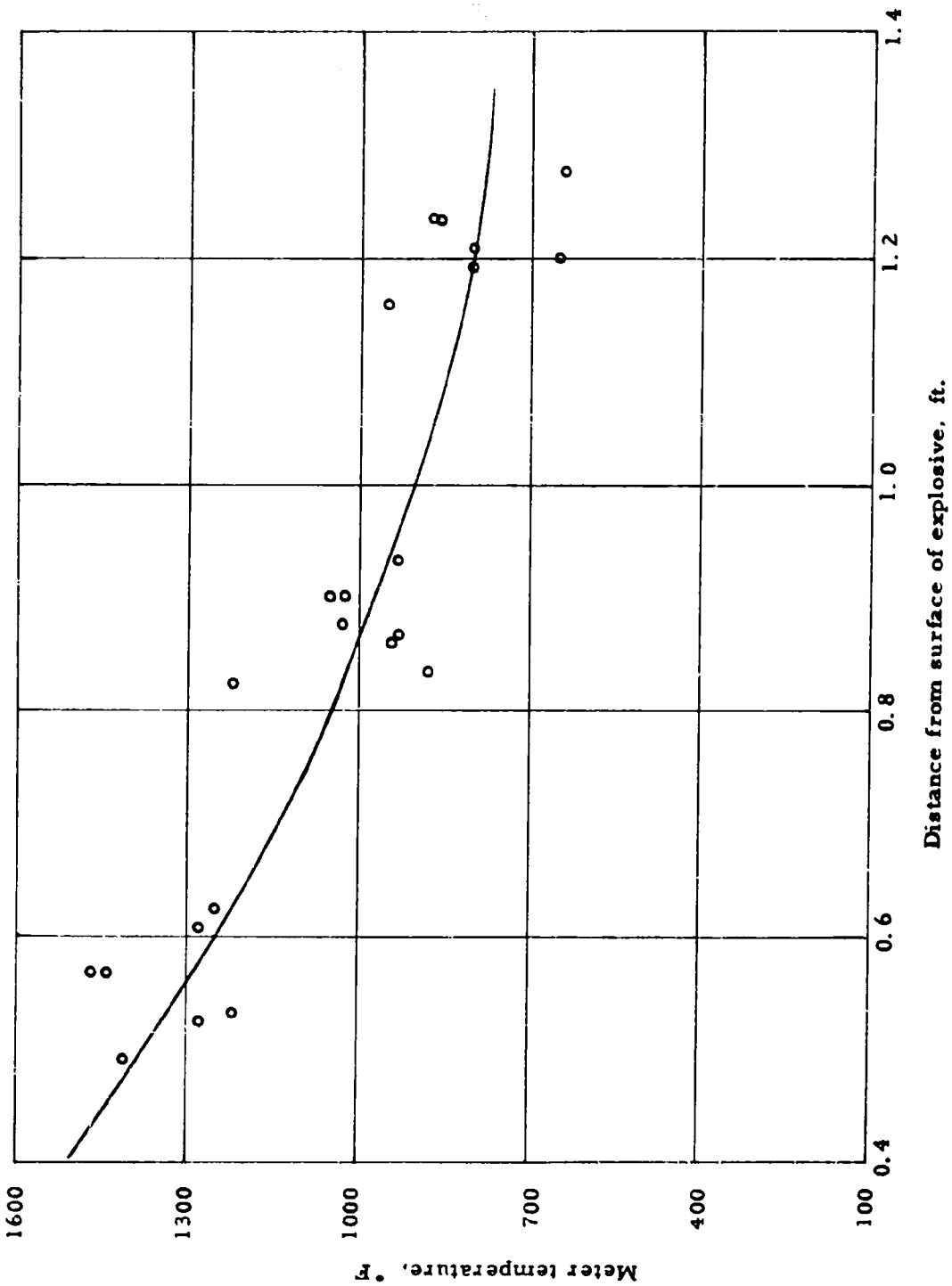

Fig. 22 METER TEMPERATURES (BURNING RATE COMPOSITION B, 7.5FT/HR)

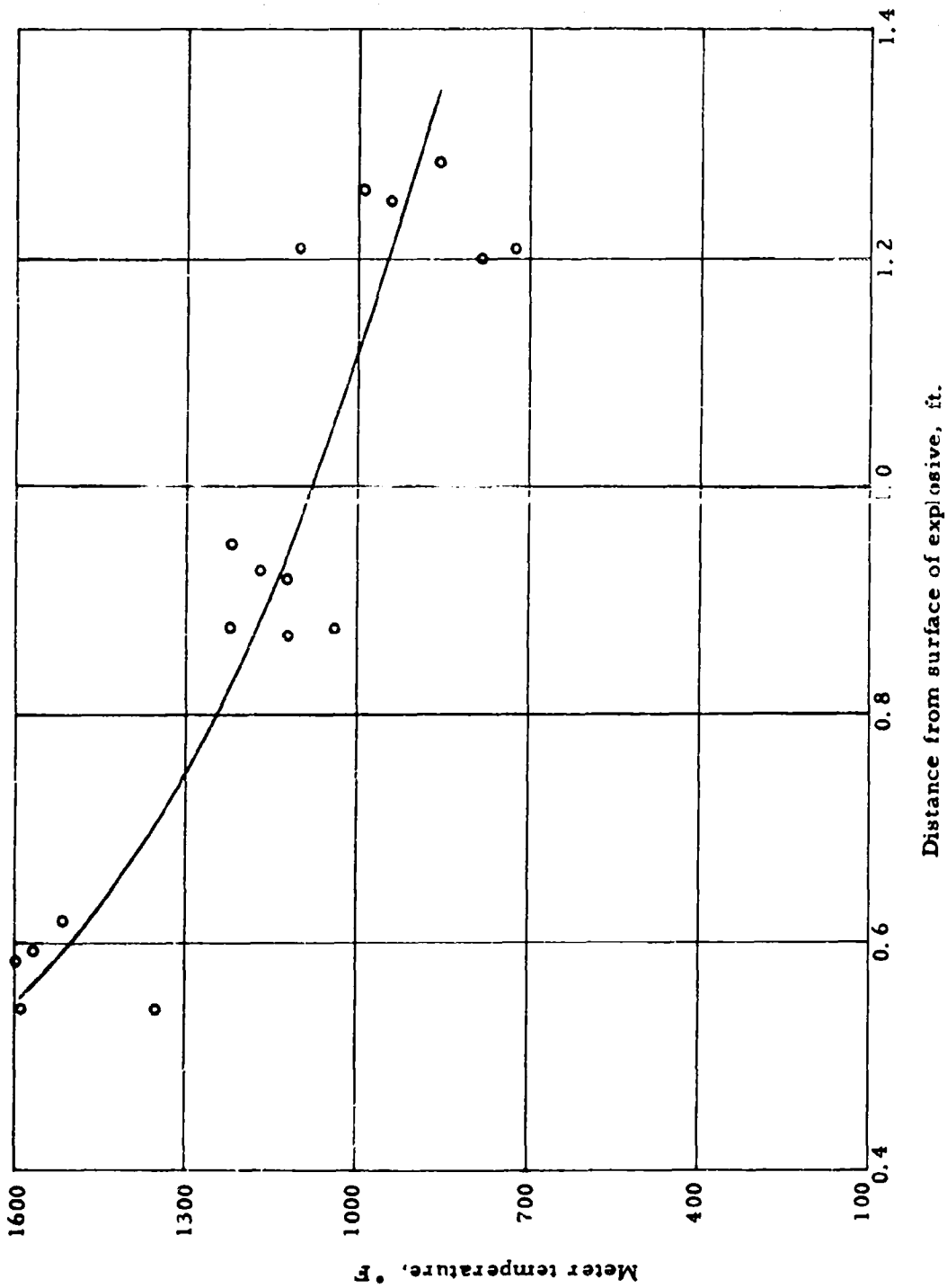

Fig. 23 METER TEMPERATURE (BURNING RATE COMPOSITION B, 10FT/HR)

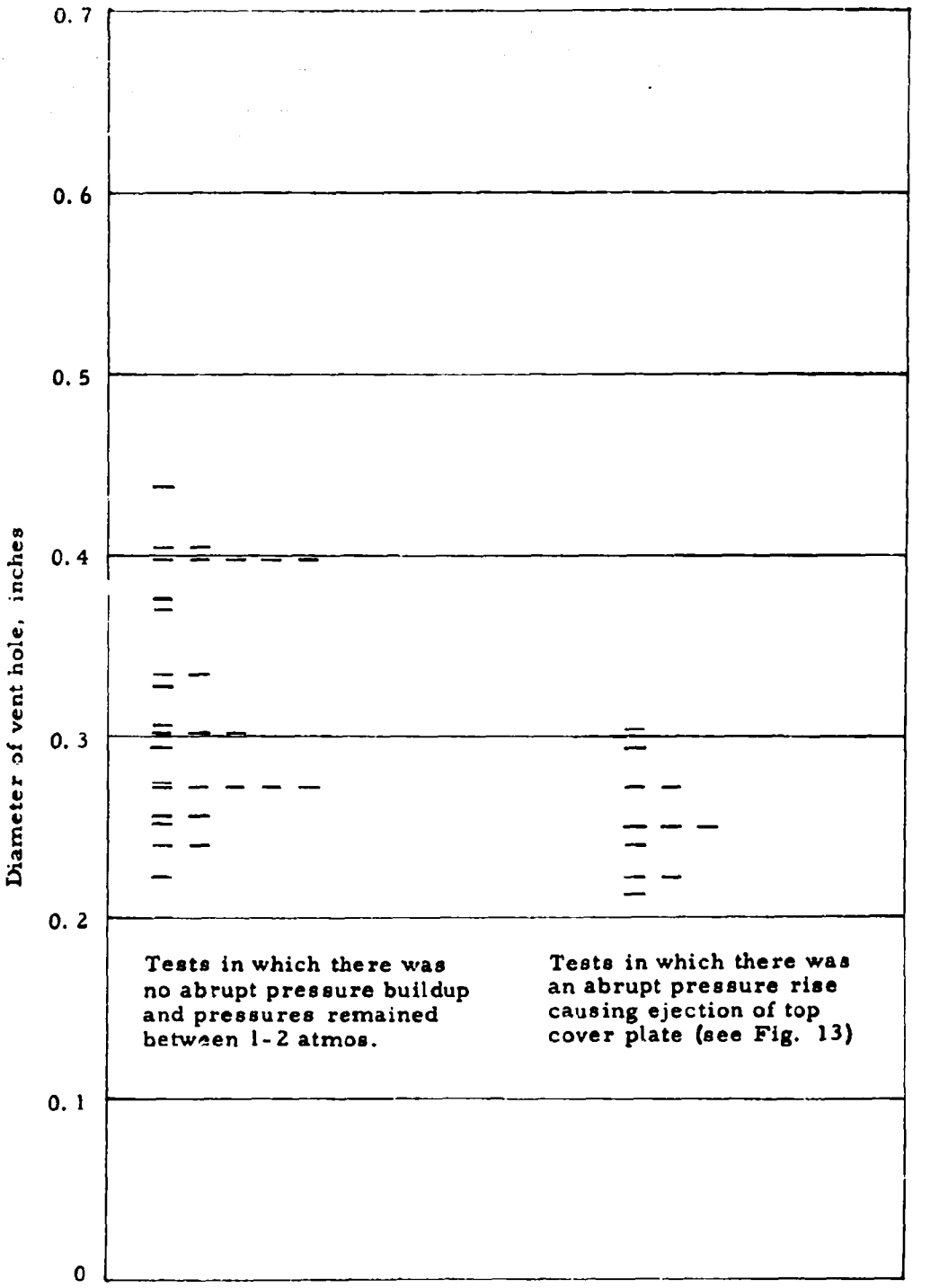

Fig. 24 EFFECT OF VENT HOLE ON BURNING OF COMPOSITION B

caused ejection of the top cover plate. Therefore, the critical diameter of the vent hole associated with the burning of Composition B in the chamber shown in Figure 13 lies somewhere between 0.222 and 0.304 inches. This topic, as well as previous ones in this section, will be returned to later in this section.

A number of chamber temperatures were acquired during the tests in which Composition B was burned in an "unconfined" manner in the chamber shown in Figure 1. The Composition B cylinders were 4 inches in diameter and 4 inches in length. Temperatures were measured along the length of the chamber and serve as one of several means of checking the theoretical work. A temperature profile along the length of the chamber is shown in Figure 25, for the case of "unconfined" burning of Composition B. These data were obtained with 7 thermocouples located along the length of the chamber by averaging the temperatures from 6 tests. The burning rate was 2.5 ft/hr and remained very uniform during each of the tests. It may be observed that the chamber reached its maximum temperature at about 0.5 feet from its base. This was due to the fact that the lower portion of the chamber was thermally protected at the early times by the presence of the cylinder of Composition B and at the later times by the layer of Adiprene used to bond the Composition B to the chamber.

c. Unconfined Burning of PBX 9404

Cylinders of PBX 9404 of 4 inch diameter and 5 inches long were also burned in the chamber shown in Figure 1 to determine the heat evolved by the burning. These results are given in Section 2a. The test procedure was identical to that for the "confined" burning of Composition B. During the course of this work, a number of chamber temperatures were procured. Unfortunately, due to the very high temperatures of the gas, measurements of the gas temperature could only be made near the exhaust end of the 2 foot chamber. To overcome this problem, the chamber was lengthened to 4 feet. Three tests were conducted with the longer chamber. In each of these tests, as well as in the earlier tests, the PBX 9404 burned very uniformly at a rate of 5 ft/hr. Gas and chamber temperatures from the 4-foot chamber are presented in Figure 26. At a distance of 2 feet from the burning surface, the temperature of the gas from the unconfined burning of Composition B (see Figure 15) was only about 960°F as compared to about 2520°F for PBX 9404. This is due to the faster burning rate of PBX 9404. Also PBX 9404 reacts almost completely at these low burning rates while Composition B does not.

Summaries of the temperatures along the lengths of the 2-foot and 4-foot chambers are presented in Figures 27 and 28. It may be observed that the shapes of the curves are similar to that for Composition B. The fact that the maximum temperatures were not at the base of the chamber is due to the protection afforded the lower 5 inches of the chamber wall by the explosive and by the 0.050 inch layer of Adiprene cement used to bond the high-explosive to the chamber.

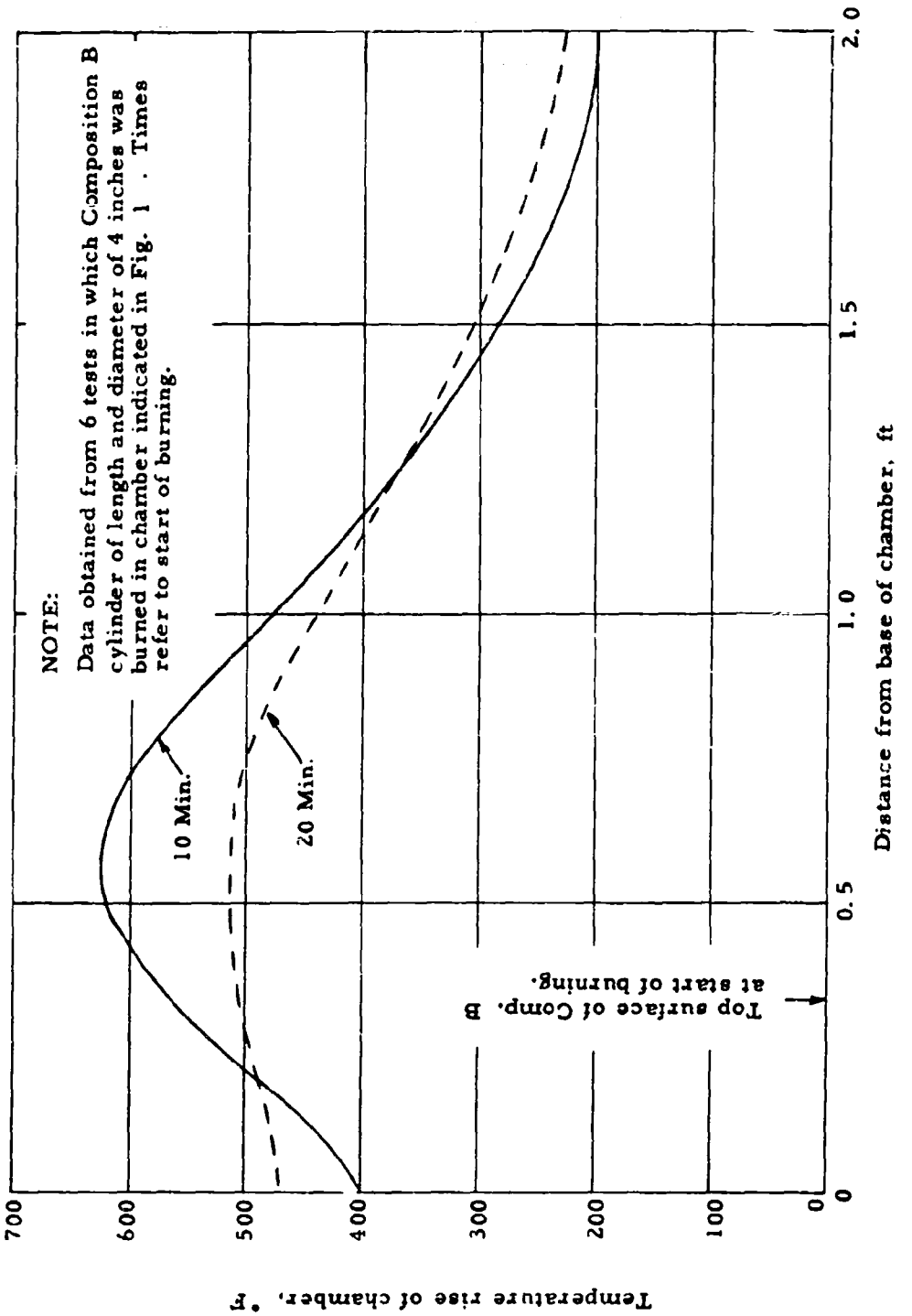

Fig. 25 CHAMBER TEMPERATURES (BURNING RATE OF COMPOSITION B, 2.5 FT/HR)

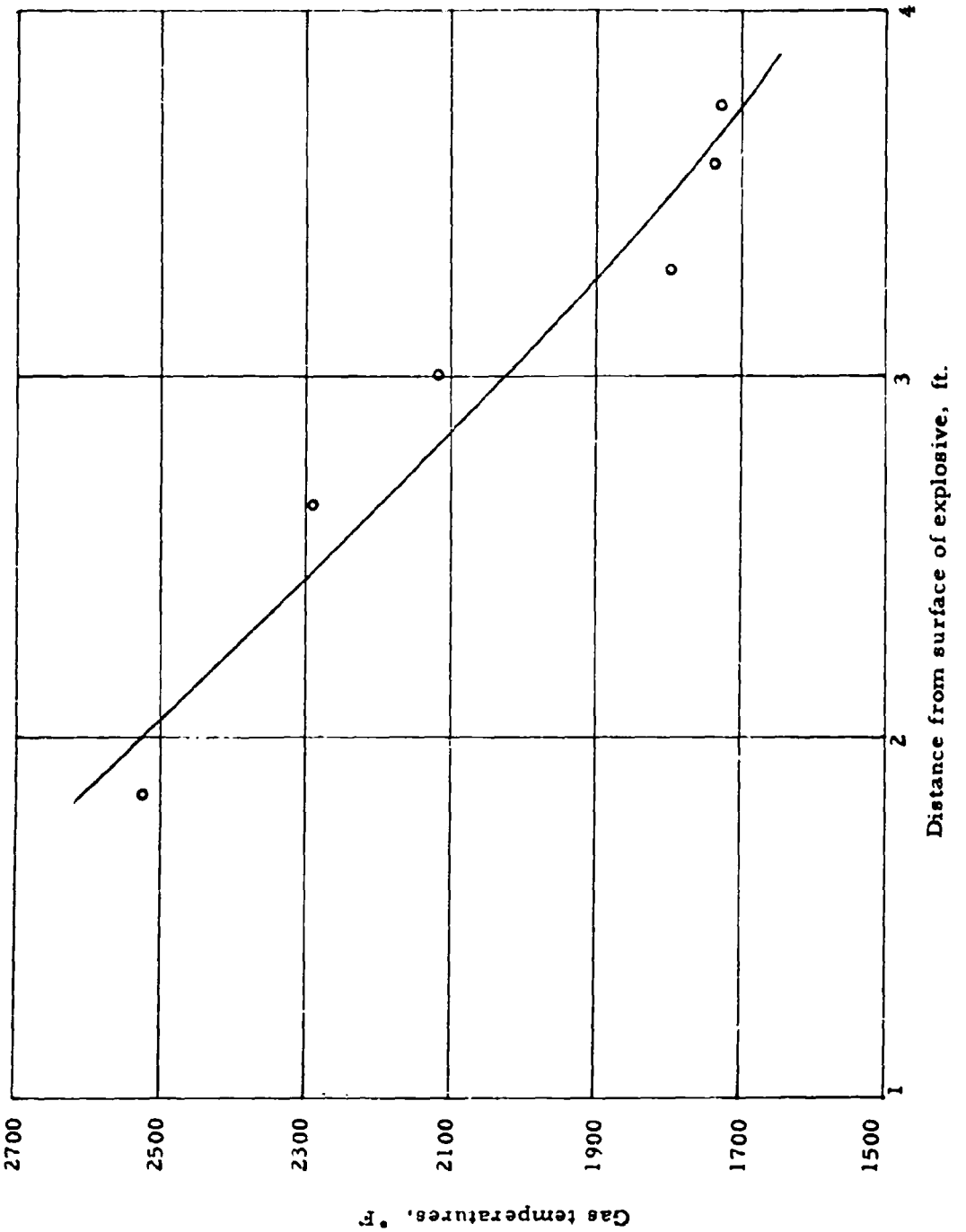

Fig. 26 GAS TEMPERATURES (BURNING RATE PBX 9404, 5.0 FT/HR)

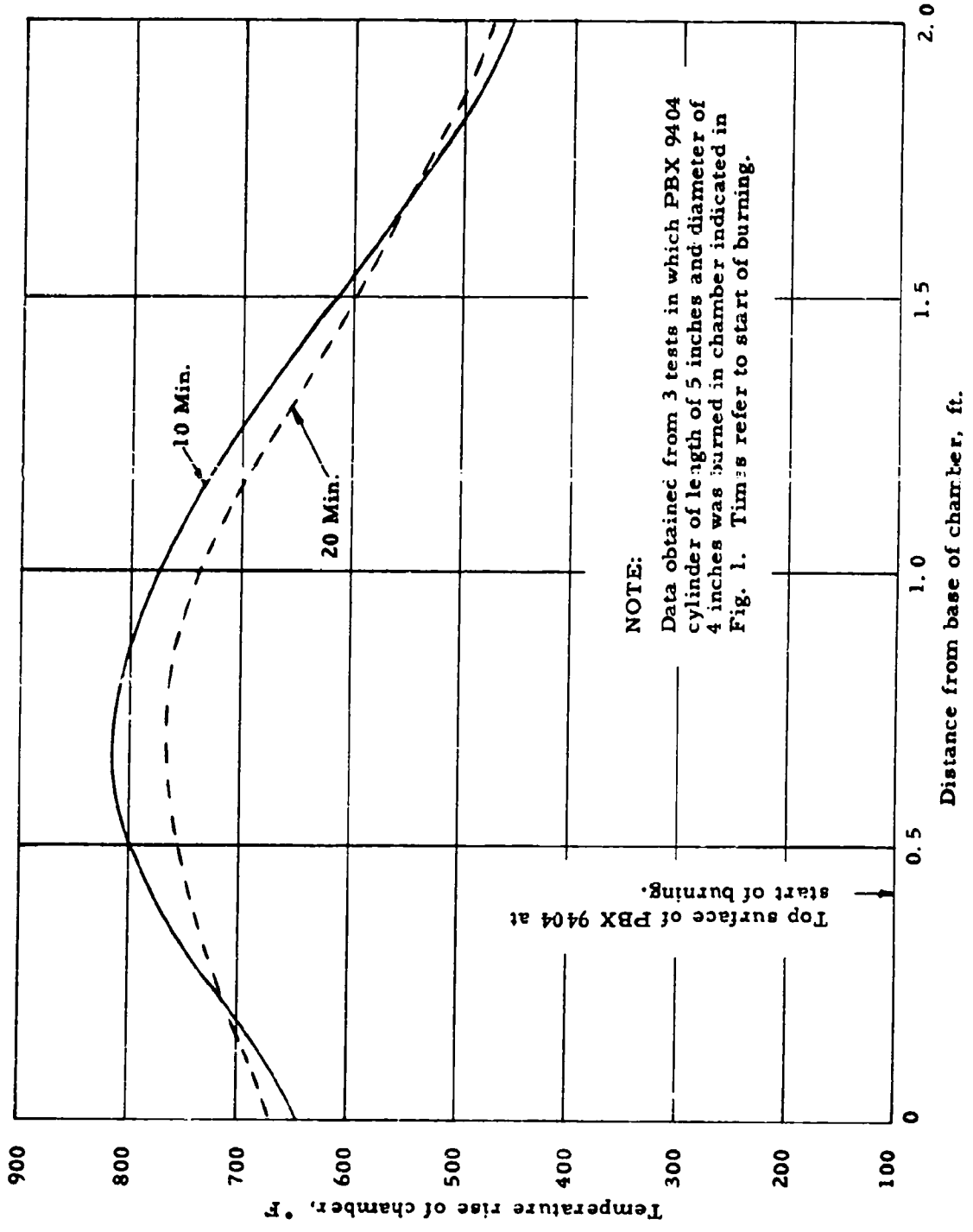

Fig. 27 CHAMBER TEMPERATURES (BURNING RATE PBX 9404, 5.0 FT/HR)

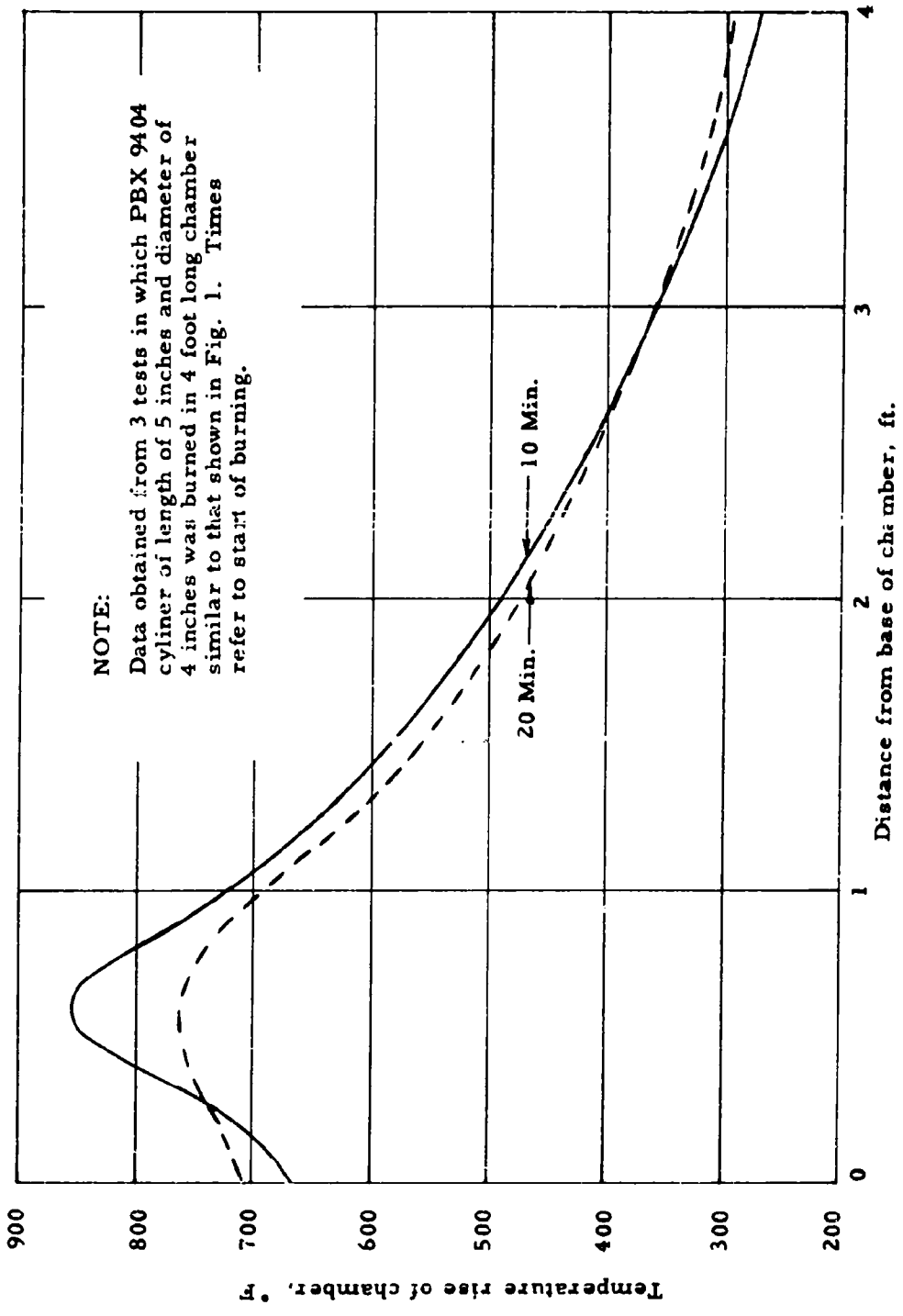

Fig. 28 CHAMBER TEMPERATURES (BURNING RATE PBX 9404, 5.0 FT/HR)

d. Theoretical Analysis of the Effects of Burning High-Explosives Under Low Pressure

The principal parameters affecting the burning rate of high-explosives such as Composition B and PBX 9404 are the temperature and the amount of the explosive undergoing reaction. An indication of the temperature, thickness and density of the reacting layer was gained from the Composition B experiments noted earlier. These measurements indicated that the layer is in the form of a foam which has a thickness of approximately 0.05 inches. The temperature of the foam during the burning of Composition B under near atmospheric pressure was about 540°F. Throughout this study it will be assumed that the amount of reacting material (or the thickness and density of the foam) is constant. It is obvious that the temperature of the foam must be maintained or increased to perpetuate the burning. This can only be brought about by a net heat flux to the foam layer. As a result, this study will be initiated by a consideration of the effect of the heating this layer on the burning rate of the explosive.

As was mentioned earlier, the principal sources of heat flow into the layer of foam are conduction and radiation from the hot gas stream. The rate at which heat is carried away from this layer is approximately equal to the product of the enthalpy of the explosive in the layer (above that of the material entering the layer) times the rate at which material is evolved. In this analysis, the heat lost by convection and conduction into the solid explosive beneath the foam is considered to be reabsorbed by the moving layer. The results of this discussion may be expressed in the following mathematical formula

$$q_T(t) = \rho_f x_f \frac{dH(T_f)}{dt} + \rho_f x_f (H(T_f) - H(T_{fo}))Z \exp-(E/R_{go}T_f) \quad (41)$$

where

$q_T(t)$ = rate of heat flow into layer due to conduction and radiation, B/ft^2 hr

t = time, hr

ρ_f = density of foam = 17.5 lb/ft^3

x_f = thickness of layer, = 0.0042 ft

$H(T_f)$ = enthalpy of foam, B/lb

$H(T_{fo})$ = enthalpy of high-explosive entering foam layer (incoming explosive), B/lb

Z = frequency factor, 1/hr

E = activation energy of explosive, cal/mole

R_{go} = universal gas constant, cal/mole °R

T_f = temperature of foam material, °R

Throughout this report all values of enthalpy are referred to a temperature of 70°F.

For steady-state conditions, i.e., steady uniform burning,

$$\frac{dH(T_f)}{dt} = 0 \tag{42}$$

Therefore Eq. 41 becomes

$$q_T = \rho_f x_f (H(T_f) - H(T_{fo}))Z \exp -(E/R_{go}T_f) \tag{43}$$

The velocity of burning, V, may be expressed as

$$\rho_E V(T_f) = \rho_f x_f Z \exp -(E/R_{go}T_f) \tag{44}$$

where

ρ_E = density of original explosive lb/ft^3

$V(T_f)$ = velocity of burning, ft/hr

Substitution of this expression into Eq. 43 yields the following relationship for steady burning

$$q_T = \rho_E V(T_f)(H(T_f) - H(T_{fo})) \tag{45}$$

This is the same relationship expressed in DASA Report 1234.

The dominant parameter in this equation is the temperature of the foam, T_f. As may be noted in Eq. 44, small changes of this temperature will produce very large changes in the burning velocity in comparison to the changes in the enthalpy of the foam. The result is that for steady-state burning, the velocity of burning is approximately proportional to the heat flux entering the explosive.

The next topic of concern is the enthalpy of the gas just after reaction of the vapors released by the foam. The enthalpy of the vapors prior to reaction is approximately equal to $H(T_f)$, (see Figure 3). The burning of a pound of the vapor releases a quantity of heat Q_E (see Figure 2) which is added to the heat or enthalpy already in the vapor. By conduction a certain amount of this heat is returned to the foam within a few mean free paths of the molecules. Since this heat loss occurs so close to the foam, the enthalpy of the gas shortly after leaving the foam is

$$H(T_g) = H(T_f) + Q_E - \frac{q_c P'_g}{W} \tag{46}$$

where

$H(T_g)$	=	enthalpy of gas, B/lb
$H(T_f)$	=	enthalpy of foam at temperature T_f, B/lb
Q_E	=	heat released by burning of 1 pound of explosive, B/lb
q_c	=	rate of conductive heating per atmosphere of pressure, B/ft^2 hr atmos.
P'_g	=	gas pressure, atmos.
W	=	rate of gas flow, lb/ft^2 hr

The terms $H(T_f)$ and Q_E are the dominant terms in this equation and both will tend to increase with the burning velocity. As a result of this, the gas temperature will increase with the velocity of burning. The increase of gas temperature may be as much as 200 to 300°F.

Since the gas temperature may be as high as 6000°R, the radiant heat loss from the gas is appreciable. The rate of radiant heat loss may be determined by the equations derived in Section 2. Let us consider a gas element of radius a and thickness Δz that is located at a distance of z from one end of a cylindrical volume of gas having a temperature T(z), and a length ℓ. From Eq. 27, 37 and 38, the rate of radiant heat loss from this element is

$$\Delta q_r = T^4_g(z)\left[P_1(z, a, \beta'_g P_g) + P_1(\ell - z, a, \beta'_g P_g) + S_1(z, a, \beta'_g P_g) + S_1(\ell - z, a, \beta'_g P_g)\right] \Delta z \tag{47}$$

where P_g and $T_g(z)$ are the pressure and temperature of the gas.

This relationship presumes that the radiant flux between the several gas elements cancel out. This is considered to be a good first order approximation. The functions P_1 and S_1 are defined by Eq. 26 and 36 and are associated with the heat losses through the circumferential surface and the two ends enclosing the cylindrical gas volume. The expression within the brackets will be simplified by setting it equal to $U_1(z, a, l, \beta'_g P_g)$. The result of this substitution is

$$\Delta q_r = T^4_g(z) U_1(z, a, \ell, \beta'_g P_g) \Delta z \tag{48}$$

Since Δq_r is equivalent to $-\pi a^2 \Delta z \rho_g(T_g) \frac{dTg}{dt}$ for a particular increment of gas, the rate of temperature change of this gas element as it moves away from the explosive is

$$\pi a^2 \Delta z \rho_g c_p(T_g) \frac{dTg}{dt} = -T^4_g U_1(z, a, \ell, \beta'_g P_g) \Delta z \tag{49}$$

The total derivative of the temperature may be written as

$$\frac{dTg}{dt} = \frac{\partial Tg}{\partial t} + \dot{z}\frac{\partial Tg}{\partial z} \tag{50}$$

Since the rate of temperature change at a fixed point within the gas stream is insignificant compared to the change of temperature of a given gas element as it moves through the chamber, it is possible to rewrite Eq. 49 as follows

$$\pi a^2 \rho_g c_p(T_g)\dot{z}\frac{\partial Tg}{\partial z} = -T_g^4 U_1(z, a, \ell, \beta_g' P_g) \tag{51}$$

The product $\rho_g \dot{z}$ may be replaced by the term for mass flow W to yield

$$\pi a^2 c_p(T_g) W \frac{\partial Tg}{\partial z} = -T_g^4 U_1(z, a, \ell, \beta_g' P_g) \tag{52}$$

Due to the fact that the terms c_p and U_1 are variable in T_g and z respectively, this equation must be solved numerically. In the next two sections, this equation, in conjunction with other equations and information, will be utilized to explore the effects and behavior of burning Composition B and PBX 9404 under pressures of a few atmospheres. This will be followed by a consideration of the behavior of burning Composition B under pressures as high as a few thousand atmospheres.

(1) Analysis of the Effects of Burning Composition B Under Low Pressures

This section will be concerned with the determination of the constant β_g' and the prediction of thermal data to serve as a check on the theory. At the end of the section, an analysis will be conducted to determine the minimum size of vent hole which will prevent an appreciable pressure buildup. The evaluation of β_g' was made by adjusting its value until the theoretical relationship between heat and mass flow was satisfied. To accomplish this, it was necessary to determine the temperature distributions of the gas associated with arbitrary values of W, β_g', and P_g. These evaluations were made by substituting these values into Eq. 52. In each case, the temperature of the gas at z = 0. was determined from Eq. 46 and Figures 2 through 5. The radiant flux to the explosive was calculated by substituting these temperatures into Eq. 38 and integrating over the several gas elements. These computations were performed on the UNIVAC 1105 computer for several sets of parameters. The heat flux which is conducted to the explosive at the assumed pressure was determined from the data shown in Figure 4 and added to the radiant flux to yield the total heat flux to the explosive. The results were then checked against the heat flux indicated by Eq. 45 for the

assumed mass flow. Appropriate modifications were made in the parameters until the relationship between heat and mass flow was closely satisfied. From these calculations, several sets of values of the parameters W, β_g' and P_g were found in which the value of β_g' was 2.83×10^{-4} ft^2 °cm°R/ft-lb (pressure in units of lb/ft^2). This value of β_g' appears reasonable since it indicates that the gas evolved by the burning of Composition B at one atmosphere of pressure has an opacity which is comparable to that of flames from ordinary hydrocarbon fuels. The results of these computations are shown in Table VII.

The fact tnat the pressure and the mass flow are consistent with test results will be discussed at the end of this section. It may be observed that at these low pressures the radiant flux is generally several times larger than the flux due to conduction. At pressures of the order of tens of atmospheres, the heat flux due to conduction will exceed the flux due to radiation. This is due to the fact that the radiant flux gradually levels off with pressure while the conductive flux continues to increase.

Before applying these results, it is desirable to check various predictions of the theory against experimental results. There are three types of thermal data which may be used as a heck on the theory. These are the temperature distribution of the gas, the irradiation or temperatures associated with the meters, and the temperature distribution along the length of the chamber at various times.

The gas temperatures were calculated as indicated earlier using Eq. 52 and are presented in Figure 29 for the several burning velocities noted in Table VIII. The experimental temperature distributions corresponding to these burning velocities were found by interpolating between the data shown in Figures 15 through 19. A summary of the theoretical and experimental temperatures is shown in Table VIII. It may be observed that in general the agreement is quite good. However, it also should be noted that in most cases the calculated temperatures exceed the experimentally determined temperatures. This may be explained by the difficulty in experimentally bringing the temperature of thermocouples in a partically transparent, low-velocity gas stream up to the temperature of the gas. As indicated earlier from a rough calculation, the experimental values could be low by as much as 50 to 200°F. This would account for the pattern of the discrepancies shown in Table VIII.

The first step in the evaluation of the irradiation to the meters was the substitution of the gas temperature into Eq. 38 and replacement of the term ℓ by the distance of the meter (see Figure 13) from the base of this chamber. The irradiation was evaluated by numerical integration of the expression over the several increments of gas. The values of irradiation were then substituted into Eq. 40, to determine the temperatures of the meters for the several meter

Table VII

SUMMARY OF ANALYTICAL RESULTS

Pressure, Atmospheres	Mass Flow, lb/ft^2 hr	Burning Velocity, ft/hr	Temperature of Foam, °R	Heat Flux Conducted to Explosive, B/ft^2 hr	Heat Flux Radiated to Explosive, B/ft^2 hr	Total Heat Flux to Explosive, B/ft^2 hr
1.0	263	2.5	1004	25,000	42,500	67,500
1.5	578	5.5	1024	38,600	116,800	155,400
2.0	961	9.15	1035	67,200	202,800	270,000
5.0	2546	24.25	1060	142,500	627,500	770,000

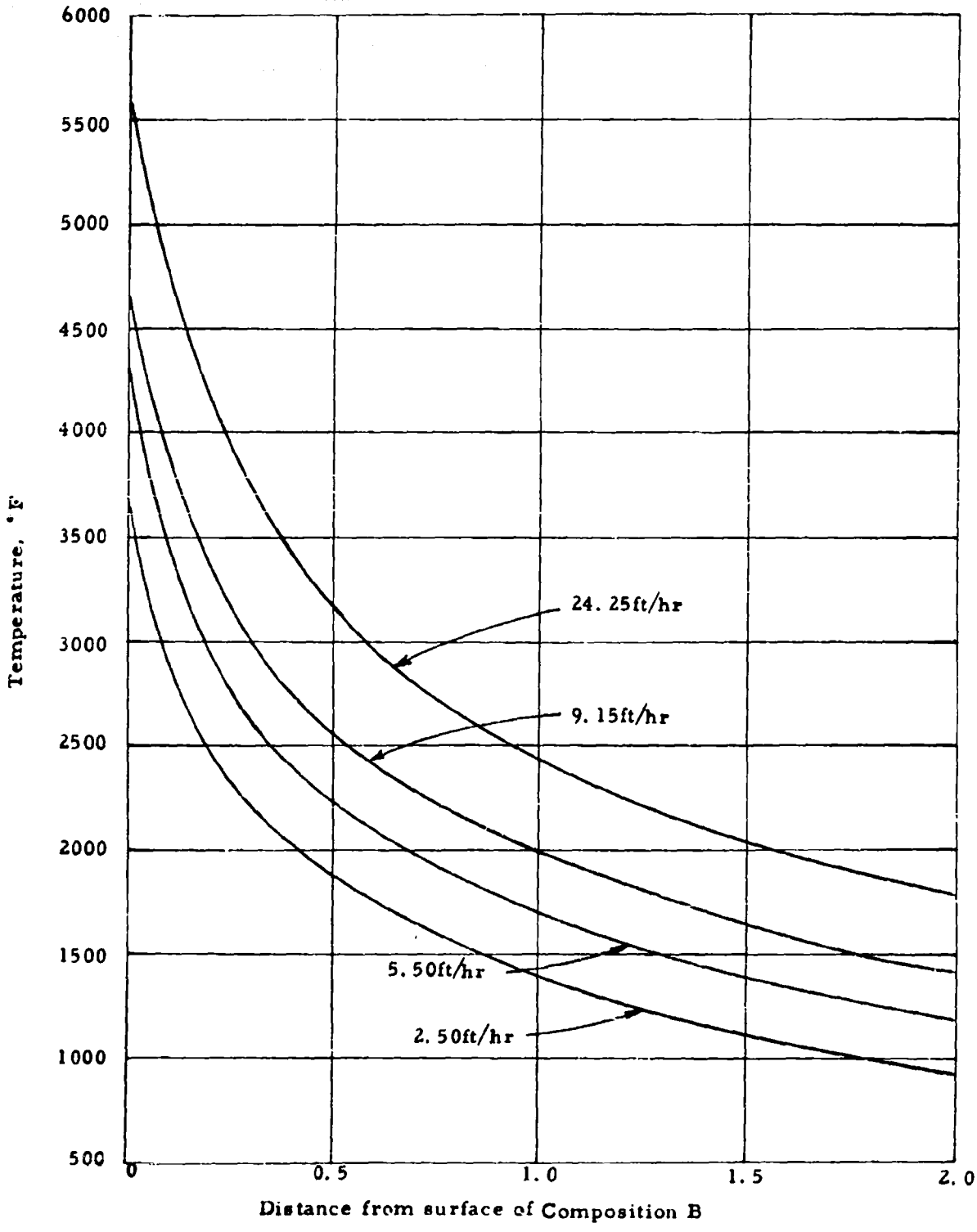

Fig. 29 GAS TEMPERATURE (COMPOSITION B)

Table VIII

GAS TEMPERATURES (COMPOSITION B)

Burning Velocity, ft/hr	Distance from Explosive, ft	Temperatures of Gas, °F	
		Experimental*	Calculated
2.5	1.4	1090	1140
	1.6	1040	1050
	1.8	990	980
	2.0	960	910
3.5	.6	1590	1860
	.8	1450	1650
	1.0	1320	1500
	1.2	1210	1350
	1.4	1110	1250
	1.6	1040	1160
	1.8	1000	1080
	2.0	970	1000
5	.8	1750	1830
	1.0	1510	1660
	1.2	1310	1520
	1.4	1170	1410
	1.6	1080	1300
	1.8	1020	1220
	2.0	990	1140
7.5	1.4	1490	1610
	1.6	1350	1500
	1.8	1250	1400
	2.0	1180	1320
10	1.6	1580	1650
	1.8	1450	1550
	2.0	1370	1460

*See Figures 15 through 19.

locations and burning velocities. These temperatures are presented in Table IX. The experimental results were obtained from the curves shown in Figure 20 to 23. When the accuracy of the meter temperatures is considered, it may be observed that the agreement is very satisfactory.

Another means of checking the theory is to compute the temperature distribution along the length of the chamber (see Figure 1) and compare it to the experimental distribution shown in Figure 25. This computation is much more complex than the preceeding ones due to the fact that the heat flux must be calculated for a number of increments of the chamber. In addition, allowance must be made for the fact that the burning front is moving, causing a shift of the gas temperatures with respect to the chamber. Allowance must also be made for the conduction of heat along the length of steel wall of the chamber during and after the burning.

The irradiance of the elements of the chamber was calculated by first modifying Eq. 27. This equation represents the rate of heat loss from a particular gas element to the total curved surface of the chamber. For purposes of the computation, it is necessary to determine the total heat loss from all the gas elements to a particular ring-shaped element of the chamber wall. If the height of each chamber element and the thickness of each gas element are represented by $\Delta z'$ and Δz (see Figure 9), then by manipulation of Eq. 27

$$\Delta q''_r = T^4_g(z) \frac{\partial P(z', a, \beta' P_g)}{\partial z'} \Delta z \Delta z' \tag{53}$$

This represents the radiation which is emitted by a gas element and is incident on a chamber element that is located at a distance z' from the gas element. To find the total radiation incident on the chamber element it is necessary to integrate this expression over the several gas elements. If b and ℓ are used to represent the distances of the chamber element and top of the chamber from the surface of the high-explosive and all quantities such as z', z, b and ℓ are taken as positive, then

$$\Delta q''_r = \left\{ - \int_0^b T^4_g(z) \frac{\partial P}{\partial z}(b-z, a, \beta' P_g) \, dz + \int_b^\ell T^4_g(z) \frac{\partial P}{\partial z}(z-b, a, \beta' P_g) \, dz \right\} \Delta z' \tag{54}$$

Table IX

METER TEMPERATURES (COMPOSITION B)

Burning Velocity, ft/hr	Distance from Explosive, ft	Temperature of Meter, °F	
		Experimental*	Calculated
3.5	0.42	1100	990
	0.82	780	730
	1.22	550	580
5.0	0.42	1200	1160
	0.82	890	890
	1.22	640	720
7.5	0.42	1480	1390
	0.82	1040	1090
	1.22	800	900
10.0	0.82	1220	1240
	1.22	930	1030

*See Figures 20 through 23

This represents the total radiation incident on a chamber element that has a thickness $\Delta z'$ and is located a distance b from the high-explosive. In this analysis it was assumed that all radiation was absorbed by the chamber since the walls were blackened by the soot. Also, the emission of radiation from the surface of the chamber was neglected. Convection may be accounted for by computing the heat transfer coefficient, h, from McAdams [9] and applying the standard relationship of

$$\Delta q''_c = h(T_g - T_w)\, 2\pi a \Delta z' \tag{55}$$

Where T_w represents the wall temperature.

Due to the approximate nature of the evaluation of the heat transfer coefficient, the value of h was considered constant along the length of the chamber for each of the several burning rates. The values ranged from 1 to 7 $B/ft^2\ hr^\circ R$.

In addition to the radiant and convective heat fluxes from the gas each element of the chamber either gains or loses heat due to heat conduction along the length of the steel wall. This heat flow may be represented by the following finite difference equation

$$\Delta q''_{cond} = -K_{stl} \frac{\partial T(z')}{\partial z'} \pi d\,(2a + d)\Delta z' \tag{56}$$

where

K_{stl} = thermal conductivity of steel.

As a result, the rate of change in temperature, ΔT, of a given element of the chamber may be determined by the following equation:

$$\rho_{stl} C_{stl}\, \pi d(2a + d)\Delta z' \frac{\Delta T}{\Delta t} = \Delta q''_r + \Delta q''_c + \Delta q''_{cond} \tag{57}$$

where

C_{stl}	=	specific heat of steel, $B/lb^\circ R$
ρ_{stl}	=	density of steel, lb/ft^3
d	=	thickness of steel wall, ft
a	=	radius of chamber, ft
$\Delta z'$	=	height of element of chamber, ft
Δt	=	increment of time, hr

The specific heat of the steel was varied with temperature in accordance with the values shown in Table VI while the thermal diffusivity, i.e., $\frac{K_{stl}}{\rho_{stl} C_{stl}}$ was maintained at a value of $0.52\ ft/hr^2$.

The calculated and experimental temperature rises of the chamber are shown in Tables X and XI at 10 and 20 minutes following the start of burning of a 4-inch-long cylinder of Composition B at the base of the chamber. It may be observed that the agreement between the temperature near the base of the chamber is poor while the agreement is reasonably good at distances in excess of about 0.6 feet from the base. The low experimental temperatures near the base of the chamber are attributed to the presence of the thermal barrier effected by a 0.050-inch-thick coating of Adiprene over the lower 4 inches of the chamber. This layer of Adiprene was bonded both to the chamber and to the high-explosive to prevent burning along the sides of the Composition B cylinder.

One of the most useful predictions evolved by this theory is the minimum size of the vent hole which will prevent a significant pressure buildup. The pressure within the chamber can be maintained at relatively low levels if the rate of mass flow through the vent hole is sufficient to counteract the flow of gas evolved by the burning explosive. To determine whether or not this condition is satisfied requires an evaluation of the rates at which gas escapes through vent holes of various sizes. This evaluation may be accomplished by use of the following two equations[10] describing the rate of mass flow W' through a vent hole which presents a throat area of A_t. For subsonic flow through the throat

$$W' = \frac{\sqrt{2\,gJ}}{R_g} A_t P_c \left\{ \frac{C_p}{T_c} \left[\left(\frac{P_t}{P_c} \right)^{2/k} - \left(\frac{P_t}{P_c} \right)^{\frac{k+1}{k}} \right] \right\}^{1/2} \tag{58}$$

for sonic flow

$$W' = A_t P_c g \left\{ \left(\frac{2}{k+1} \right)^{\frac{k+1}{k-1}} g R_g T_c \right\}^{1/2} \tag{59}$$

where

W' = rate of mass flow through vent hole, lb/hr

g = gravitational constant = 4.15×10^8 ft/hr^2

J = mechanical equivalent of heat = 778 ft-lb/B

T_c = temperature of gas at entrance of vent hole, °R

R_g = gas constant, ft-lb/lb°R

P_c = pressure within chamber, lb/ft^2

P_t = pressure at throat, lb/ft^2

k = ratio of "specific heat" at constant pressure to the "specific heat" at constant volume

C_p = "specific heat" at constant pressure, B/lb°R

Table X

TEMPERATURE RISES OF CHAMBER AT 10 MINUTES AFTER START OF BURNING COMPOSITION B

Distance from Base of Chamber, ft	Experimental Temperature Rise, °F	Calculated Temperature Rise, °F
0	405	885
0.2	495	861
0.4	590	791
0.6	625	686
0.8	570	567
1.0	475	455
1.2	390	359
1.4	305	284
1.6	255	232
1.8	215	202
2.0	195	192

Table XI

TEMPERATURE RISES OF CHAMBER AT 20 MINUTES AFTER START OF BURNING COMPOSITION B

Distance from Base of Chamber, ft	Experimental Temperature Rise, °F	Calculated Temperature Rise, °F
0	470	730
0.2	490	718
0.4	510	682
0.6	510	627
0.8	490	561
1.0	440	490
1.2	385	422
1.4	350	363
1.6	285	318
1.8	250	290
2.0	225	280

In this analysis, the throat area and pressure will be taken as equal to the cross-sectional area of the vent hole and the environmental pressure, respectively. It may be observed that in a given external environment, the flow is a function of the pressure within the chamber and the temperature of the gas just prior to entering the vent hole. If uniform flow through the chamber is assumed, the gas temperature may be fixed by a specification of the pressure, the rate of burning, and the distance between the high-explosive and the vent hole. From this information the gas temperature may be found from the data shown in Table VII and Figure 29. In order to determine the flow escaping through a vent hole, it is first necessary to determine whether the flow is subsonic or sonic. This may be determined by the following equation[10]

$$\left(\frac{P_t}{P_c}\right)_{max} = \left(\frac{2}{k+1}\right)^{\frac{k}{k-1}} \tag{60}$$

The values of k are shown as a function of gas temperature in Table IV. The temperature of the gas entering the vent hole will range from 1370 to 5240°R for Composition B with vent-hole distances between 0.1 and 2.0 feet and with chamber pressures between 1 and 5 atmospheres. These temperatures will yield values of k ranging from 1.13 to 1.36. Substitution of these values into Eq. 60 yields chamber pressures of 1.73 and 1.87 atmospheres. Therefore, for chamber pressures below about 1.73 atmospheres the flow will be subsonic and the use of Eq. 58 is indicated. Chamber pressures above 1.87 atmospheres will produce sonic flow at the throat and the use of Eq. 59 will be required.

The gas temperatures for each of the several cases were obtained from the data shown in Table VII and Figure 29. The dependence of R_g and k on temperature may be found in Table IV while values of "C_p" may be determined from the slopes of the enthalpy temperature curve shown in Figure 5. The mass flow was determined for the various pressures, distances, and vent sizes by substitution of appropriate values either into Eq. 58 if the flow is subsonic or into Eq. 59 is the flow is sonic. The results are shown as dashed curves in Figures 30 through 32. The solid curve in each figure refers to the rate at which gas is evolved by the burning Composition B. By comparing the figures, it may be observed that the critical size of the vent hole (for which the inlet flow generated by the burning explosive is always equal to or greater than the exit flow passing through the vent) increases from 0.28 to 0.31 to 0.35 inch as the distance of the hole from the explosive decreases from 2.0 to 0.5 to 0.1 feet. With the larger hole sizes shown in the figures, the inlet and outlet flow would tend to stabilize at chamber pressures between 1.1 to 1.2 atmospheres and result in mass flows of about 30 to 40 lb/hr. This range of mass flows corresponds to burning velocites between 3.3 and 4.4 ft/hr and is consistent with the burning velocities of about 3.5 ft/hr that were encountered in tests in which the Composition B

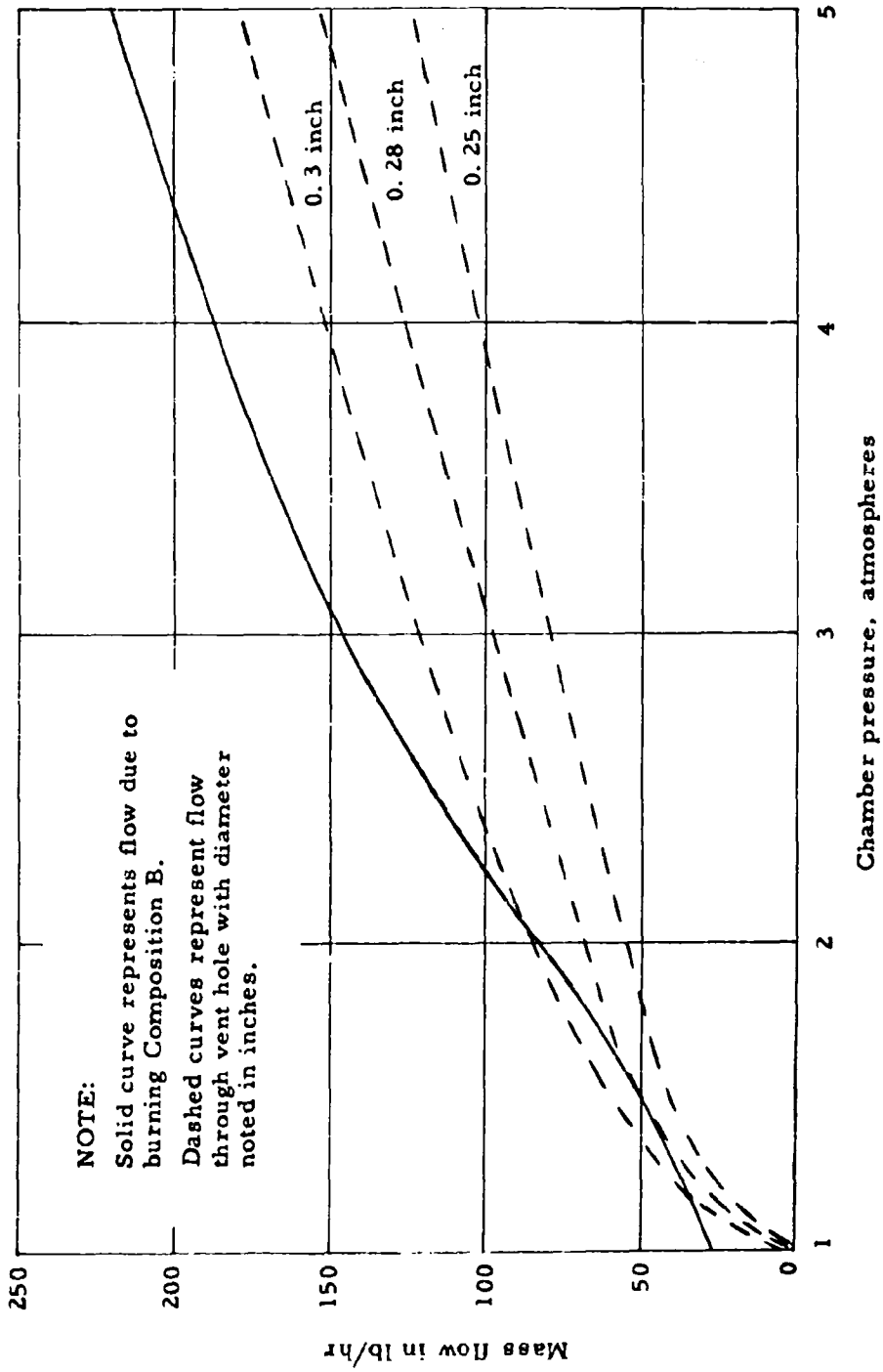

Fig. 30 INLET AND EXIT MASS FLOW TO CHAMBER (DISTANCE-COMPOSITION B AND VENT - 2FT)

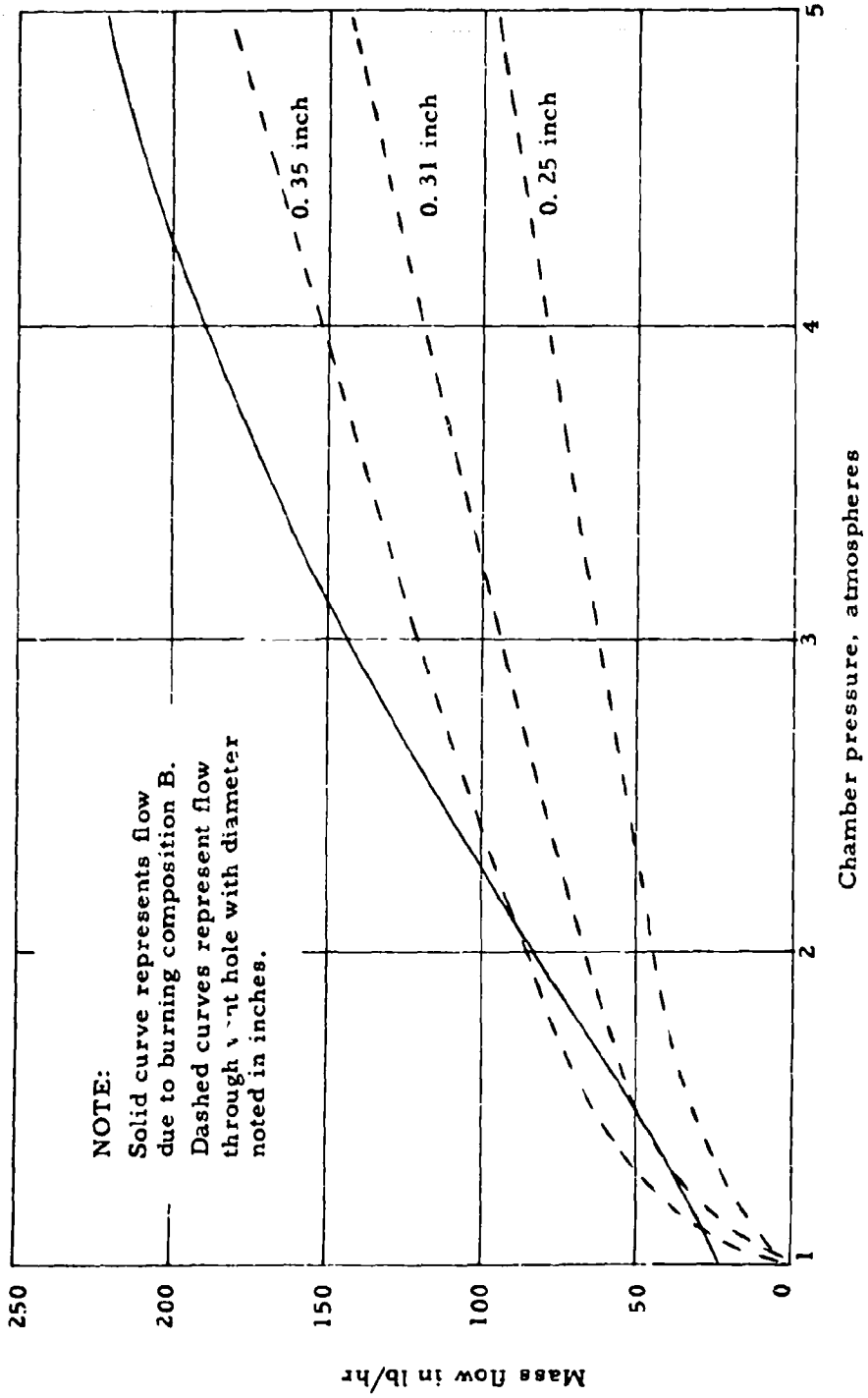

Fig. 31 INLET AND EXIT MASS FLOW TO CHAMBER (DISTANCE-COMPOSITION B AND VENT - 0.5 FT)

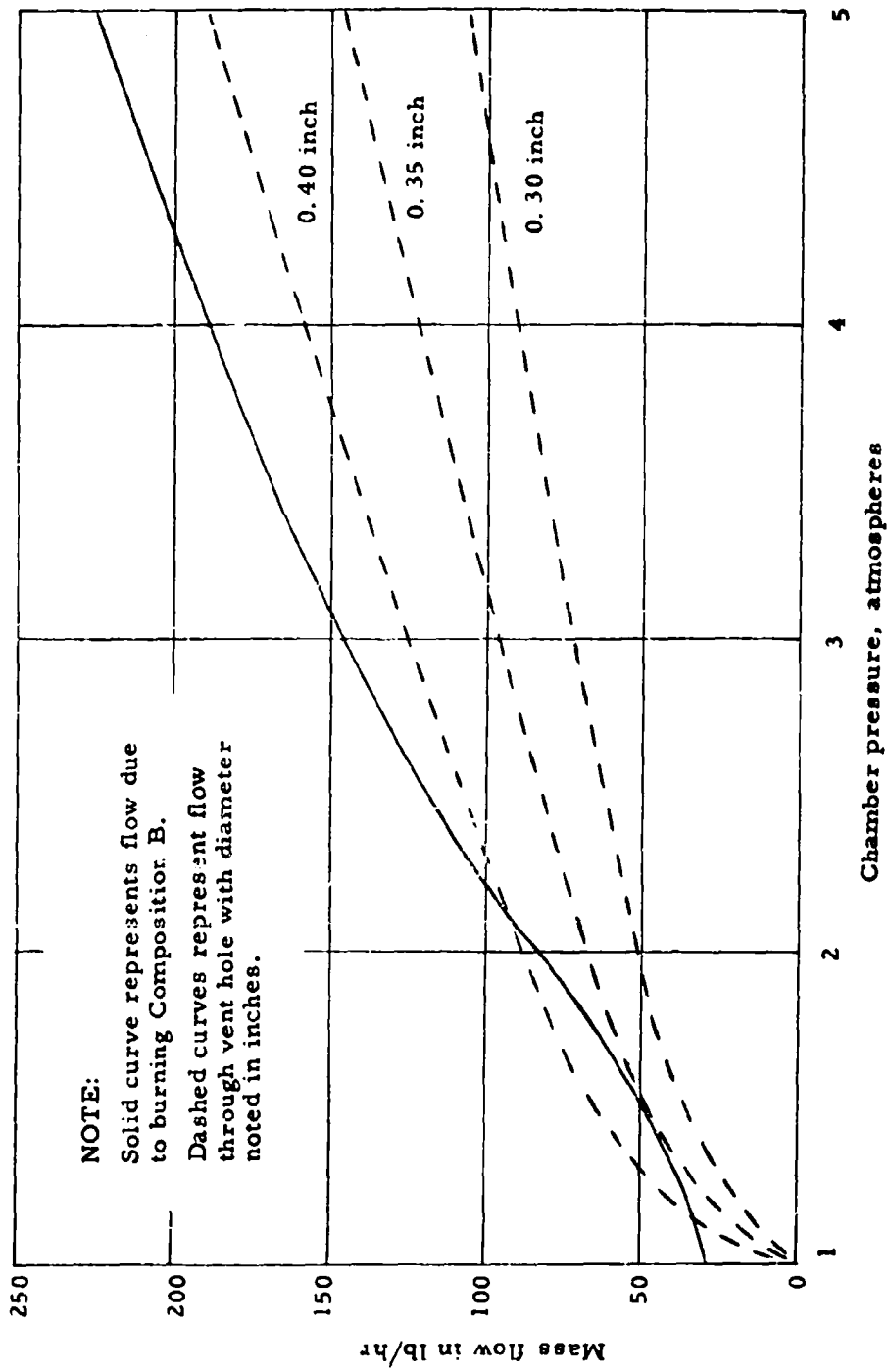

Fig. 32 INLET AND EXIT MASS FLOW TO CHAMBER (DISTANCE-COMPOSITION B AND VENT - 0.1 FT)

burned uneventfully. In addition, the chamber pressures are in agreement with the values indicated above. During these tests, it was frequently observed that the gas and smoke escaped in a pulsating manner. This may be attributed to pressure oscillations about the pressure indicated by the first intercept of the dashed curve with the solid curve. It may be observed that if the pressure is lower than this value the flow from the burning Composition B will exceed the flow escaping through the vent hole. The reverse is true if the pressure exceeds this value. In either case, the pressure will tend to move towards the value indicated above. This could cause oscillations of the pressure and burning rate which would explain the puffs of escaping gas and smoke. The amplitude of the pressure oscillations must have been less than about 0.1 atmospheres since no oscillations were detected by a catenary type pressure gage whose sensitivity was about 0.1 atmosphere. The experimental data shown in Figure 24 also provide a check on the results. Those data indicate that the critical diameter of the vent hole associated with the 2 foot chamber shown in Figure 13 lies between 0.222 and 0.304 inch, and is in good agreement with the value of 0.28 inch shown in Figure 30.

As noted previously the pressure may be maintained at tolerably low levels by use of vent holes whose diameters exceed the critical values of 0.28 to 0.35 inch associated with vent-explosive distances of 0.1 to 2.0 feet, respectively. The cross-sectional areas of these holes are equivalent to 0.49 to 0.77 percent of that of the burning surface. It may be observed that the critical area of the vent hole will increase according to the proximity of the vent hole to the explosive. Except for minor differences, these data may be applied to systems employing Cyclotol type explosives for which the burning rate and gas temperatures are nearly the same as those for Composition B. If these data are to be applied to larger systems, such as actual weapon systems, care should be taken to provide adequate coverage of the pressure hull with the vent holes to ensure that no significant pressure gradients develop as a result of internal resistances to gas flow.

(2) Preliminary Analysis of the Effects of Burning PBX 9404 Under Low Pressures

As was noted in Section 3, PBX 9404 burns approximately twice as fast as Composition B at atmospheric pressures. The faster burning rate is attributed to the fact that PBX 9404 reacts more completely than Composition B. This results in higher gas temperatures and hence, higher radiant fluxes to the explosive.

Unfortunately, due to the lack of strand burn data for either PBX 9404 or HMX which is its major constituent, it was not possible to accurately determine the heat flux to this explosive due to conduction. For this reason, the study was confined to a preliminary examination of the heat flux based on the temperatures of the gas and of the chamber shown in Figure 1. This analysis indicates that the value

of β_g' is close to 0.47×10^{-4} ft^2 cm°R/ft-lb, while the rate of conductive heating at a pressure of 1 atmosphere is in the neighborhood of 75,000 B/hr-ft^2. The fact that the value of β_g' is appreciably less than the value for Composition B, i.e., 2.83×10^{-4}, indicates that the flames from PBX 9404 are much cleaner and transparent than those of Composition B. This is consistent with the observation that the burning of Composition B results in considerably more soot than the burning of PBX 9404.

4. BURNING OF COMPOSITION B AND PBX 9404 UNDER HIGH PRESSURES

The experimental studies were performed by burning Composition B and PBX 9404 under pressures ranging from one to several thousand atmospheres. In addition, an analysis was conducted to predict the pressure using the theoretical and experimental results discussed previously. The purpose of this work is two-fold: first to see if it is possible to predict the transient pressure rises during normal burning; and second, to search for analytical criteria which could be used to predict the type or order of explosion which may occur. The first objective was successfully accomplished and the second objective was only partially successful.

The remainder of this section will discuss the results of the experimental work and will present an analytical means of predicting the pressure history during normal burning.

a. Experimental Results from High Pressure Burning of Composition B

This section will cover the burning of Composition B under pressures up to several hundred atmospheres. The pressures were obtained by burning the high-explosive in tubular chambers which were sealed to prevent gas leakage and which were strengthened to maintain pressures of the order of 100 atmospheres. A sketch of the chamber assembly is shown in Figure 33. Photographs of one of the steel chambers are shown in Figures 34 and 35. The space of about 0.05 inches between the Composition B and the wall of the chamber was sealed with Adiprene to prevent ignition of the sides of the Composition B cylinder by exposure to the hot gas. The diameter of the rods and the thickness of the cover plates were increased above the values used in the low-pressure chamber shown in Figure 13 to cause very violent explosions or low order detonations. During assembly of the chamber, the rods were elongated to within 70 percent of their yield strength in order to retain the cover plates for as long as practical. This was accomplished by measuring the elongation of the rods with a dial gage as torque was applied to the nuts. The upper face of the explosive was heated and ignited using the same technique illustrated previously for the low-pressure tests. This was assomplished by passing a current through the 122-watt heater shown in Figure 14 for a period of 10 minutes. This initiated melting of the surface of the Composition B. Ignition was accomplished by passing a current of 10 amperes through a 0.56-ohm wire which was located in a shallow groove across the face of the Composition B. An average delay of 5.4 seconds was noted between the delivery of this current and the start of burning (detected by an abrupt decrease of the current through the igniter wire). Various types of ionization probes were used to measure the passage of the flame front across various

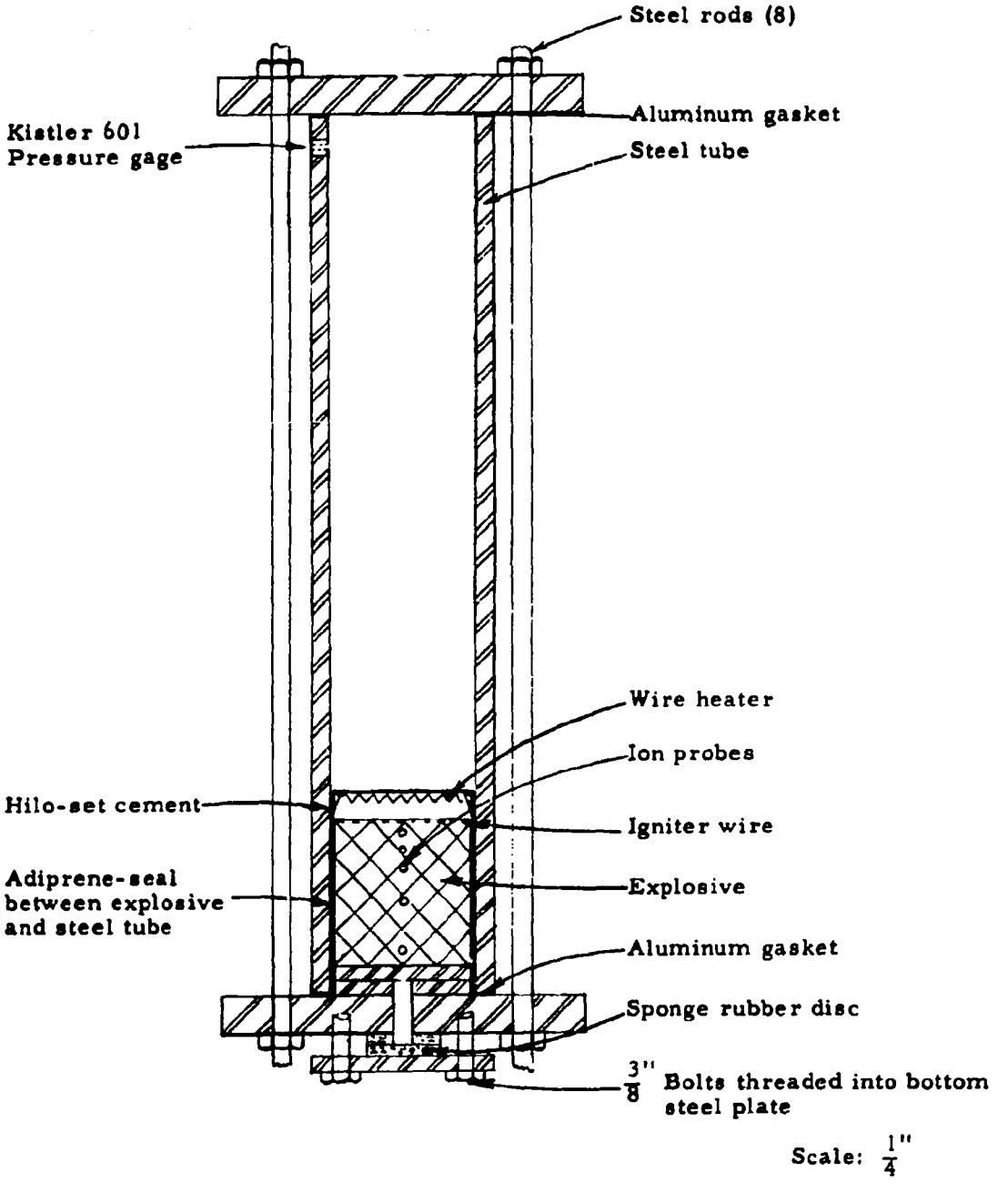

Fig. 33 CROSS SECTION OF "CLOSED" TEST CHAMBER

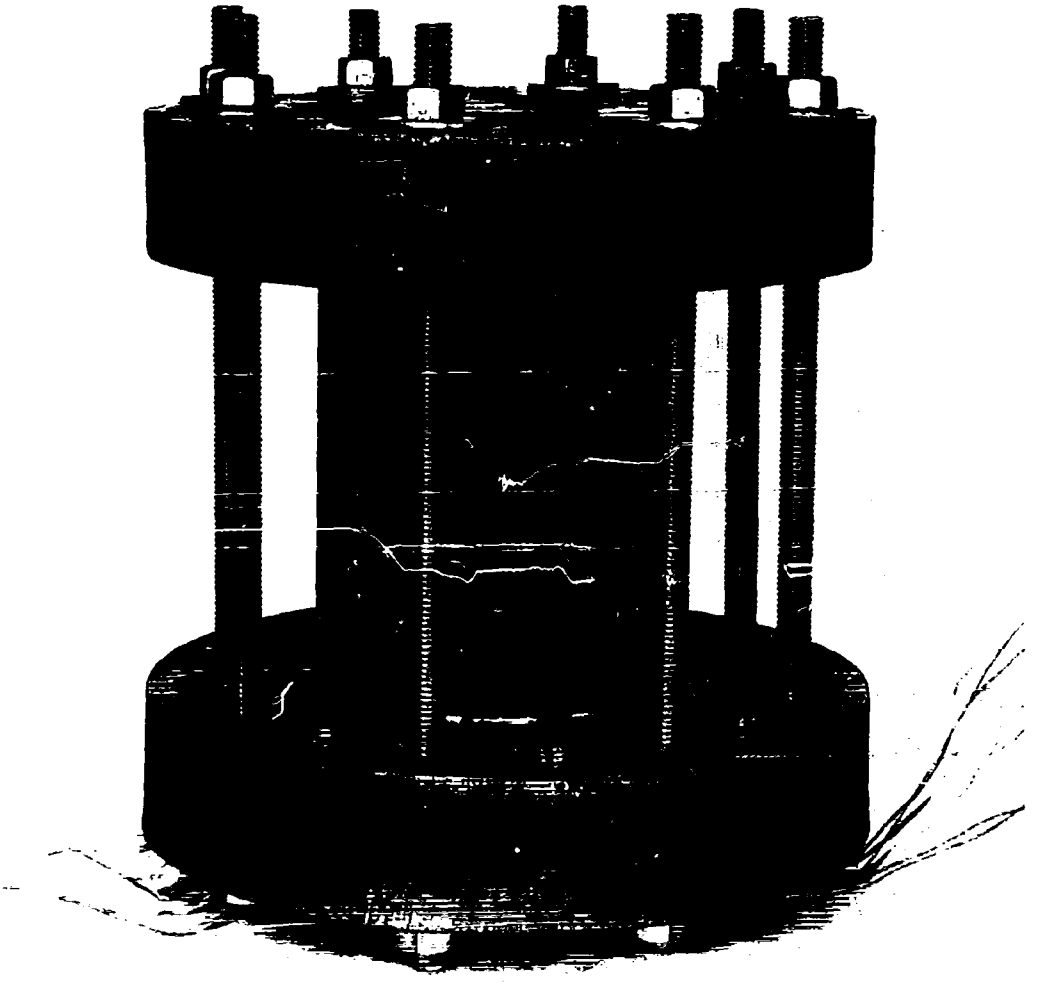

Fig. 34 SIDE VIEW OF "CLOSED" CHAMBER FOR HIGH-PRESSURE BURNING

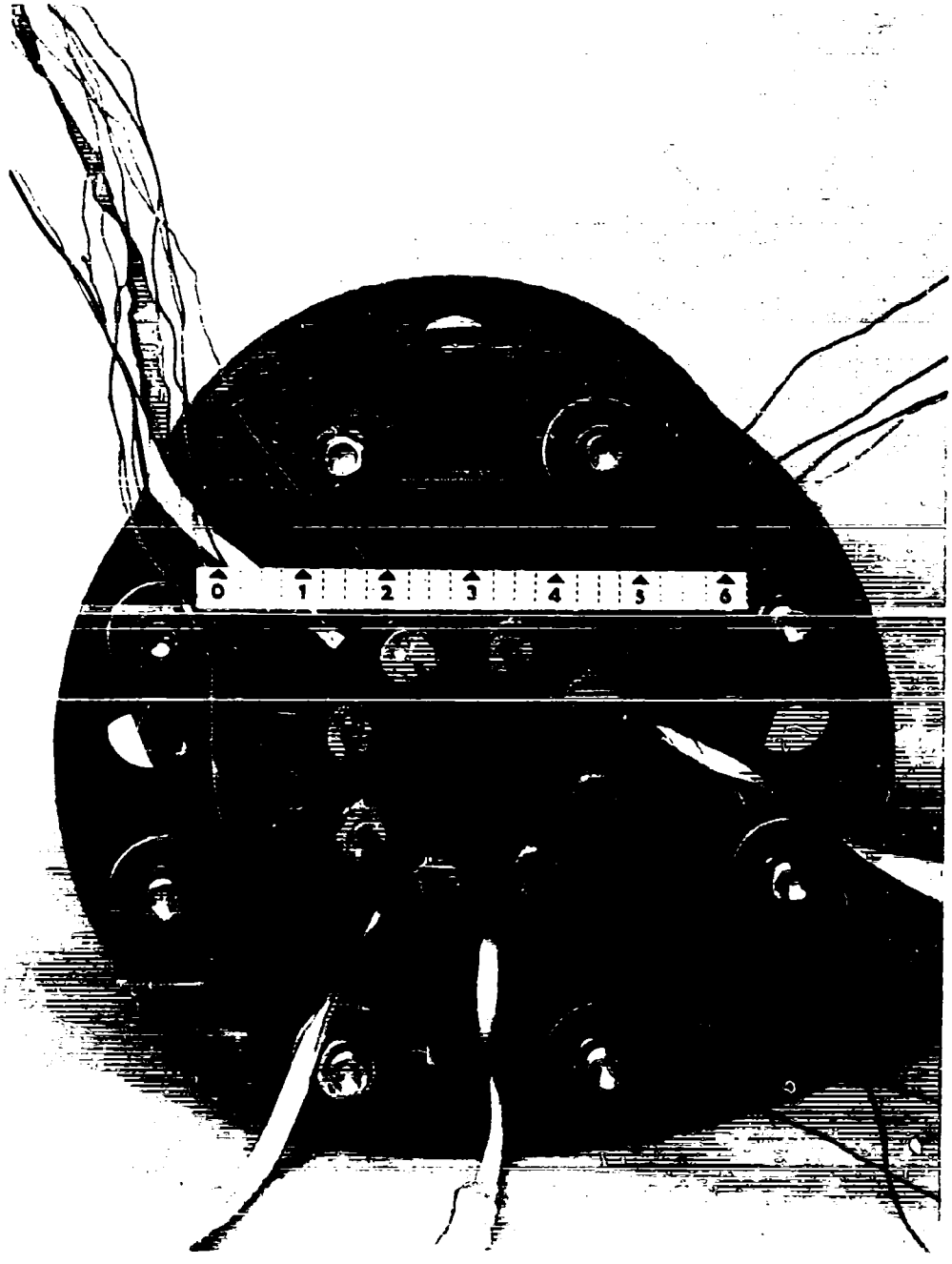

Fig. 35 BOTTOM VIEW OF "CLOSED" CHAMBER FOR HIGH-PRESSURE BURNING

points along the axis of the explosive. Sketches of two of the most commonly used probes are shown in Figures 36 and 37. The probes were inserted into the Composition B through small holes in the chamber wall. The technique of positioning the probes and sealing the holes is illustrated in Figure 38. This figure also contains a sketch which shows the method used to mount a Kistler pressure gage in the wall of the chamber.

During the course of this work, a total of 30 tests were conducted in which the distance between the explosive and the top of the chamber was varied from 1/4 to 31 inches while the minor diameter of the rods was varied from 0.19 to 0.85 inches. Two types of burning were noted which were distinguished from each other by a marked difference in the rates of pressure rise within the chamber. Illustrations of this may be seen in Figures 39 through 41. These figures show the pressure histories of three tests in which the distance between the high-explosive and the lower surface of the top-cover plate was varied. The portions of the curves between 14.7 and about 65 psia were omitted due to the appreciable times required for this transition as compared to the time scales shown in the figures. In each case, it may be observed that the pressure built up relatively slowly to about 1000 psia and then rose very abruptly as evidenced by the discontinuity of the slope of the pressure-time curve. A similar anomaly was noted by Wachtell[3] with smaller (~ 1 inch diameter) Composition B samples at pressures of 4000-5000 psia. The portion of the pressure-time curve up to about 1000 psia is consistent with what would be expected if the burning is confined to the face of the Composition B cylinder. This will be illustrated in the next section. The very abrupt rise in pressure is attributed to an increase of the burning area caused by cracking of the explosive.

There are three pieces of evidence which indicate that the Composition B cracked. The most conclusive evidence is illustrated by a photograph of a number of pieces of Composition B shown in Figure 42. These pieces of explosive were recovered from a test in which the top cover plate was ejected and caused the burning to be extinguished due to the rapid decrease of gas pressure and temperature. The porous surfaces are those surfaces which were formed during burning and in the process of very vigorous reaction. It may be observed that this porous condition exists on irregular surfaces of practically all the pieces of Composition B and could happen only if the high-explosive cracked and exposed these surfaces to hot, high-pressure gas prior to ejection of the cover plate. The second piece of evidence that indicates the Composition B cracked is the random sequence in which the probes fired. This happened with each of the several types of probes. Extensive cracking of the high-explosive would result in random firing of the probes and appears to be the most likely cause of the irregular firing sequence. The last evidence which supports the theory of cracking is the apparent susceptibility of Composition B to thermal shock. The Composition B was stored

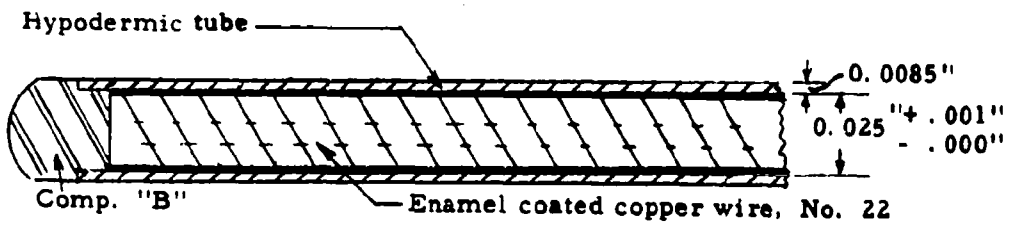

Type A

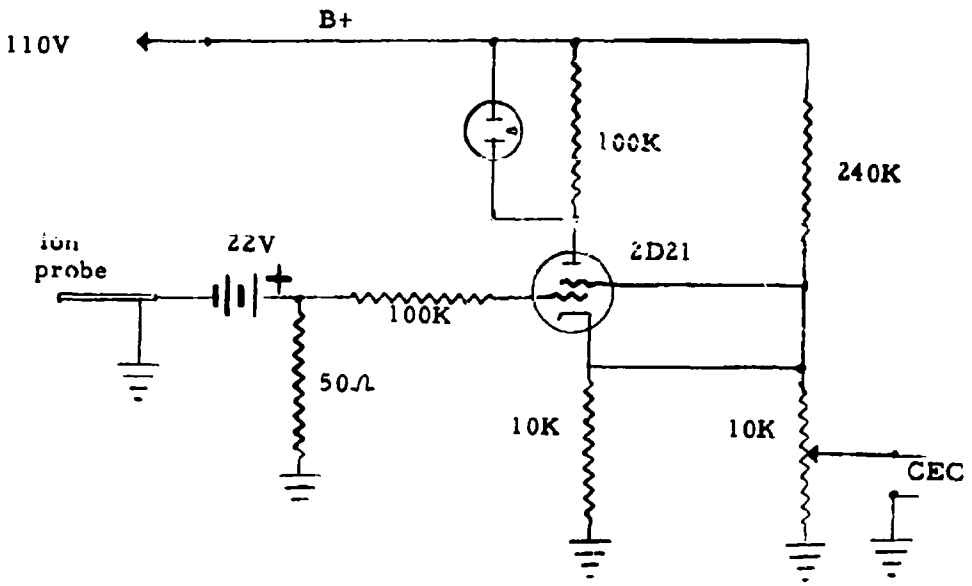

Fig. 36 TYPE-A ION PROBE AND ASSOCIATED CIRCUIT

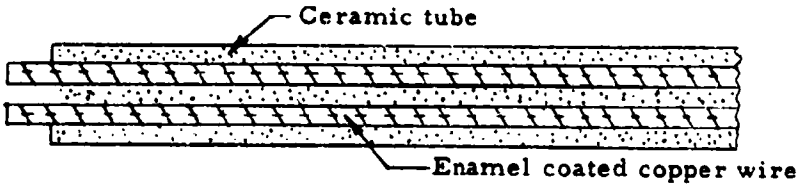

Type "B"

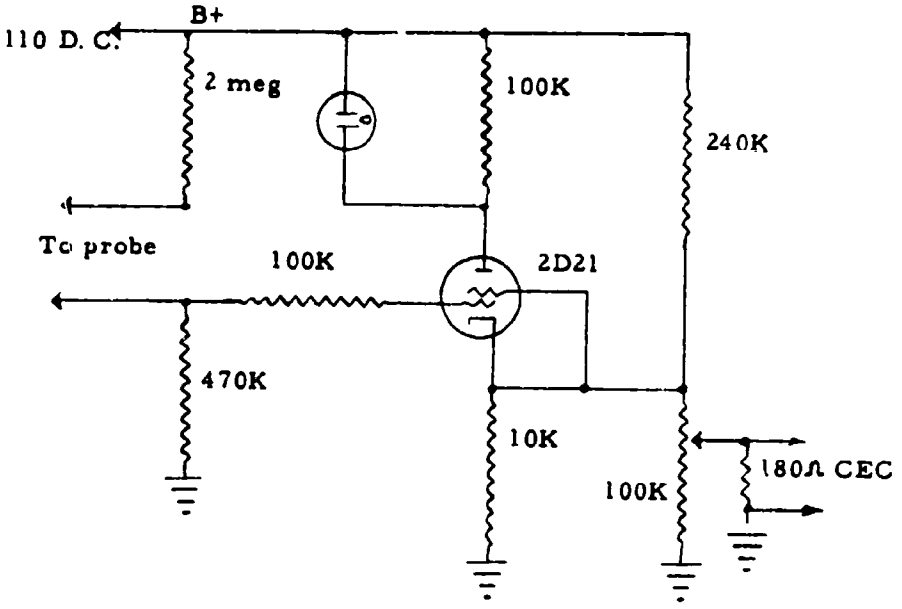

Fig. 37 TYPE-B ION PROBE AND ASSOCIATED CIRCUIT

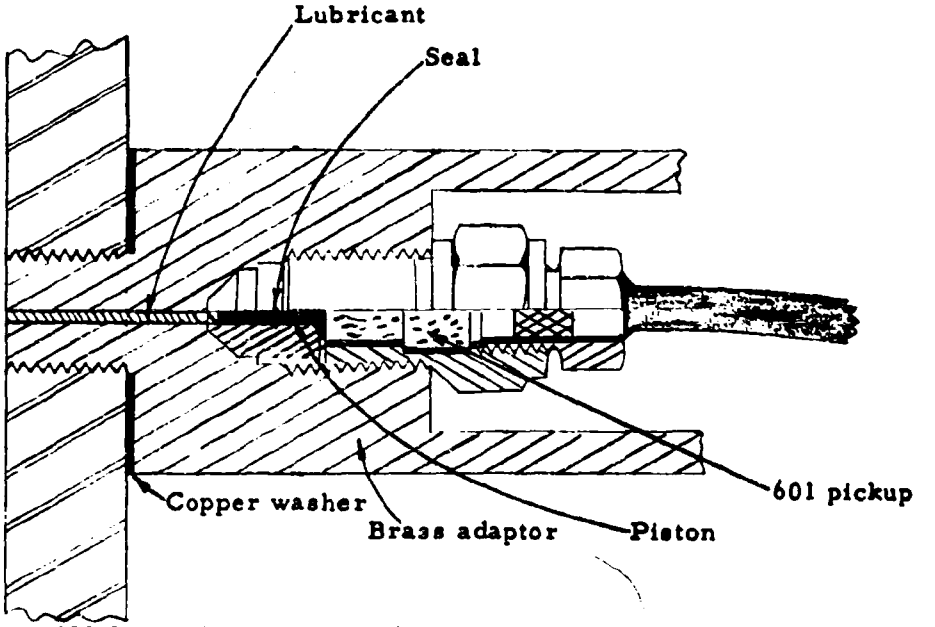

CROSS SECTION O. KISTLER PRESSURE PICKUP (601) MOUNTED INTO CHAMBER WALL

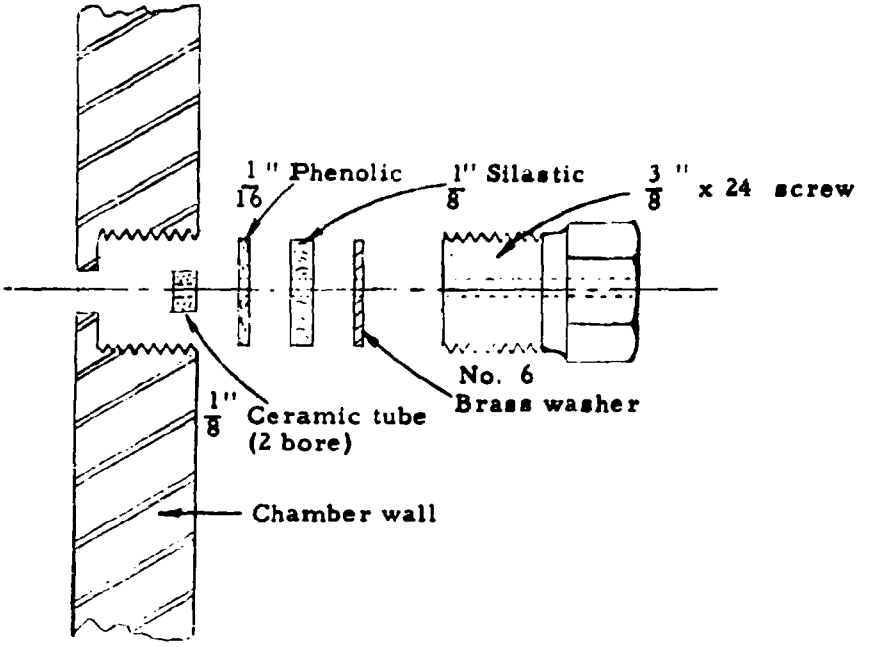

ASSEMBLY OF PRESSURE SEAL FOR THERMOCOUPLE LEADS

Fig. 38 METHOD OF INSERTING THERMOCOUPLES AND PRESSURE PROBE THROUGH CHAMBER WALL

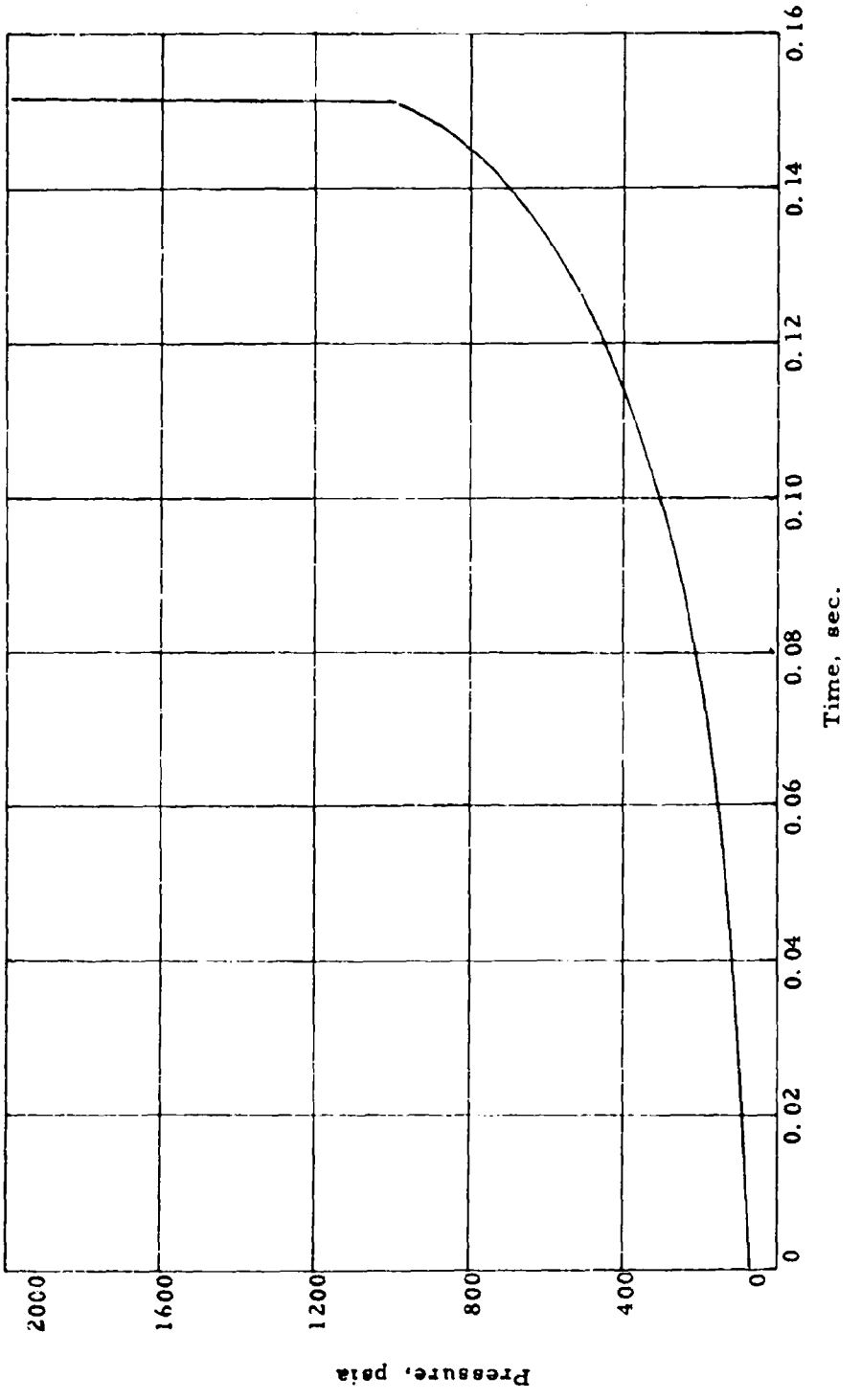

Fig. 39 PRESSURE TIME HISTORY (COMPOSITION B, ℓ = 1.75 inches)

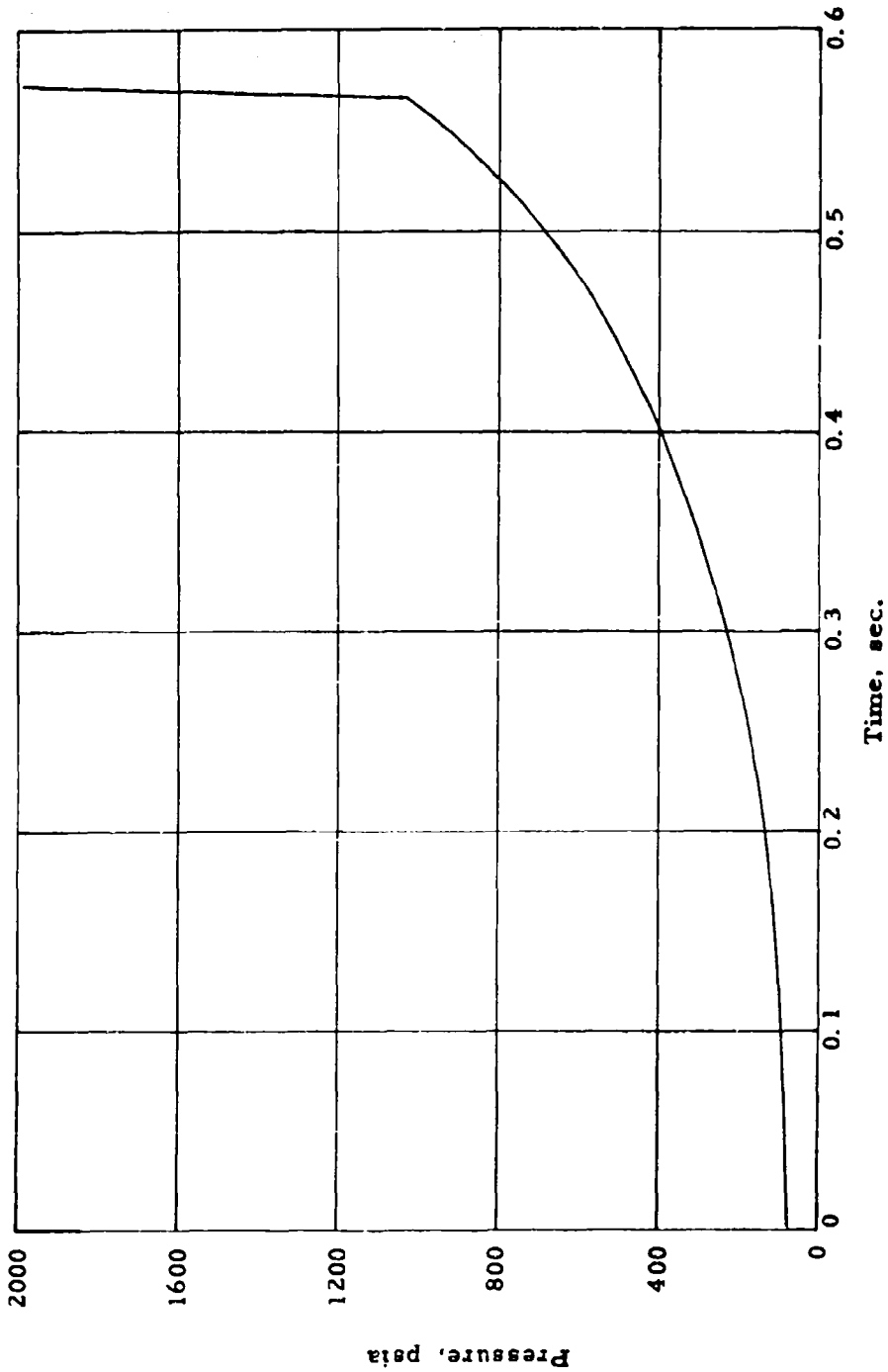

Fig. 40 PRESSURE TIME HISTORY (COMPOSITION B, ℓ = 8 inches)

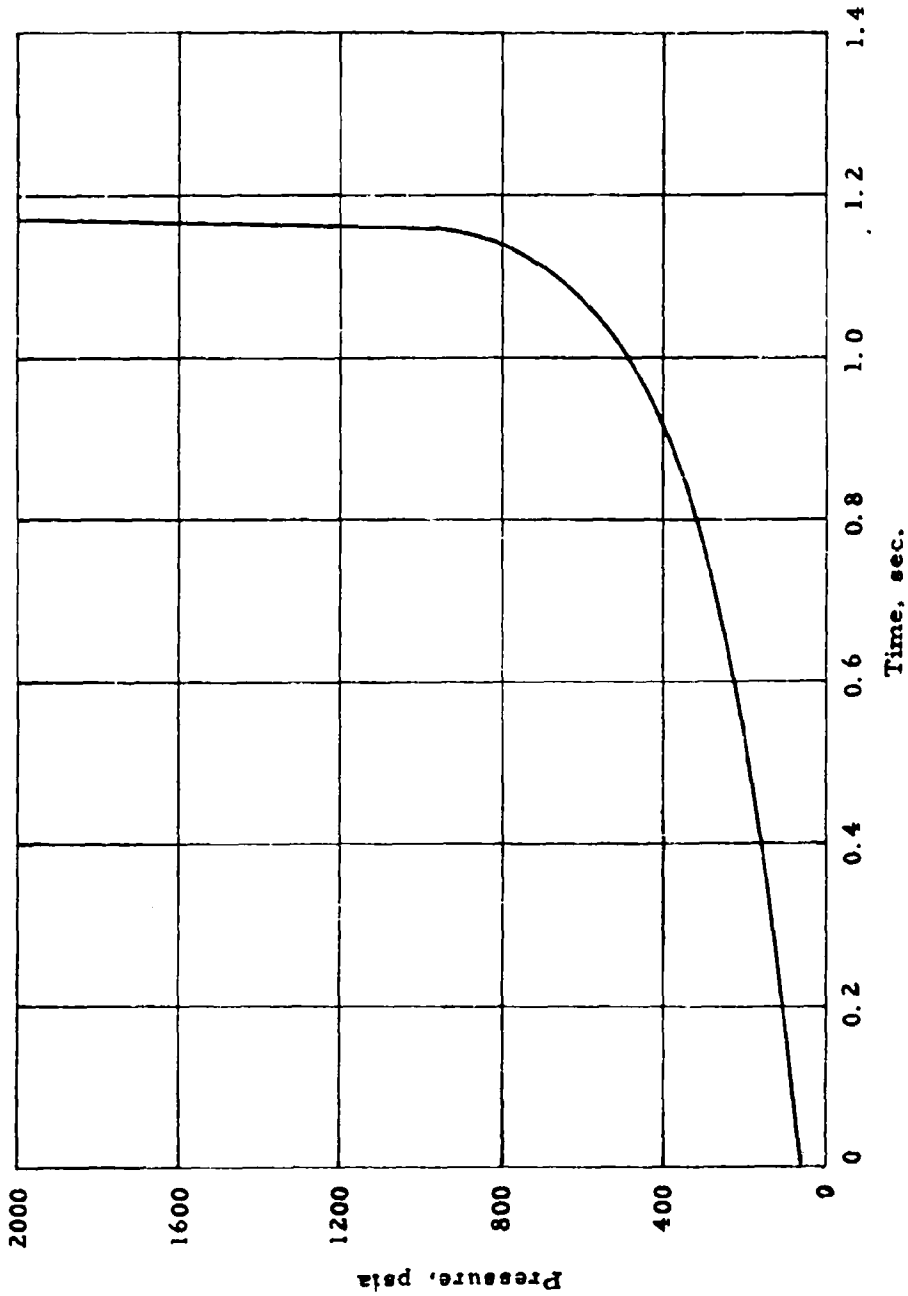

Fig. 41 PRESSURE TIME HISTORY (COMPOSITION B, ℓ = 17.75 inches)

Fig. 42 COMPOSITION B PIECES FOUND IN CHAMBER FOLLOWING EJECTION OF TOP COVER PLATE

in an igloo which often reached temperatures of 0°F or less. Upon exposure of the high-explosive to normal room temperatures, it commenced to emit audible cracking noises although no visual changes were discernable. When sawed, the Composition B cracked into a number of pieces. This gives an indication of the susceptibility of the explosive to thermal shock. During the burning, the solid explosive beneath the layer of foam is subjected to very appreciable temperature gradients. An appreciation of the magnitude of these temperature gradients may be gained by a consideration of their magnitude during constant-velocity burning. Under this condition, the temperature, T, of the solid Composition B may be described by [11]

$$T = (T_m - T_o) \exp -\left(\frac{u}{\alpha} x\right) + T_o \tag{61}$$

where

T_m = melt temperature of high-explosive, °F

T_o = initial temperature of high-explosive, °F

u = burning velocity, ft/hr

α = thermal diffusivity of solid high-explosive, ft^2/hr

x = distance from melt surface, ft.

The temperature gradient at the surface may be found by differentiating this expression with respect to x and setting $x = 0$ to yield

$$\frac{dT}{dx} = -(T_m - T_o) \frac{u}{\alpha} \tag{62}$$

From Table A-1, T_m and α are approximately equal to 176°F and .0044 ft^2/hr where the value of the thermal conductivity of Cyclotol 70/30 was used in the evaluation of α. Therefore, if the initial temperature of the explosive is 70°F, the temperature gradient at the surface is

$$\frac{dT}{dx} = -2.4 \times 10^4 u \tag{63}$$

Even for the lowest burning velocities of 2.5 ft/hr, the gradient is substantial, i.e., -6×10^4 °F/ft. The magnitude of the temperature gradient will increase in a linear fashion with the velocity of burning and probably contributes to the cracking. An exhaustive consideration of the problem of cracking is outside the scope of this investigation. Future studies are needed in this area.

The effect of the pressure rise on the chamber varied according to the strength of the weakest portion of the chamber, i.e., the 8 ordinary steel rods holding the cover plates. These tests were conducted utilizing rods with the following threads and minor diameters:

Thread Size	Minor Diameter
1/4 x 20	.189 inches
5/16 x 18	.244 inches
8/8 x 16	.298 inches
7/16 x 14	.350 inches
1/2 x 13	.406 inches
5/8 x 11	.514 inches
1 x 8	.847 inches

With small threaded rods having a minor diameter of 0.189 inches, the pressure reached levels of several hundred psia and raised the top cover plate by either elongating or breaking the rods. The smallest rod which caused destruction of the chamber had a minor diameter of 0.244 inch. This would indicate that the critical value of the minor diameter (which may or may not cause destruction of the chamber) lies somewhere between 0.189 and 0.244 inch. The static pressure which will cause separation of the cover plate from the steel tube for these two rod sizes is only slightly less than the dynamic pressure at separation and may be determined by the following equation

$$P_s = \gamma\sigma_y \left(1 + \frac{N\pi r_b^2}{A_c}\right) \frac{N\pi r_b^2}{A} \tag{64}$$

P_s = static pressure to cause separation of cover plate from steel tube, psia

γ = preload fraction of yield stress = .7 (dimensionless)

σ_y = yield stress of bolts = 75,000 psia

N = number of bolts = 8

r_b = minor radius of bolts, in.

A_c = area of tube face = 7.07 in.^{2}

A = area of cover plate subjected to gas pressure = 12.57 in.^{2}

Substitution of these quantities and the radius of the critical sizes of bolts into this equation indicates that the critical pressure necessary to initiate the destruction of the chamber lies somewhere between 960 and 1650 psia. This conclusion is reasonably consistent with the evidence which indicates that normal Composition B cracks during burning upon exposure to pressures in the vicinity of 1000 psia.

With the large threaded rods that had a minor diameter of 0.51 inch or greater, the chamber was always destroyed by the reaction. The damage varied from test to test with rods having intermediate diameters. In approximately 1/4 of the tests utilizing rods with minor

diameters of 0.24 to 0.51 inch, the chamber was destroyed. In the remaining tests, the damage was principally confined to the rods, even though the pressure exceeded 1000 psia or 68 atmospheres in each of these tests. This anomaly may be explained by variations in the extent of cracking of the explosive which resulted in significant variations in the increase of burning area and/or the development of high pressures or shocks between crevices. This of course, would cause variations in the violence of the explosions. Photographs of the remains of two chambers are shown in Figures 43 and 44. Figure 43 represents a plastic failure of the chamber in which the walls were thinned out and ruptured along lines extending along the length of the chamber. The damage was typical of the lower order explosions. The effects of a high order explosion are shown in Figure 44. This debris represents the remains of the chamber shown in Figures 34 and 35. The inner surface of a number of the pieces of the chamber were wrinkled as shown by the photographs at the bottom of Figure 45. This gives an indication of the violence of the explosion. The pressure within the chambers that were destroyed must have been considerably higher than the 1300 atmospheres required to cause plastic failure of the ordinary carbon steel tube under static loads. The relatively slow response time, i.e., 2.8 milliseconds, of the galvonometers in the CEC recorder did not resolve the high pressure portion of the curves, which included these peak pressures.

b. Experimental Results from High Pressure Burning of PBX 9404

Three high pressure tests were conducted using PBX 9404. Except for the omission of the heater which was not deemed necessary to initiate a vigorous burning, the tests were identical to those with Composition B. The chamber was 12 inches long in each of the three tests, and the rods had 1/4-20 and 3/8-16 threads. Within times of the order of milliseconds following the ignition of 5 inch long samples of PBX 9404, the pressure built up and destroyed the chamber and stand. A photograph of the remains of one of the chambers is shown in Figure 46. It may be observed that all components of the chamber were fractured and reduced to many more pieces than in the Composition B tests (see Figures 43 and 44). Plastic flow along the inner surface of the chamber was noted on a number of the pieces. These observations indicate that the reaction was a detonation.

Due to the wide variation in the rise times of the pressures, i.e., by a factor of at least 10, it is suspected that these samples cracked. This would account for large differences in burning since it would not be expected that each sample would crack in the same fashion. Unfortunately, due to the very rapid rise times relative to the response time of the CEC recorder it was not possible to discern if and when the slope of the pressure time curve exhibited a discontinuity which would indicate that the PBX underwent extensive cracking. It is recommended that any future studies involving PBX type explosives utilize much faster response instruments such as oscilloscopes to

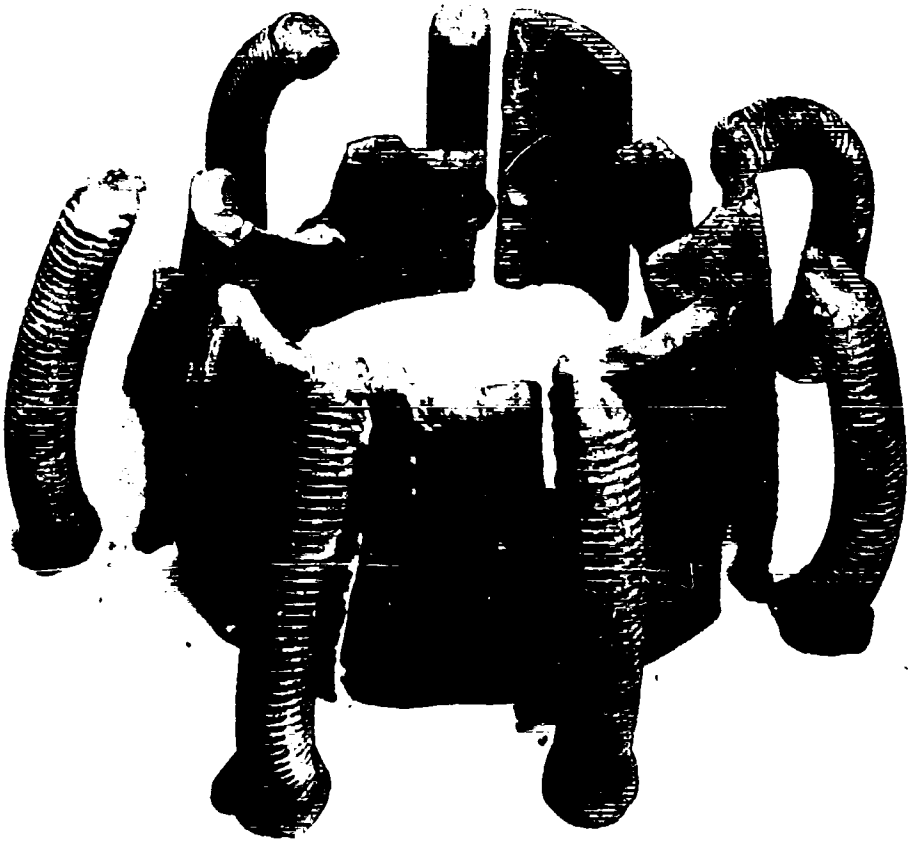

Fig. 43 PLASTIC FAILURE OF CHAMBER (COMPOSITION B)

Fig. 44 BRITTLE FRACTURE OF CHAMBER (COMPOSITION B)

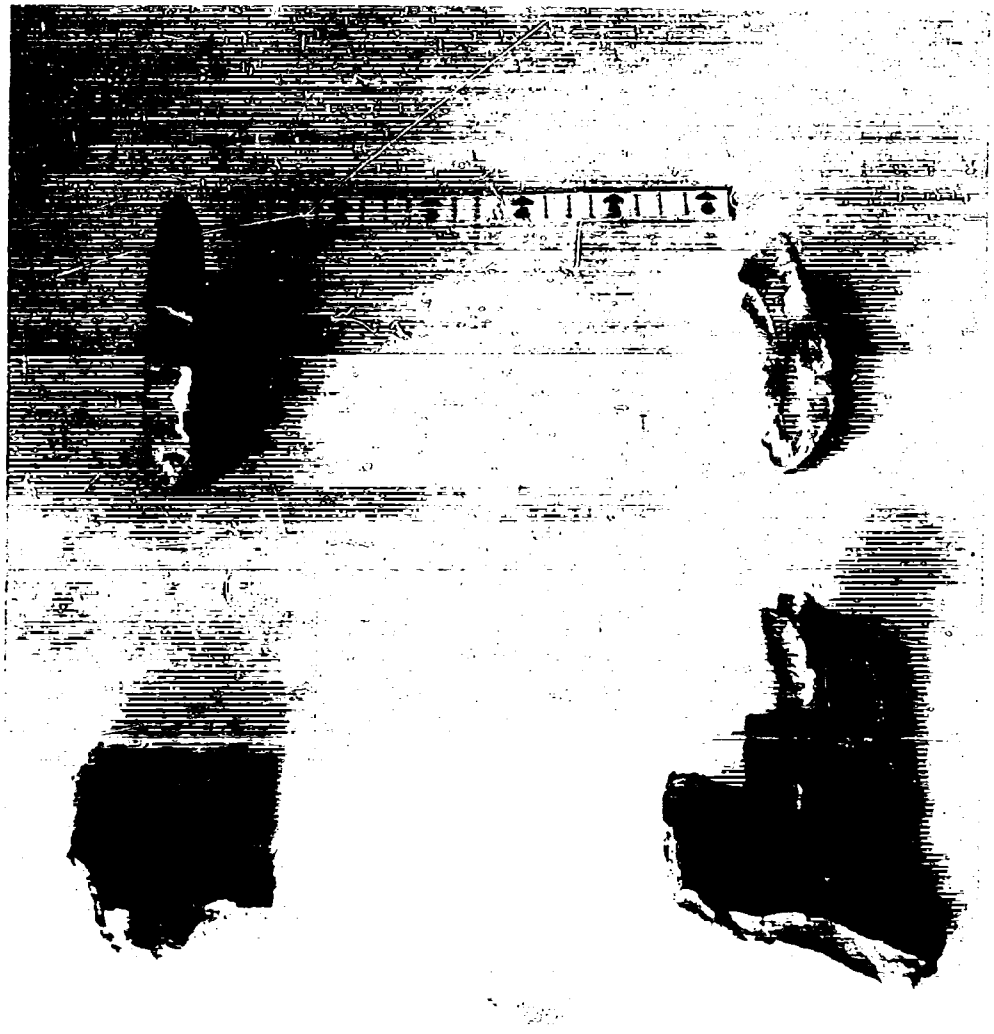

Fig. 45 EFFECT OF EXPLOSION ON INNER SURFACES OF CHAMBER (COMPOSITION B)

Fig. 46 REMAINS OF CHAMBER FROM DETONATION OF PBX 9404

detect any occurence of cracking. Elaborate triggering circuits will be required to ensure that the pressure is recorded to allow for the large differences in the time scale.

c. Theoretical Analysis of the Effects of Transient Burning of High-Explosives (High Pressure)

This section describes the development of an analytic description of the pressure rise within the closed chamber shown in Figure 34. The work was programmed for the UNIVAC 1105 computer in a manner that allows application to a wide variety of problems of this type.

The temperature distribution, $T_{fo}(x)$, along the axis of the explosive at the time current is passed through the igniter wire will be represented by

$$T_{fo}(x) = T_m \exp -(C_1 x) + T_o \tag{65}$$

where

T_m is the temperature of the high-explosive at x = 0, °R

T_o is the initial temperature of the high-explosive prior to any heating, °R

C_1 is an arbitrary constant, 1/ft

At the time current was passed through the igniter wire, the surface was in the process of melting. An average time of 5.4 seconds was required to initiate a burning reaction. The heat from the igniter would be dissipated in depth as well as along a portion of the molten film on the face of the Composition B. In order to maintain a simple geometric description of the problem, the heat will be assumed as dissipated uniformly in a thin layer across the face of the Composition B. The thickness of the layer will be taken equal to the thickness of the foam layer during the burning reaction while the width of the element will be adjusted to yield ignition times consistent with the average delay of 5.4 seconds noted above. The area of the upper surface of the element will be represented by A_1 while the remaining area of the face of the Composition B will be taken as A_2. The total area of the face, i.e., $A_1 + A_2$ will be represented by A. The gas in the chamber at the time current is passed through the igniter wire will be considered as having the same properties as the gas evolved by the explosive. The total mass M of the gas in the chamber may be represented as follows:

$$M = (A_1 x_1 + A_2 x_2 + A x_0)\rho_E \tag{66}$$

where

x_1 = distance traversed by the burning front through the element of the high-explosive containing the igniter wire, ft

x_2 = distance traversed by the burning front through the remainder of the high-explosive, ft

x_0 = depth of high-explosive presenting the same mass as gas originally in the chamber, ft

ρ_E = density of solid high-explosive, lb/ft^3

Since the volume of the gas is essentially constant, the rate of energy change of the gas may be represented by

$$\frac{d}{dt}\left(M\frac{H(T_g)}{k}\right) = A_1\rho_E \frac{dx_1}{dt}\left\{q_1(\dot{x}_1) + H_1(T_{f1})\right\} + q_{elec} + A_2\rho_E \frac{dx_2}{dt}\left\{q_2(\dot{x}_2) + H_2(T_{f1})\right\} - A_1 q_{c1} - A_2 q_{c2} - q_{r\ell} \tag{67}$$

where

$H(T_g)$ represents the total equilibrium enthalpy of the gas, B/lb

k = ratio of the "specific heat" at constant pressure to that at constant volume, dimensionless

$q_i(\dot{x}_i)$ = heat released by the reaction of material evolved from the ith element of explosive (i = 1, 2), B/lb

$H_i(T_{fi})$ = enthalpy of explosive of the ith element (i = 1, 2) just prior to reaction, B/lb

q_{elec} = rate at which gas is heated by the heater, B/ft^2

q_{ci} = rate of heat extraction from gas due to conduction to the ith element of the explosive (i = 1, 2), B/ft^2 hr

$q_{r\ell}$ = rate of heat extraction from gas due to radiant losses to the chamber and explosive, B/ft^2 hr

If the gas is ideal, the equation of state may be expressed as

$$P_g(\ell + x) = (x + x_o)\rho_E R_g T_g \tag{68}$$

where

ℓ = length of gas volume, ft

From Eq. 48 the rate of radiant heat loss, $q_{r\ell}$, from the gas is represented by

$$q_{r\ell} = \int_0^{\ell} T_g^4(z)\, U_1(z, a, \ell, \beta_g' P_g)\, dz \tag{69}$$

while the rate of heat flow, q_{gi} to the ith element of the explosive is given by

$$q_{gi} = \frac{A_i}{A} \int_0^{\ell} T_g^4(z) S_1(z, a, \ell, \beta_g' P_g) dz + A_i q_{ci} + q'_{elec\ i} \tag{70}$$

where

$q'_{elec,\ 1}$ = rate of heat deposition into element 1 from the heater and from the igniter, B/lb

$q'_{elec,\ 2}$ = rate of heat deposition into element 2 from the heater, B/lb

This heat flow will be equal to the rate at which heat is accumulated in the ith element of explosive plus the different between the rates at which heat is carried into and out of the layer by the material entering and leaving the element. This may be expressed as follows:

$$q_{gi} = A_i \rho_E \frac{dx_i}{dt} \left\{ H(T_{fi}) - H(T_{foi}) \right\} + M_i \frac{dH(T_{fi})}{dT_{Ei}} \frac{dT_{fi}}{dt}$$

where

T_{fi} = temperature of foam in ith element during burning, °R

T_{foi} = temperature of solid HE just prior to entering foam layer of ith element

This equation assumes that the amount of high-explosive material in the foam layer remains constant and that the solid HE under the foam layer remains at its initial temperature until it enters the foam layer. Any heat abstracted from the foam by evaporization is neglected.

From Eq. 4 the rate at which mass is evolved by the ith element of the explosive (i = 1, 2) is

$$\dot{M}_i = M_i Z \exp -(E/R_{go} T_{fi}) \tag{71}$$

This completes the specification of the several phenomena. All the quantities are well defined except for the heat flow to the explosive by conduction, i.e., q_{ci}. During the time the explosive is burning, the values of q_{ci} are defined by the data shown in Figure 4. The problem is to specify when these data are applicable, i.e., when burning commences. The temperature of the foam layer during steady burning at a pressure of 1 atmosphere is approximately 540°F. If one uses this temperature as a criterion of ignition it will be found that the pressure at which the pressure commences to rise rapidly is much higher than the value found experimentally, i.e., by a factor of about 2. This would indicate that burning started at a lower foam temperature. By trial and error methods it was found that a good criterion to prescribe the start of burning is the time at which the foam temperature reaches 510°F. At this time the theoretical pressure is consistent with the experimental values at which the pressure

commences to rise rapidly. Furthermore, this foam temperature is consistent with the surface temperatures of Composition B and Cyclotol type explosives that are generally encountered in model and full-scale tests just prior to a rapid temperature rise.

These results were programmed for the UNIVAC 1105 computer to determine the pressure and temperature histories of the gas, the temperature of the layers of explosives, and the burning velocity of the Composition B in the chamber shown in Figure 34. In addition, the temperature histories of the chamber wall and the top cover plate were computed. The parameters used in these computations are as follows

E = 47,500 cal/mole

R_{go} = universal gas constant = 1.987 cal/mole°K
= 1.104 cal/mole°R

Z = frequency factor = $10^{18.5}$/sec
= 1.14×10^{22}/hr

M_1 = 0.0238 lb

M_2 = 0.0491 lb

R_g = 73 ft-lb/lb°R

β'_g = 0.6 atmos. lb^2 °R ft/(ft-lb)^2 cm or 2.83×10^{-4} lb^2 °R/ft^2 ft-lb cm

k = 1.31 (dimensionless)

q_{elec} = heat absorbed by gas from heater = 83B/hr

q'_{elec} = rate of heating of high-explosive from igniter wire = 209 B/hr

q''_{elec} = rate of heating of high-explosive by heater = 1.9×10^3 B/ft^2 hr

Three calculations were conducted utilizing the chamber dimensions associated with the three tests indicated by the data shown in Figures 39 through 41. In these tests, the distances between the Composition B and the lower surface of the top cover plate (see Figure 33) were 1.75, 8.0 and 17.5 inches. The calculated and experimental pressures are shown in Tables XII through XIV. It may be observed that the agreement between the experimental and calculated pressures is reasonably good up to about 1000 psia. Beyond this point the experimental pressures are considerably higher than the calculated values. This is attributed to the increase of the burning area caused by the cracking of the explosive. While these data are consistent, it should not be expected that all Composition B samples will crack at about 1000 psia. The fact that the 1-1 1/4 inch diameter samples of Composition B cracked in the Picatinny Arsenal tests[3] at 4000 - 5000 psia suggests that size, as well as other parameters, such as severe cycling of the environmental temperature and rate of pressure rise,

Table XII

TEMPERATURES AND PRESSURES FROM BURNING COMPOSITION B IN CHAMBER WITH ℓ = 1.75 INCHES

Time, sec	Foam Temperatures,* °F	Gas Temperature, °F	Av. Temperature rise of chamber wall, °F	Gas Pressure, psia	
	calc.	calc.	calc.	exp.	calc.
0	555, 332	2126	.5	65	70
0.02	565, 338	2380	.6	80	84
0.04	575, 347	2673	.7	100	105
0.06	586, 363	2976	.8	150	137
0.08	597, 380	3256	1.1	210	184
0.10	608, 393	3516	1.5	290	256
0.12	619, 450	3751	2.2	410	367
0.13	624, 478	3857	2.7	510	533
0.14	629, 514	3974	3.2	680	700
0.15	633, 594	4182	3.8	970	1126
0.153	635, 604	4360	4.0	(3080)**	1320
0.16	640, 632	4843	4.6	---	2065
0.17	668, 668	5066	6.1	---	3906

*Temperature of foam surrounding igniter wire, temperature of remainder of foam.

**Start of cracking of Composition B.

Table XIII

TEMPERATURES AND PRESSURES FROM BURNING COMPOSITION B IN CHAMBER WITH ℓ = 8.0 INCHES

Time, sec	Foam Temperatures,* °F	Gas Temperature, °F	Av. Temperature rise of chamber wall, °F	Gas Pressure, psia	
	calc.	calc.	calc.	exp.	calc.
0	574, 349	2134	.9	70	75
.1	581, 380	2293	1.4	80	97
.2	589, 395	2410	2.0	120	124
.3	595, 446	2507	2.9	220	158
.4	602, 510	2631	3.9	380	207
.5	625, 625	4031	6.4	690	556
.54	638, 638	4330	8.9	870	840
.56	647, 647	4450	10.8	990	1070
.563	651, 651	4460	11.1	1020	1120
.57	654, 654	4493	11.7	(1500)**	1214
.6	663, 663	4644	15.4	---	1800

*Temperature of foam surrounding igniter wire, temperature of remainder of foam.

**Cracking of explosive.

Table XIV

TEMPERATURES AND PRESSURES FROM BURNING COMPOSITION B IN CHAMBER WITH ℓ = 17.5 INCHES

Time, sec	Foam Temperatures,* °F	Gas Temperature, °F	Av. Temperature rise of chamber wall, °F	Gas Pressure psia	
	calc.	calc.	calc.	exp.	calc.
0	578, 383	1833	1.4	65	84
0.2	582, 396	1896	2.0	115	99
0.4	586, 434	1938	2.7	165	118
0.6	590, 481	2003	3.5	235	141
0.8	596, 577	2267	4.5	330	189
1.0	621, 621	3368	8.0	485	471
1.1	632, 632	3616	12.1	625	733
1.17	640, 640	3890	15.3	1000	994
1.183	642, 642	3830	16.1	(2000)**	1050
1.2	644, 644	3879	17.5	---	1142
1.3	661, 661	4165	25.0	---	1881
1.4	677, 677	4455	35.0	---	3154

*Temperature of foam surrounding igniter wire, temperature of remainder of foam.

**Cracking of explosive.

may play a significant role in affecting the cracking. For these reasons, the criterion of cracking, i.e., 1000 psia, is only preliminary and should be treated accordingly until the cause is thoroughly explored.

Tables XII through XIV also show the calculated temperatures of the foam, gas and chamber. It may be observed that at the lower pressures there is a substantial difference between the temperature of the foam in close proximity to the igniter wire and the temperature of the remainder of the foam. This would indicate that the burning at the lower pressures was essentially limited to the high-explosive surrounding the igniter wire. At later times, the computation indicates that the complete face of the Composition B burned at the same rate. The amount of material that is burnt away during the transition was quite small, i.e., of the order to 0.1 inch. However, since much of this material was evolved in close proximity to the igniter wire, there is a possibility that a groove may have been formed across the face of the Composition B which could initiate the cracking. This would explain the difference between the pressures of 1000 psia at which the Composition B cracked in these studies and the pressure range of 4000 - 5000 psia found at Picatinny Arsenal. This point, however, remains to be resolved.

The calculations also revealed that the average temperature rise of the chamber is relatively small in spite of the fact that the heat fluxes are very high. This is due to the small times for heat transfer. The fact that the temperature rises of the chamber are only 4° to 16°F at the time of cracking for the different tests leads one to suspect that the thermal expansion of the chamber was not a primary cause of the high-explosive cracking. It remains to be seen whether or not the expansion of the chamber by the pressure played any role in the cracking of the Composition B.

5. SUMMARY AND CONCLUSIONS

This report indicates it is feasible to make reasonably accurate predictions of the build up of gas pressure within systems containing burning high-explosives at least until the high-explosive cracks. For this purpose, computer programs have been developed to determine the pressure within closed and vented systems. For these computations, it is necessary to know the enthalpy and opaqueness of the gas, the amount of material in the layer of foam, the conductive heat flux to the explosive, the heat evolved by the burning reaction, the enthalpy of the solid and liquid high-explosive, and the rate at which the high-explosive reacts as a function of temperature. These data have been determined for Composition B and are presented in this report. The problem of predicting the pressure rise during normal burning for other explosive materials is basically one of accumulating these data. While some of the data is in the literature, most of it must either be estimated or determined by experimentation. Fortunately, this is not a major endeavor.

Once the high-explosive cracks, the pressure rises at such a rapid rate that much higher pressures are reached than the system can maintain under conditions of static loading. As a result of the various modes by which an explosive may crack, the rate of pressure rise following the cracking (or the violence of the resulting explosion) is not predictable. As a general rule the order of the explosion should be related in some inverse manner with the volume of the void space between the explosive and the confining vessel. This is due to the fact that a decrease in the void space would accentuate the rate of pressure rise and enable the confining vessel to remain intact until higher pressures are reached. Furthermore, the order of the explosion should increase with the depth of the explosive. The increased depth would allow the cracking to expose greater surface areas to the burning and thereby result in more pronounced pressure rises. This would partially explain the fact that thin layers of explosive have never initiated an explosion in any full-scale test.

From these studies, it is possible to catagorize the behavior of any system by one of the following descriptions:

a. Complete burning of the high-explosive without any hazardous pressure building up.

b. Burning of the high-explosive that evolves a sufficient buildup of pressure to cause a pressure burst or plastic failure of the confinement vessel without initiating cracking of the high-explosive. While this type of reaction would be a hazard to personnel in the immediate vicinity of such a reaction, no extensive damage would be anticipated.

c. Burning of the high-explosive that evolves sufficient buildup of pressure to crack the explosive material and thereby produce a violent explosion. In this situation, the very rapid pressure rise may cause

a brittle failure of the confinement vessel with the evolution of considerable shrapnel. The explosion may or may not be a detonation.

The criterion which determines whether (b) or (c) occurs is the size of any holes in the vessel at the time the high-explosive commences to burn. As noted previously from the Composition B studies, small holes of about 1 percent of the burning area will maintain the pressure at near atmospheric levels. With minor adjustments, these data are also applicable to actual systems containing Cyclotol-type explosives. The critical hole size will increase with the proximity of the hole to the surface of the burning explosive. This is due to the lower density of the gas caused by the higher gas temperatures. Vent holes should be sufficiently well dispersed about the high-explosive system to prevent any appreciable pressure buildup as a result of the internal resistance presented to gas flow. Determination of the hole sizes requires a knowledge of the parameters noted previously and is a relatively simple procedure.

REFERENCES

1. Zinn, J., and C. L. Mader, "Thermal Initiation of Explosives," University of California, Los Alamos Scientific Laboratory, 1959, (UNCL).

2. ORDP-20-177, "Properties of Explosives of Military Interest," Army Ordnance Corps., May 1960, (UNCL).

3. Wachtell, S., "Establishment of Improved Standards for Classification of Explosives and Propellants," Report No. 1, Picatinny Arsenal, Dover, New Jersey, June 1960, (UNCL).

4. Huff, V. N., and C. S. Calvert, "Charts for the Computation of Equilibrium Compositions of Chemical Reactions in Carbon-Hydrogen-Oxygen-Nitrogen System at Temperatures from 2000 to 5 000°K," Technical Note 1653, Flight Propulsion Research Laboratory, Cleveland, Ohio, (UNCL).

5. Hershey, R. L., J. E. Eberhards, H. C. Hottel, "Thermodynamic Properties of the Working Fluid in Internal Combustion Engines," SAE Trans., 31, No. 4, Oct. 1936, pp. 409-424.

6. Goldsmith, A., Handbook of Thermophysical Properties of Solid Materials, 1, MacMillian Co., New York, 1961.

7. Schack, A., A. Tech. Physik 6, 530, 1925, (UNCL).

8. Jakob, M., Heat Transfer, 1, John Wiley and Sons, Inc., New York, London, May, 1962.

9. Mc Adams, W. H., Heat Transmission, McGraw-Hill Book Co., Inc., New York, Toronto, London, 1954.

10. Boelter et al., Space Technology, John Wiley and Sons, Inc., New York, London, 1959.

11. Carslaw and Jaeger, Conduction of Heat in Solids, Clarendon Press, Oxford, 1959.

12. Takata, A. N., "Factors Affecting the Vulnerability of Atomic Weapons to Fire," (U), Full Scale Tests AFSWP (DASA) Rept. No. 1060, Oct. 1957, (SRD).

13. Takata, A. N., and W. J. H. Murphy, "Factors Affecting the Vulnerability of Atomic Weapons to Fire," (U), Full Scale Tests, AFSWP (DASA), Rept. No. 1066, June, 1958, (SRD).

14. Takata, A. N., "Development and Analysis of Models of Nuclear Weapons Exposed to Fire," (U), Model Tests, DASA Rept. No. 1130, June 1959, (SRD).

15. Takata, A. N., "Vulnerability of Nuclear Weapon Systems to Fire," DASA Rept. No. 1234, July 1961, (SRD).

16. Takata, A. N., A. Goldsmith, H. Hirschhorn, W. J. H. Murphy, G. Nagumo, DASA Rept. No. 1276, Vols. I, II, III, IV. 1963, (SRD).

APPENDIX

Table A-1 is a compilation of data pertaining to high-explosives. These data were obtained from a literature study during the course of this work.

TABL 1 L AN

Explosive Material	Density (lb/ft^3)	Temperature Melting (°F)	Latent Heat of Fusion (B/lb)		Specific Heat, c, (B/lb at Sp				l Con ures
					-103	-74 to 32	32	32 to 79	79 to 140
Baratol (67/33)	159(a) 159(b)	177(j)	5.04(j)	c	0.152(j)	0.131(a)	0.147(j)	0.162(a) 0.180(j)	0.213(a) 0.229(j)
				k		0.174(a)		0.193(a)	0.248(a)
Composition B	101(c) 103(b)	172-176(b) 169-176(c) 172-176(j)	14.4(b) 14.4(j)	c	0.235(j)		0.220(j)	0.254(j)	0.305(j)
				k					
Cyclotol (75/25)	107(b) (cast)	172-176(j)	9.0(b) 9.0(j)	c	0.220(j)		0.225(j)	0.254(j)	0.296(j)
				k				0.259(d)	
Cyclotol (70/30)	109(a) 107(b)			c		0.208(a)		0.238(a)	0.283(a)
				k		0.135(a)		0.129(a)	0.139(a)
Cyclonite (RDX)	114(b)	399(b)		c	0.215(a)		0.228(a)	0.298(b)	0.331 0.331(b) (104°F)
				k	0.152(a)		0.235(a)		0.288(a)
HMX	114(a) 118(b)	529(j)		c	0.115(a)	0.210(a)	0.228(a)	0.262(a)	0.262(a)
				k		0.201(a)		0.202(a)	0.209(a)
PETN	111(b) (crystal)	285(b)		c					0.260(b)
				k					
TNT	103(b) (crystal)	178(b) 177.6(j)	40.2(b) 37.8(j) (calc)	c	0.232(j)	0.226(a)	0.242(j) 0.309(b)	0.254(j) 0.259(a) 0.264(d)	0.315(j) 0.294(a)
				k		0.114(a)		0.117(a)	0.121(a)

(a) ORD. BB. THI-095 Picatinny Arsenal, Dover, N.J. Samuel Feldman, Ammunition Lab. April 1958

(b) ORDP 20-177 "Properties of Explosives of Military Interest" May 1960

(c) APC Exp

(d) The "Eig

TABLE A1 PHYSICAL AND THERMAL PROPERTIES OF EXPLOSIVES

, c, (B/lb °F) and Thermal Conductivity, k, (B/hr ft °F) at Specified Temperatures (°F)							Heat of Explosion (B/lb)	Heat of Formation (B/lb)	AC GY	
2	32 to 79	79 to 140	167	185	194	212			Cal/Mole	Temperature Range (°F)
7(j)	0.162(a) 0.180(j)	0.213(a) 0.229(j)	0.280(j)	0.213(j)	0.201(j)	0.171(j)				
	0.193(a)	0.248(a)								
0(j)	0.254(j)	0.305(j)	0.376(j)	0.354(j)	0.341(j)	0.312(j)	2232(b)			
5(j)	0.254(j)	0.296(j)	0.352(j)	0.325(j)	0.332(j)	0.351(j)	2205(b) (calc)		47,500(h) 43,600(d)	311-356(d)
	0.259(d)									
	0.238(a)	0.283(a)								
	0.129(a)	0.139(a)								
8(a)	0.298(b)	0.331 0.331(b) (104°F)	0.292(a)	0.384(b) (176°F)		0.427(a) 0.406(b)	2304(b)	-173(b)	57,200(d) 43,400(d) 34,400(d) 47,500(b)	338-392(d) 460-530(d) 428-500(d) 415-570 (b)
5(a)		0.288(a)	0.288(a)							
3(a)	0.262(a)	0.262(a)	0.282(a)				2441(b)	-109(b)	52,700(b)	520-597(b)
	0.202(a)	0.209(a)								
		0.260(b)					2493(b)	689(b)	50,900(b) 52,300(b) 47,000(b)	226-248(b) 279-314(b) 322-451(b)
2(j) 9(b)	0.254(j) 0.259(a) 0.264(d)	0.315(j) 0.294(a)	0.354(j)	0.513(j)	0.478(j)	0.275(j)	1944(b)	141(b)	43,400(b) 34,400(b)	460-531(b) 527-590(b)
	0.117(a)	0.121(a)								

(c) APG. ORD School APG, Md. "Fundamentals of Explosives" Jan. 1953

(d) The Williams and Wilkes Co., Baltimore 2, Md. "Eighth Symposium (International) on Combustion" 1962

(h) Robertson A. J. B., Trans.

(j) R. Velicky, C. Lenchitz and "Enthalpy Change, Heat of Specific Heat of Basic Expl PATR No. 2504, Jan. 1959

ERMAL PROPERTIES OF EXPLOSIVES

vity, k, (B/hr ft °F)				Heat of Explosion (B/lb)	Heat of Formation (B/lb)	ACTIVATION ENERGY (E)		FREQUENCY FACTOR (Z)	
67	185	194	212			Cal/Mole	Temperature Range (°F)	1/Sec.	Temperature Range (°F)
.280(j)	0.213(j)	0.201(j)	0.171(j)						
.376(j)	0.354(j)	0.341(j)	0.312(j)	2232(b)					
352(j)	0.325(j)	0.332(j)	0.351(j)	2205(b) (calc)		47,500(h) 43,600(d)	 311-356(d)	$10^{18.5}$(h)	
292(a)	0.384(b) (176°F)		0.427(a) 0.406(b)	2304(b)	-173(b)	57,200(d) 43,400(d) 34,400(d) 47,500(b)	338-392(d) 460-530(d) 428-500(d) 415-570(b)	 $10^{12.19}$(d) $10^{11.4}$(d) $10^{18.5}$(b)	 460-560(d) 428-500(d) 415-570(b)
288(a)									
282(a)				2441(b)	-109(b)	52,700(b)	520-597(b)	$10^{19.7}$(b)	520-597(b)
				2493(b)	689(b)	50,900(b) 52,300(b) 47,000(b)	226-248(b) 279-314(b) 322-451(b)	$10^{20.6}$(b) $10^{23.1}$(b) $10^{19.8}$(b)	226-248(b) 279-314(b) 322-451(b)
154(j)	0.513(j)	0.478(j)	0.275(j)	1944(b)	141(b)	43,400(b) 34,400(b)	460-531(b) 527-590(b)	$10^{12.2}$(b) $10^{11.4}$(b)	460-531(b) 527-590(b)

D School APG, Md. "Fundamentals of
s" Jan. 1953

ams and Wilkes Co., Baltimore 2, Md.
ymposium (International) on Combustion" 1962

(h) Robertson A. J. B., Trans. Far. Soc. 45, 85 (1949)

(j) R. Velicky, C. Lenchitz and W. Beach "Enthalpy Change, Heat of Fusion, and Specific Heat of Basic Explosives" PATR No. 2504, Jan. 1959

DISTRIBUTION

No. cys	
	HEADQUARTERS USAF
1	Hq USAF (AFCOA), Wash, DC 20330
1	Hq USAF (AFOCE), Wash, DC 20330
1	Hq USAF (AFORQ), Wash, DC 20330
1	Hq USAF (AFRNE-A), Wash, DC 20330
1	USAF Dep, The Inspector General (AFIDI-A-3), Norton AFB, Calif 92409
1	USAF Directorate of Nuclear Safety (AFINS-E-1), Kirtland AFB, NM 87117
1	Hq USAF (AFRDC-NE, Lt Col Trogdon), Wash, DC 20330
	MAJOR AIR COMMANDS
	AFSC, Andrews AFB, Wash, DC 20331
1	(SCT)
1	(SCSSN, Maj Berrier)
1	(SCIZ)
1	TAC (DORQ-M), Langley AFB, Va 23365
	SAC, Offutt AFB, Nebr 68113
1	(OA)
1	(OAWS)
2	AFLC, Wright-Patterson AFB, Ohio 45433
2	ADC (Ops Anlys), Ent AFB, Colorado Springs, Colo 80912
1	AUL, Maxwell AFB, Ala 36112
1	USAFIT (USAF Institute of Technology), Wright-Patterson AFB, Ohio 45433
1	USAFE (Ops Anlys), APO 633, New York, NY
1	PACAF (PFODC), Camp Smith, Hawaii
	AFSC ORGANIZATIONS
2	ASD (ASNXRR, Tech Info Ref Br., Reports Div.), Wright-Patterson AFB, Ohio 45433
2	RTD (RTN-W, Lt Col Munyon), Bolling AFB, Wash, DC 20332
	BSD, Norton AFB, Calif 92409
2	(BSR)
1	(BSOR, Lt Col Schmidt)
1	SSD (SSSC), AF Unit Post Office, Los Angeles, Calif 90045
1	ESD (ESAT), Hanscom Fld, Bedford, Mass 01731

DISTRIBUTION (cont'd)

No. cys	
	AF Msl Dev Cen, Holloman AFB, NM 88330
1	(RRRT)
1	(MDRGT, Lt Col Bogard)
1	AFMTC (MU-135, Tech Library), Patrick AFB, Fla 32925
1	APGC (PGAPI), Eglin AFB, Fla 32542
1	RADC (Document Library), Griffiss AFB, NY 13442
	KIRTLAND AFB ORGANIZATIONS
	AFSWC, Kirtland AFB, NM 87117
1	(SWEH)
1	(SWT)
	AFWL, Kirtland AFB, NM 87117
40	(WLL)
1	(WLAX)
1	(WLAS)
1	(WLD)
1	(WLDW)
1	ADC (ADSWO), Special Weapons Office, Kirtland AFB, NM 87117
1	ATC Res Rep (SWN), AFSWC, Kirtland AFB, NM 87117
1	AFLC, Albuquerque Ln Ofc (MCSWQ), AFSWC, Kirtland AFB, NM 87117
1	SAC Res Rep (SWL), AFSWC, Kirtland AFB, NM 87117
1	TAC Liaison Office (TACLO-S), AFSWC, Kirtland AFB, NM 87117
	OTHER AIR FORCE AGENCIES
	Director, USAF Project RAND, via: Air Force Liaison Office, The RAND Corporation, 1700 Main Street, Santa Monica, Calif 90406
1	(RAND Physics Div)
1	(RAND Library)
1	SAAMA (SAW), Directorate of Special Weapons, Kelly AFB, Tex 78241
1	2705 Airmunitions Wing (OOYS), Hill AFB, Utah 84401
1	Det 1, 2701st Explosive Ordnance Disposal Squadron, Ellsworth AFB, S Dak 57706

DISTRIBUTION (cont'd)

No. cys	
	ARMY ACTIVITIES
1	US Army Materiel Command, Harry Diamond Laboratories, (ORDTL 06.33, Technical Library), Wash, DC 20438
1	Commanding Officer, US Army Combat Developments Command, Nuclear Group (USACDCNG), ATTN: Top Secret Control Officer, Ft Bliss, Tex 79916
3	Redstone Scientific Information Center, US Army Missile Command, Chief, Document Section, Redstone Arsenal, Ala 35809
	Commanding Officer, Picatinny Arsenal, Samuel Feltman Ammunition Laboratories, Dover, NJ 87801
2	(Document Control Office)
1	(AMSMU-D)
2	Commanding Officer, US Army Signal Research & Development Laboratory (SIGFM/EL-SAT), Weapons Effects Section, Fort Monmouth, NJ 07703
1	Research Analysis Corp (Margaret L. Emerson, Librarian), 6935 Arlington Road, Bethesda 14, Md
1	Commandant, Command and General Staff College (Archives), Ft Leavenworth, Kans 66027
1	President, US Army Air Defense Board, Ft Bliss, Tex
2	Chief of Engineers (ENGNB), Department of the Army, Wash 25, DC
1	Director, US Army Engineer Research & Development Laboratories, ATTN: Tech Documents Center, Ft Belvoir, Va
2	Commandant, US Army Ordnance School, ATTN: BRL-W, Survival Branch, Aberdeen Proving Ground, Md 21005
1	Office, Chief of Engineers, Department of the Army, Classified Records Section, Bldg T-7, Room G-401, Gravelly Point, Wash 25 DC
1	Chief, NWSSG, USA Nuclear Weapons Systems Safety Group, Ft Belvoir, Va
1	Chief of Research & Development, Department of the Army, Room 3D-442, The Pentagon, ATTN: Atomic Div., Wash 25, DC
1	Commandant, US Army Artillery & Guided Missile School, Ft Sill, Okla
1	Commanding General, US Army Combat Development Command, Ft Belvoir, Va
1	Commandant, Army War College, Carlisle Barracks, Penna
2	Chief Signal Officer, Room 2D-260, ATTN: SIGRD-4B, The Pentagon, Wash 25, DC

DISTRIBUTION (cont'd)

No. cys	
1	Commanding General, US Continental Army Command, ATTN: G-3, Ft Monroe, Va
1	Deputy Chief of Staff for Military Operations, Department of the Army, ATTN: OPS CD MD, Wash 25, DC
3	Commanding General, US Army Materiel Command, Department of the Army, ATTN: AMCOR, Wash 25, DC
1	Commanding Officer, Ammunition Procurement & Supply Agency, ATTN: SMUAP-SW, Joliet, Ill
6	Commander-in-Chief, US Army Pacific, ATTN: Ord Office, APO 958, San Francisco, Calif
1	Commander-in-Chief, United States European Command, ATTN: ECJS-A, APO 128, New York, NY
1	Commanding General, Army Mobility Command, ATTN: ORDMC-RR-1, Detroit, Mich
3	Commanding General, US Army Combined Arms Group, Fort Leavenworth, Kans
1	San Francisco Ordnance District, 1515 Clay Street, ATTN: BR & SP Branch, Oakland 12, Calif
1	President, Airborne & Electronics Board, ATTN: ARBF-AB, Ft Bragg, North Carolina
2	Commander, US Strike Command, MacDill AFB, Fla
	NAVY ACTIVITIES
4	Office of the Chief of Naval Operations (OP-75), Department of the Navy, Wash, DC 20350 ATTN: Director, Atomic Energy Division
	Chief, Bureau of Naval Weapons, Department of the Navy, Wash 25, DC
3	(RAAV)
3	(RRNU)
2	Bureau of Ships, Department of the Navy, BS 390, Wash 25, DC
1	Commanding Officer, Nuclear Weapons Training Center (Nuclear Warfare Department), Atlantic, Naval Base, Norfolk, Va 23511
1	Commanding Officer, Naval Weapons Training Center, Pacific, Naval Air Station, ATTN: Director, Weapons Employment & Planning Dept., North Island, San Diego 35, Calif
1	Commanding Officer, US Naval Schools Command, US Naval Station, Treasure Island, San Francisco, Calif
2	Commander, Naval Ordnance Test Station (Code 753), China Lake, Calif 93557
1	Commander, Naval Ordance Laboratory, ATTN: Dr. Rudlin, White Oak, Silver Spring, Md

DISTRIBUTION (cont'd)

No. cys	
1	Director, Special Projects (SP-43, Tech Library), Department of the Navy, Wash 25, DC
	Commanding Officer, US Naval Explosive Ordnance Disposal Facility, US Naval Propellant Plant, Indian Head, Md
1	(Explosive Ordnance Disposal)
1	(Explosive Ordnance Disposal School)
1	Commander-in-Chief, US Atlantic Fleet, US Naval Base, Norfolk 11, Va
1	Commandant of the Marine Corps, Department of the Navy (Code AO3H), Wash 25, DC
2	Office of Naval Research, ATTN: Dr. W. Thaler, Wash 25, DC
1	Commanding Officer, US Naval Weapons Evaluation Facility (NWEF) (Code 404), Kirtland AFB, NM 87117
1	Commander, US Naval Weapons Laboratory, Dahlgren, Va
1	Commander, Training Command, US Pacific Fleet, c/o US Fleet SONAR School, San Diego 47, Calif
1	Director, Marine Corps Development Center, Marine Corps Schools, Quantico, Va
1	Bureau of Naval Weapons Representative (Special Projects), Lockheed Aircraft Corporation, ATTN: LCDR Loper, Sunnyvale, Calif
1	Inspector of Naval Materiel, 495 Summer Street, ATTN: RCA, Box 2276, Boston, Mass
	OTHER DOD ACTIVITIES
4	Chief, Defense Atomic Support Agency (Document Library, Miss Gertrude Camp), Wash, DC 20301
9	Commander, Field Command, Defense Atomic Support Agency, (FCAG3, Special Weapons Publication Distribution), Sandia Base, NM 87115
1	Director, Weapon Systems Evaluation Group, Room 1D-847, The Pentagon, Wash, DC 20330
2	Director Advanced Research Projects Agency, Department of Defense, The Pentagon, Wash, DC 20301
1	Office of Director of Defense Research & Engineering, ATTN: John E. Jackson, Office of Atomic Programs, Rm 3E 1071, The Pentagon, Wash, DC 20330
1	Chairman, Armed Services Explosives Safety Board, Wash 25, DC
20	Hq Defense Documentation Center for Scientific and Technical Information (DDC), Bldg 5, Cameron Sta, Alexandria, Va 22314

DISTRIBUTION (cont'd)

No. cys	
2	Chairman, Military Liaison Committee to AEC, Department of Defense, Wash 25, DC
	AEC ACTIVITIES
	Sandia Corporation, Box 5800, Sandia Base, NM 87115
5	(Div. 1261)
1	(Div. 1541-2, B.E. Bader)
2	(Information Distribution Division),
1	Sandia Corporation (Technical Library), P.O. Box 969, Livermore, Calif 94551
3	Chief, Division of Technical Information Extension, US Atomic Energy Commission, Box 62, Oak Ridge, Tenn 37831
4	University of California Lawrence Radiation Laboratory (Technical Information Division), P.O. Box 808, Livermore, Calif 94551
4	Director, Los Alamos Scientific Laboratory (Helen Redman, Report Library), P.O. Box 1663, Los Alamos, NM 87554
1	US Atomic Energy Commission, San Francisco Operations Office, 2111 Bancroft Way, Berkeley 4, Calif
1	Director, Division of Military Application, US Atomic Energy Commission, Wash 25, DC
	OTHER
1	Central Intelligence Agency (OSI/RD), 2430 E Street, NW, Wash 25, DC
1	Convair, A Division of General Dynamics Corp., ATTN: Chief Librarian, P.O. Box 1950, San Diego 12, Calif
5	Illinois Institute of Technology Research Institute, ATTN: Security Office, 10 West 35th Street, Chicago 16, Ill
1	Director, Lincoln Laboratory, Massachusetts Institute of Technology, ATTN: Technical Library, P.O. Box 73, Lexington 73, Mass
1	Official Record Copy (Capt L.S. McChristian, WLAX)